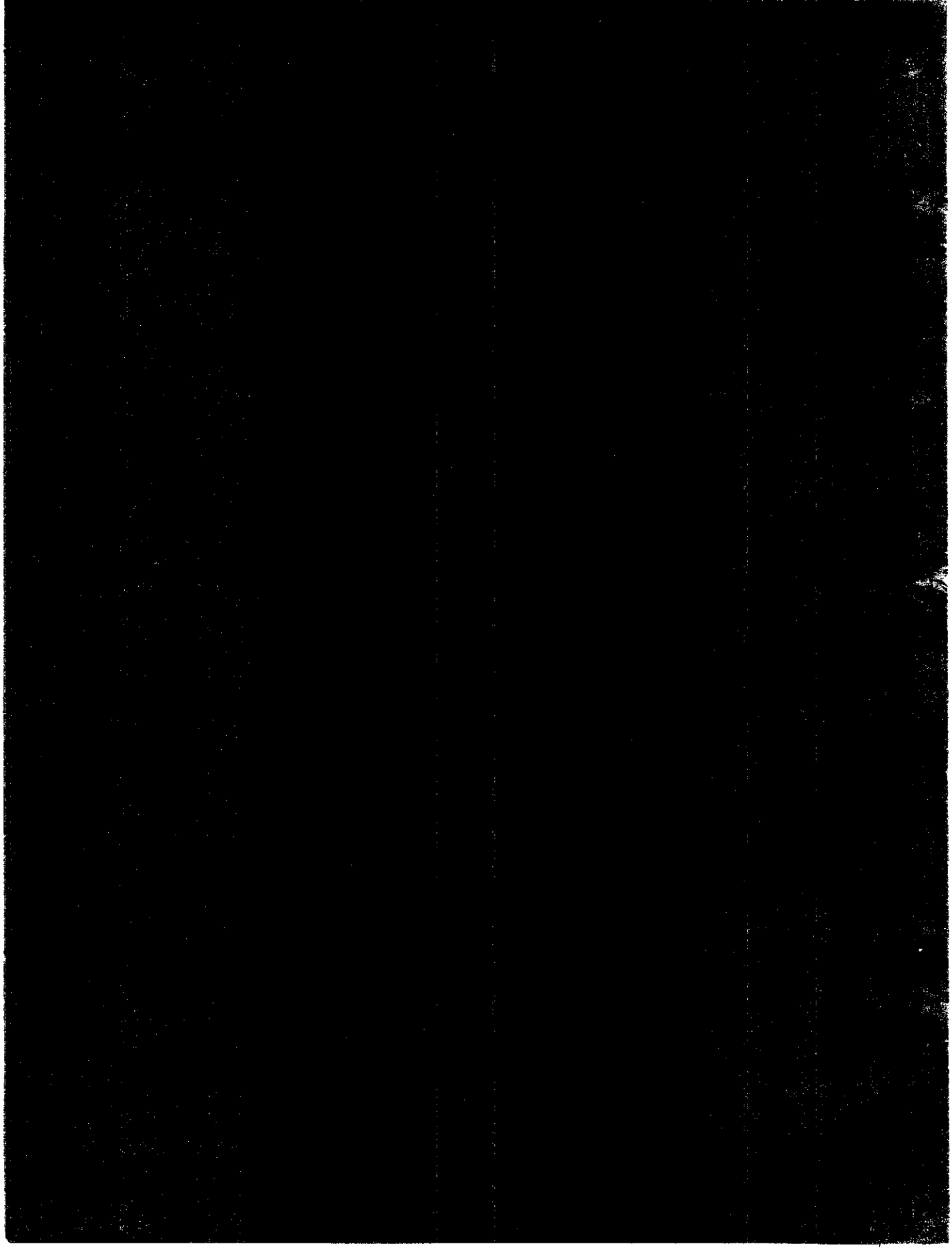

COMMONWEALTH OF AUSTRALIA
DEPARTMENT OF EXTERNAL AFFAIRS

AUSTRALIAN NATIONAL ANTARCTIC RESEARCH EXPEDITIONS

ANARE SCIENTIFIC REPORTS

SERIES A (IV) GLACIOLOGY

PUBLICATION No. 96

RADIATION FLUXES OVER AN ANTARCTIC ICE SURFACE, MAWSON, 1961-62

by
G. E. WELLER

ISSUED BY THE ANTARCTIC DIVISION
DEPARTMENT OF EXTERNAL AFFAIRS, MELBOURNE
1967

Registered at the G.P.O. Melbourne
for transmission by post as a book.

Printed in Australia by
Brown Prior Anderson Pty Ltd 5 Evans Street Burwood Victoria

CONTENTS

LIST OF FIGURES

RADIATION FLUXES OVER AN ANTARCTIC ICE SURFACE, MAWSON, 1961-62

By

G. E. WELLER

Antarctic Division, Department of External Affairs, Melbourne
Present Address: Department of Meteorology, University of Melbourne

(Manuscript received March 1967)

ABSTRACT

The solar radiation fluxes over an Antarctic ice surface were measured for two years and the radiation spectrum was analysed by dividing it into the usual short-wave and long-wave regions, the former having wave-lengths of less than 3 microns, the latter wave-lengths greater than 3 microns. Both downward-and-upward-directed fluxes were considered separately.

Normalized curves representing the average condition at Mawson were constructed for the short-wave downward flux with the aid of the theoretical considerations of Ångström and Hoelper. Numerous checks with measured data agree well. The long-wave downward flux was computed, using the Elsasser radiation diagrams and the water vapour content of the atmosphere obtained from aerological soundings. Also, various empirical formulae (Ångström, Brunt, etc.) and the semi-empirical Swinbank equation were tested. The long-wave upward flux was measured and found to agree well with the Stefan-Boltzmann temperature radiation law. Finally, the upward-directed short-wave flux was determined as a remainder term in the radiation balance and compared with measured values of the albedo. All separate radiation components were analysed for the conditions of clear and overcast sky.

The final radiation balance was compared with other stations. At Mawson, as elsewhere in the Antarctic, the radiation balance of the ice surface is negative for the greater part of the year. The total radiation loss of the ice is 5·6 k cal cm^{-2} $year^{-1}$. In summer, the radiation balance remains negative up to a solar altitude of 17 degrees on clear days.

Finally, the amount of radiation absorbed by the ice was computed and the importance of radiation in the total energy exchange through an ice surface indicated.

0. INTRODUCTION

The different radiation fluxes to and from the earth's surface are amongst the most important terms in the heat economy of the earth as a whole and of any individual place at the earth's surface or in the atmosphere. These fluxes consist basically of the extra-terrestrial radiation emitted by the sun, and the temperature radiation of the atmosphere and the earth's surface.

The solar radiation or short-wave radiation is conveniently defined as radiation with wave lengths smaller than 3 μ although some energetically negligible radiation from the sun up to 25 μ has been shown to be present (Möller 1957). The solar radiation is scattered, absorbed and reflected by the atmosphere and the earth's surface resulting in both upward and downward directed fluxes. The temperature or long-wave radiation i.e., radiation with wave lengths larger than 3 μ, also has upward and downward directed components.

Observation and measurement of these fluxes have now been carried out over a few decades at numerous points on the earth's surface, making it possible to construct an atlas of the radiation balance of the earth's surface (Budyko 1963). Many measurements made, however, may unfortunately be seriously in error since the physical principles of the instruments involved were not fully investigated. It must be stressed that a proper physical analysis of what is actually measured is of high importance if correct and meaningful values of the measured quantities are required.

Despite careful investigation of the performance of radiation instruments, the limitations of available instruments result in some error in the determination of integrated radiation fluxes, unless a prodigious amount of work is done on reducing the measured data. Nicolet (1948) has claimed that, in a continuous record of the radiation of sun and sky, an accuracy of $\pm$ 5% represents the result of good and careful work. It will be shown below that the error estimate of the radiation measurements presented in this thesis will fall within this margin.

A complete study of the radiation fluxes must achieve a number of aims. To quote from the Commission for Instruments and Methods of Observation of the World Meteorological Organization (1953): "Radiation measurements within meteorological networks must contribute to the following purposes:

(a) the study of the transformation of energy within the system earth-atmosphere and its variation in time and space;
(b) the analysis of the atmosphere with regard to its turbidity and constituents such as dust and water-vapour;
(c) the study of the distribution and its variation of incoming, outgoing and net radiation."

The radiation measurements discussed in this thesis fitted into these requirements and consisted of the following separate investigations of :

(a) the direct solar radiation, the turbidity and the water-vapour absorption in the atmosphere.
(b) the global radiation;
(c) the duration of sunshine;
(d) the net outgoing long-wave radiation from the snow;
(e) the atmospheric long-wave radiation;
(f) the albedo of the snow surface.

A precise determination of the radiation fluxes is of interest in climatological and meteorological studies. It is also required in a study of the physical processes determining the mass balance of an ice cap, and in the study of the total energy exchange of such an ice cap with the atmosphere.

The measurements to be described were made in the coastal ablation zone of the Antarctic ice cap. The location was the Australian National Antarctic Research Expedition's Station at Mawson, situated at latitude 67° 36′ S, longitude 62° 53′ E, on a small flat rock exposure on the coast of Mac. Robertson Land. The surface of the continental ice there rises steeply from the sea-level at Mawson to a height of 1500 metres about 80 kilometres from the coast. Further inland the slopes are more gentle; an altitude of 2500 metres is reached at 300 km inland and a maximum of 3000 metres is reached 600 km from the coast.

The instruments were located over a sloping blue ice surface facing North, half a kilometre from the coast at an altitude of 40 metres. The nature of the surface underneath the instruments varied with season. In summer, heavy ablation produced a smooth ice surface, whereas in the winter months snow drifts, generally only a few centimetres thick, partially or wholly covered the ground. There was no exposed rock in the immediate vicinity of the instruments.

Measurements of solar radiation have been carried out at Mawson since 1954. In 1954, soon after Mawson station had been established by the ANARE spot readings of direct solar radiation were taken by Dingle with an actinometer specially designed by H. J. Albrecht (Albrecht and Dingle 1957).

In 1956, a Robitzsch actinograph was installed at Mawson by the Commonwealth Bureau of Meteorology, and operated until May 1958, when it was damaged in a blizzard. A similar instrument replaced it and operated until April 1962. Daily radiation totals and monthly totals of the short-wave global radiation were published by the Bureau of Meteorology (Bureau of Meteorology Publication 1963). A Campbell-Stokes sunshine recorder was also installed in 1957 and has been operating since.

In 1959, two Moll-Gorczynski solarimeters were installed, one recording global radiation and the other, provided with a shade ring, recording diffuse sky radiation. A polythene-shielded net radiometer (Funk 1959) was also installed, and a Linke-Feussner actinometer was provided for the calibration of this instrument set.

Continuous recording was obtained from the solarimeters and the net radiometer from October 1959 to January 1960 (Norris and Funk 1961).

The data presented in this volume were collected at Mawson station during the period January 1961-January 1963. The author gathered the 1961 data. The meteorological staff of the 1962 wintering party obtained the data for that year. The purpose of the investigation was to give a careful and accurate evaluation of the components of the radiation balance at Mawson which, despite the previous collection of data, had hitherto not been undertaken.

0.1. NOMENCLATURE

For the fluxes of radiation the following symbols were used as taken partly from the IGY Instruction Manual IV, 1958.

S	direct solar radiation
D	diffuse sky radiation
G	global radiation (total (sun + sky) radiation) $G = S \sin h + D$
R	reflected short-wave radiation from below
N_s	short-wave radiation balance; $N_s = G - R$
A	long-wave atmospheric radiation
E	long-wave (temperature) radiation of the surface; $E = \sigma T^4$
N_L	long-wave radiation balance; $N_L = A - E$
Q_o	total (short-wave and long-wave) incoming radiation from the upper hemisphere; $Q_o = A + G$
Q_u	total (short-wave and long-wave) outgoing radiation from the lower hemisphere; $Q_u = E + R$
N	total radiation balance; $N = Q_o - Q_u$

The following radiation fluxes were measured directly:

solarimeter 1 : G
solarimeter 2 (with shade ring) : D
net radiometer : N
net radiometer (during night) : N_L

Details of the instruments used will be considered below in Section 1.

1. INSTRUMENTS AND MEASURING TECHNIQUE

1.1. INSTRUMENTS

To measure the components of the radiation balance, the following instruments were used:

a. one Linke-Feussner actinometer No. 56 (Kipp and Zonen, Delft) against which all other instruments were calibrated;

b. one Moll-Gorczynski solarimeter (Kipp and Zonen) to measure the global radiation and the albedo by turning the instrument through 180° on a fixed axis;

c. one Moll-Gorczynski solarimeter (Kipp and Zonen) with a shade ring 5 cm wide and 30 cm in diameter to measure the diffuse sky radiation;

d. one CSIRO polythene-shielded net radiometer Mk. 1, No. 3, to measure the net flux of short-wave and long-wave radiation;

e. one portable CSIRO polythene-shielded net radiometer Mk. 1, No. 5.

The mounting of the instruments over the ice surface was achieved by means of steel pipes of 5 cm diameter let into the ice surface, scaffold clamps attaching horizontal pipes approximately 2 metres above the surface to the vertical pipe supports. The instruments were clamped to these horizontal pipes. The mounting was quite rigid, one being provided for each instrument. The ice surface was undisturbed below the instruments. The height of the instruments above the surface could be adjusted and was not quite constant due to ablation and accumulated snow. Occasional adjustment of the instruments in a horizontal plane was necessary due to slow ice movement.

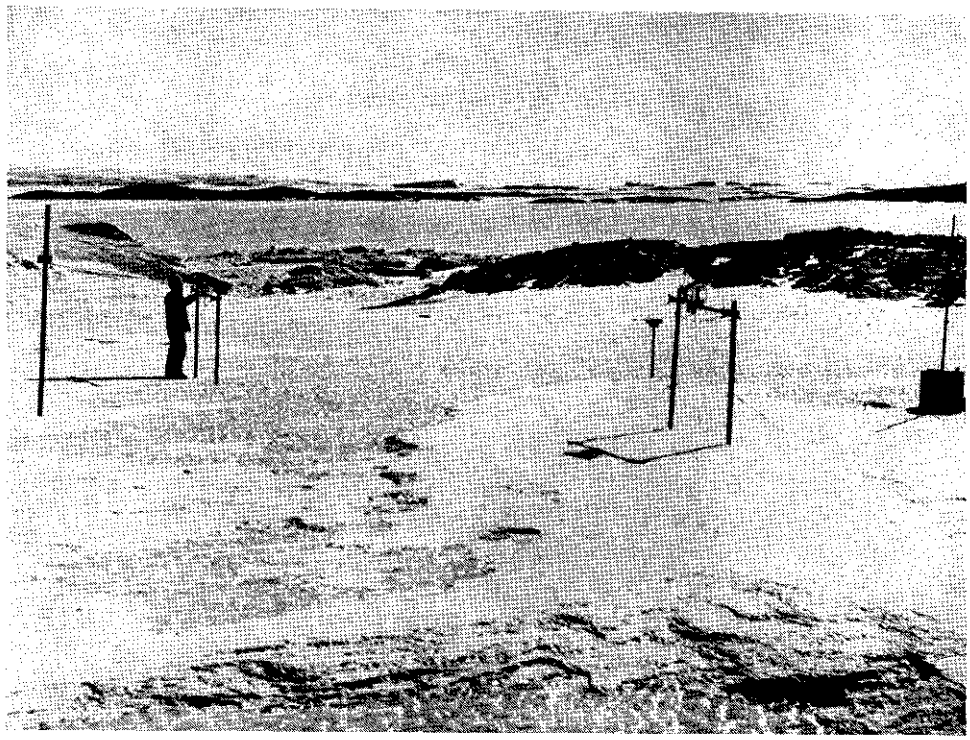

FIG. 1.1.1. Installation of the radiation instruments at Mawson.

Fig. 1.1.1 shows the installation of the three instruments. The underlying surface is typical of winter conditions, when a partial snow cover existed. From left to right are seen the mast for telephone cables, Kipp solarimeter No. 1, the stand for the Linke-Feussner actinometer, Kipp solarimeter No. 2 with shade ring, net radiometer and inflation equipment.

Fig. 1.1.2 shows details of the Kipp solarimeter with the shade ring, measuring diffuse sky radiation. Between the supporting framework of the solarimeter can be seen the vertical mast supporting the net radiometer. The wooden box at its base contained a balloon used to inflate the polythene hemisphere of the net radiometer. Both photos were taken late in 1959, soon after the installation of the instruments.

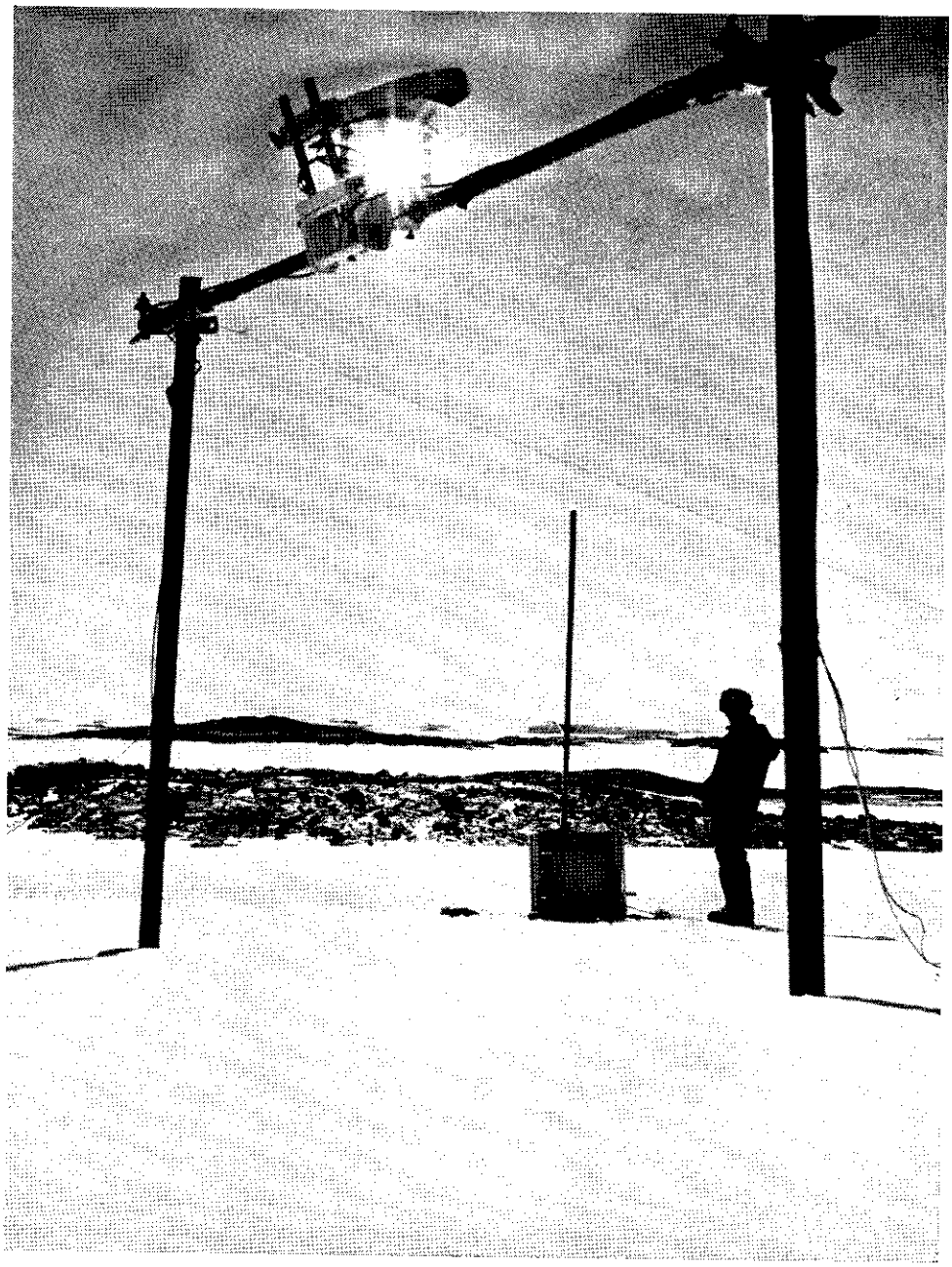

FIG. 1.1.2. Kipp solarimeter with shade-ring and net radiometer at Mawson.

In 1961 the wooden box and balloon were removed and a pair of small bellows was attached to the mast to inflate the polythene hemispheres. Frequent checks to ensure full inflation were necessary.

1.2. RECORDING EQUIPMENT

Recording of the emf output of all the instruments was by means of two Cambridge galvanometric thread recorders, one an iron case 2-channel recorder No. B684, the other an iron case single-channel recorder. Initially, these recorders were housed in a small auroral observation dome. This arrangement proved unsatisfactory when it was found that the building commenced to vibrate strongly during blizzards and the recorder trace became erratic. After their transfer to the meteorological hut, on to a more stable base, they performed satisfactorily. The distance between recorders and instruments was, however, increased to approximately 500 metres. Of the two Cambridge recorders used, the single-channel recorder measured the net flux of the long-wave and short-wave radiation at two minute intervals, and also recorded a closed-circuit zero point every two minutes. The two-channel recorder measured the global radiation on one channel and the diffuse sky radiation on the other channel. To minimize confusion between the two traces, they recorded on either side of the zero line.

The two-channel recorder recorded in the following sequence at one minute intervals:

global
global
global
global
zero
diffuse
zero
zero

Standardizing of the recorders was by means of a standardizing potentiometer using a standard cell of 1·0186V and a Multiflex galvanometer, Type MG 1. A 1·0186 volt battery potential from the potentiometer was applied across the recorder connected in series with a 1,000,000 ∽ resistance and the recorder deflection compared with the applied potential. Calibrations throughout the year showed only negligible changes in the recorder sensitivity.

The recorder sensitivity could, however, be reduced by placing a resistance in series with the recorder. Two standard post-office resistance boxes up to 500 ∽ total resistance were available for the two recorders. High resistances were used in summer and zero resistance in winter. The resistance values for instruments and cables were measured by an AVO-meter and were found to be as follows:

Kipp solarimeter No. 1 (global radn.) plus cable: 15·8 ∽

Kipp solarimeter No. 2 (diffuse sky radn.) plus cable: 15·4 ∽

Net radiometer plus cable: 25·4 ∽

The resistance of the cable alone was 4·3 ∽ connecting the solarimeters and the recorder and 4·6 ∽ connecting the radiometer and the recorder. The resistance of the two-channel recorder was 19·4 ∽ and that of the single-channel recorder 17·7 ∽. The values of the sensitivity of the recorders are shown in the table below:

TABLE 1.2.1

SENSITIVITIES OF SINGLE-CHANNEL AND TWO-CHANNEL RECORDERS, RECORDING NET AND DIFFUSE SKY AND GLOBAL RADN.

Box resistance	Sensitivity graph units/mv		
	Net	Diffuse	Global
300	3·60	8·78	9·36
200	5·08	12·50	13·34
100	8·62	21·82	23·22
40	14·86	39·25	41·70
0	28·75	84·80	89·30

Resistance values were changed on the following days in 1961:

New values (⌁) on days indicated:

Global radiation	*Diffuse sky radiation*	*Net radiation*
1. 1.61 : 300	1. 1.61 : 300	1. 1.61 : 300
14. 3.61 : 100	14. 3.61 : 100	13. 3.61 : 200
16. 5.61 : 0	23. 3.61 : 200	15. 3.61 : 100
19. 8.61 : 100	16. 5.61 : 0	16. 5.61 : 0
8.10.61 : 200	19. 8.61 : 100	3. 9.61 : 40
	5.10.61 : 200	12. 9.61 : 100
	29.11.61 : 300	24.10.61 : 200

A schematic layout of the instruments and recorders is shown in Fig. 1.2.1.

The Linke-Feussner Actinometer was only taken to the plateau during calibrations, and was normally stored in the meteorological hut. Its internal resistance was 60 ohms.

1.3. CALIBRATION OF THE INSTRUMENTS

1.3.1. The Linke-Feussner actinometer

The Linke-Feussner actinometer was calibrated by the CSIRO Division of Meteorological Physics against an Ångström compensation pyrheliometer before the expedition left in January 1961 and again after its return in March 1962. Another Linke-Feussner actinometer (Kipp and Zonen No. 60) was in use in 1962. Both instruments showed no change in the calibration constant after one year's service. The respective calibration factors were:

Linke-Feussner actinometer No. 56 : 0·146 $mVmW^{-1}$ cm^{-2}

Linke-Feussner actinometer No. 60 : 0·131 $mVmW^{-1}$ cm^{-2}

The temperature coefficient of sensitivity quoted by the manufacturers for the actinometers was —0·002/°C. The above constants are referred to 20°C. The instrument constant S at temperature T is given by the expression:

$$S_T = S_{T_0} \{1 - 0{\cdot}002\ (T - T_0)\}$$

where S_{T_0} is the instrument constant at temperature T_0. The difference between the instrument constant at the mean June temperature of —15°C and at the mean December temperature of —2°C is approximately 3%.

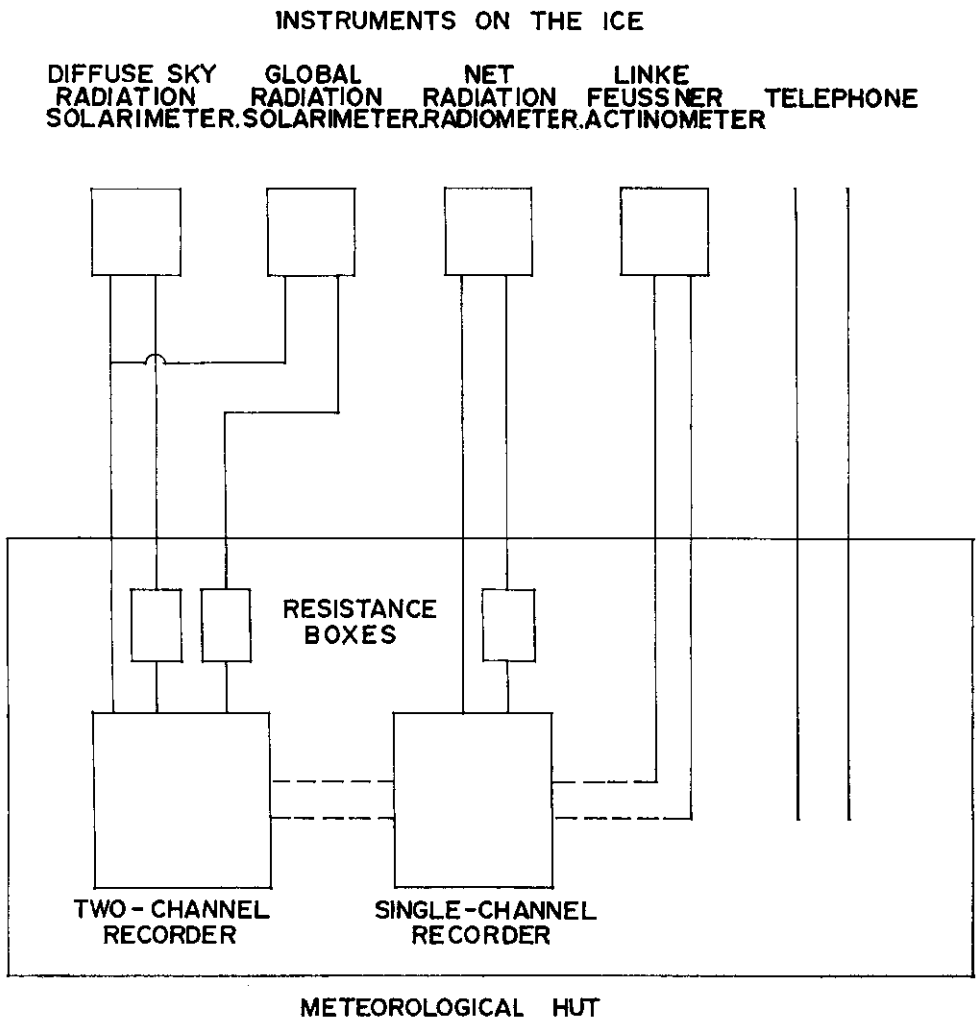

FIG. 1.2.1. Schematic layout of instruments and recorders.

1.3.2. The Kipp solarimeter No. 1

The Kipp solarimeter No. 1 (without shade ring) was calibrated by shading it with a disk fixed at a distance. The difference between the unshaded and shaded reading, being equivalent to the direct solar radiation, was compared with the reading from the Linke-Feussner actinometer pointed at the sun. The calibrations of the net radiometer were carried out in a similar fashion. The Kipp solarimeter No. 2 (with shade ring) was not calibrated independently, but against the Kipp solarimeter No. 1, with the element shaded by a small disk.

All calibrations were carried out at approximately solar noon, i.e., with approximately the same azimuthal position of the sun with respect to the orientation of the element of the instrument. Azimuthal variations of the calibration factor were thus

not obtained. No variation of the calibration factor is expected with azimuthal changes in the case of the net radiometer, due to the relatively smooth and flat surface of the radiometer element and small focussing effect of the polythene shield. The Kipp solarimeter, however, is known to be azimuth-dependent in its sensitivity. This is due to a focusing of the incident light of the inner of the glass hemispheres

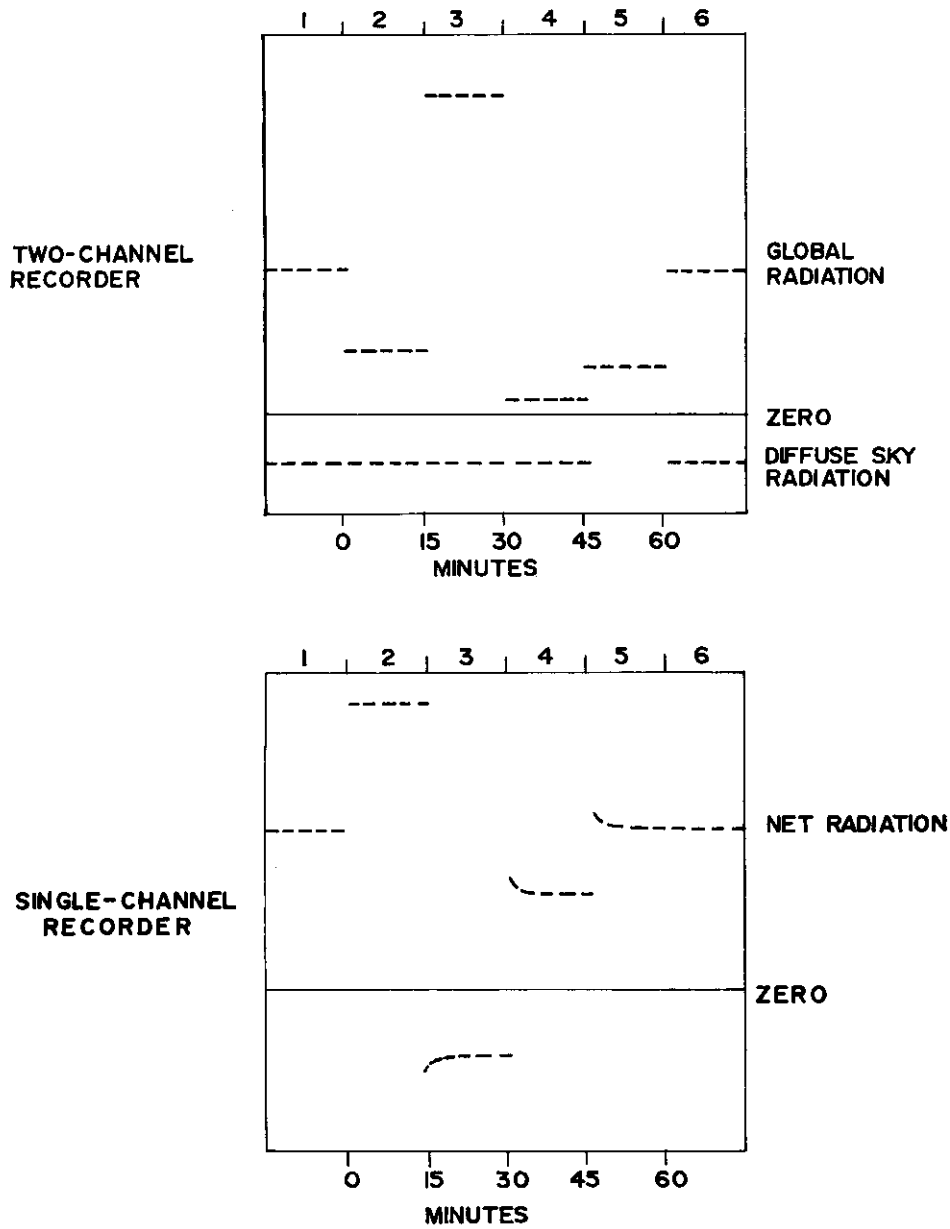

FIG. 1.3.1. Schematic diagram of the calibration procedure.

onto the element. This "Katakaustik" effect can readily be observed and has been described by Ambach (1963). The azimuth dependence also has been measured by Liljequist (1956) and others.

Since 15 minutes were allowed for the instrument to settle to the equilibrium position after or before shading, the advantage of carrying out the calibrations at solar noon was that only very small changes in solar elevation and the intensity of the direct solar radiation occurred. Changes in the instrument temperature were negligible.

A typical calibration of all the instruments used as shown by the recorder traces is shown schematically in Fig. 1.3.1.

Two-channel recorder:

1. Global radiation, Diffuse radiation } Normal recording—high recorder sensitivity
2. Global radiation —low ,, ,,
3. Linke-Feussner —low ,, ,,
4. Diffuse sky radiation (global element shaded) —low ,, ,,
5. Diffuse sky radiation (connected through "total" channel) —low ,, ,,
6. Global, Diffuse } radiation normal recording —high ,, ,,

Single-channel recorder:

1. Net radiation—normal recording —high recorder sensitivity
2. Linke-Feussner —low ,, ,,
3. "Net" element shaded —low ,, ,,
4. "Net" element unshaded —low ,, ,,
5. Net radiation—normal reading —high ,, ,,

Suitable sensitivities to give maximum recorder scale readings for all elements measured were selected by using different resistances in series with the recorders.

The screening of some diffuse sky radiation, as well as the direct solar radiation by the shading disk during calibrations, is compensated by the actinometer measuring some sky radiation, since its aperture angle is larger than the angle subtended by the solar periphery. The aperture angle of the Linke-Feussner actinometer is approximately 11°. A disk of 10 cm radius, fixed at the distance of one metre, should thus screen the same amount of sky radiation as is measured by the Linke-Feussner actinometer.

The recorder trace for the net radiometer shows some over-shooting when the radiometer is shaded or un-shaded. The radiometer thus does not reach thermal equilibrium for some minutes. In actual measurements this over-shooting effect is very small, since the shading and un-shading of the radiometer by cloud is not as abrupt as with a shading disk. The over-shooting can thus be neglected.

(a) Calibration factors for direct solar radiation. As mentioned above, the sun was screened from the solarimeter to give the diffuse clear sky radiation D. If S is

the direct solar radiation, G the global radiation and h the solar altitude, we have

$$S \sin h = G - D.$$

S and h are measured with the Linke-Feussner actinometer. $(G - D)$ corresponds to N millivolt on the recorder scale, hence,

$$\frac{N}{C} = S \sin h \quad \text{or} \quad C = \frac{N}{S \sin h},$$

where C is the calibration factor required in $mV mW^{-1}$ cm^{-2}.

The calibration factors obtained in this way are shown in Fig. 1.3.2. They are

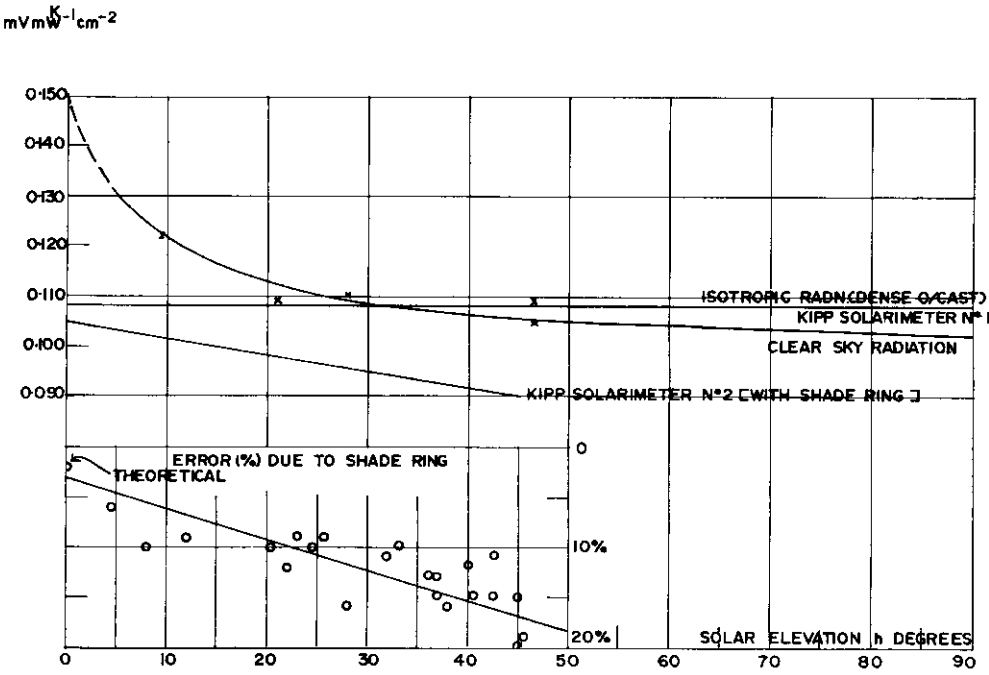

FIG. 1.3.2. Change of the calibration factors of the Kipp solarimeters with solar elevation (reduced to 20° C). Measured values at solar noon.

reduced to 20°C using a temperature coefficient of sensitivity of —0·002/°C. The calibrating factors can be seen to be higher at lower solar elevations, i.e., the instrument has an increased sensitivity at these low solar altitudes as expected from the general discussion above. Results of other calibrations to be discussed below are also shown in Fig. 1.3.2.

(b) Calibration factors for global radiation. The calibration factors determined above are only valid for the direct solar radiation on a horizontal surface. In the global radiation there is also a diffuse sky radiation component. Since this component on clear days is small, except at low solar altitudes compared with the global radiation, the calibration values for direct solar radiation were also used for global radiation. The error introduced is small.

(c) Calibration factor for isotropic radiation. The calibration curve determined above (Fig. 1.3.2) serves as a basis for the determination of the calibration factor

for diffuse sky radiation if the spatial distribution of the diffuse radiation is known. With a densely overcast sky the diffuse radiation can be considered to be practically isotropic. Designating the intensity of the radiation I and integrating the flux F over the hemisphere,

$$dF = 2\pi \cos h \; dh \; I \sin h,$$

where h is the altitude,

$$F = \frac{\pi I}{2} \int_0^{\frac{\pi}{2}} \sin 2h \, d(2h)$$

$$F = \pi I.$$

This will correspond to a reading N on the recorder. The contribution from a strip along the parallel circle h will be dN,

$$dF = \frac{1}{SK} dN = 2\pi \cos h \, dh \, I \sin h,$$

where S is the recorder sensitivity (graph unit/mV), K the clear sky calibration factor for altitude h ($mV/mW/cm^2$).

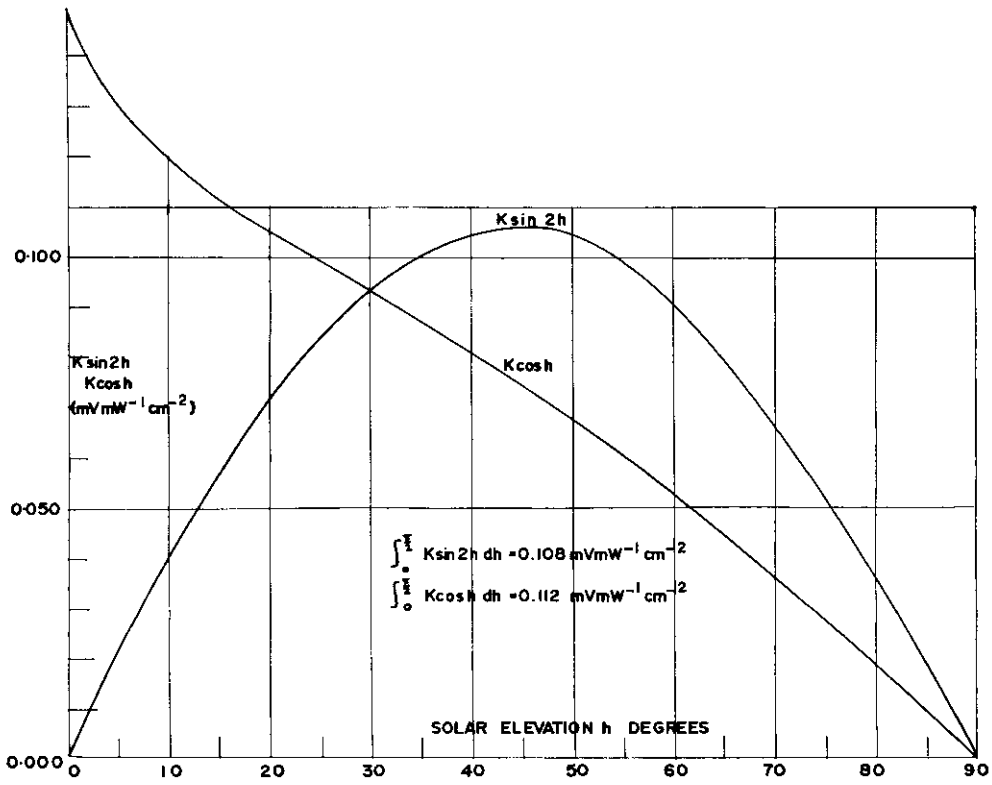

FIG. 1.3.3. Graphic determination of the calibration factors for isotropic radiation ($\int_0^{\pi/2} K \sin 2h \, dh$) and the diffuse clear sky radiation ($\int_0^{\pi/2} K \cos h \, dh$) for the Kipp solarimeter No. 1.

The relationship between K and h is given in Fig. 1.3.2,

$$N = \pi I \int_0^{\frac{\pi}{2}} SK \sin 2h \, dh.$$

If the calibration constant for isotropic radiation is K', then

$$\frac{N}{SK'} = F = \pi I$$

$$\therefore K' = \int_0^{\frac{\pi}{2}} K \sin 2h \, dh.$$

K' is obtained by graphical integration of the K sin $2h$ curve shown in Fig. 1.3.3. The integrated value is 0·108 $mV/mW/cm^2$.

(d) Calibration factor for diffuse clear sky radiation. The diffuse clear sky radiation is not isotropic but increases in intensity from the zenith to the horizon. The assumption is made by Liljequist (1956) that the intensity is proportional to the number of diffusing particles present, i.e., proportional to the air mass

$$m = \frac{1}{\sin h}.$$

This is a first approximation which will allow only rough estimates, particularly at low solar elevations.

To support this assumption, Liljequist measured the distribution of the diffuse sky radiation with a directional photometer and a blue colour filter. His measurements at 420 mμ wavelength show that his assumption is well founded down to solar altitudes of approximately 20°.

Also, using the theoretical considerations of Sekera and other investigators, summarized by Möller (1957) it can be shown that for Rayleigh-scattering, considering multiple scattering and the effect of the earth's surface albedo on the diffuse sky radiation, the distribution of the diffuse sky radiation is closely proportional to

$$\frac{1}{\sin h}$$

down to approximately 10° for a wavelength of 495 mμ. (See table 1.3.1). The values were calculated for a zenith distance of the sun of 53°, wavelength 495 mμ and a surface albedo of 80%. Measurements by Volz, (quoted by Möller (1957)) support these figures.

TABLE 1.3.1

RELATIVE DISTRIBUTION ($I_\omega d\omega = 1$) OF THE DIFFUSE SKY RADIATION IN A VERTICAL PLANE THROUGH THE SUN, WITH A ZENITH DISTANCE OF THE SUN OF 53°.

$\lambda = 495\, m\mu$, $A = 0{\cdot}8$

Altitude	Intensity		Mean Intensity	$I\lambda \sin h$
	Into sun	Away from sun	I_λ	
6·0	0·148	0·139	0·144	0·015
11·5	0·104	0·0910	0·098	0·020
23·5	0·0636	0·0496	0·057	0·023
44·5	0·0395	0·0280	0·034	0·024
90·0	0·0229	0·0220	0·022	0·022

ie., $I_\lambda \sin h$ is fairly constant down to an altitude of 10° approximately.

Taking now the intensity of the diffuse clear sky radiation in the zenith to be I, we have the intensity along a parallel circle h, $I_h = \frac{I}{\sin h}$.

D = diffuse clear sky radiation,

$$D(D) = 2\pi \cos h\, dh\, \frac{I}{\sin h} \sin h = 2\pi I \cos h\, dh$$

$$D = 2\pi I \int_0^{\pi/2} \cos h\, dh$$

$$D = 2\pi I.$$

But $D(D) = \frac{1}{SK} dN$ (as above)

$$dN = D(D)\, SK = 2\pi ISK \cos h\, dh$$

$$N = 2\pi IS \int_0^{\pi/2} K \cos h\, dh.$$

But $D = \frac{N}{SK'}$,

where K' is the calibration constant for diffuse clear sky radiation;

$$K' = \int_0^{\pi/2} K \cos h\, dh.$$

K' is again obtained by graphical integration of the $K \cos h$ curve shown in Fig. 1.3.3 and has magnitude 0·112 $mV/mW/cm^2$. Both these integrals were originally applied by Liljequist (1956).

(e) Calibration factors for a broken cloud cover. Calibrating an instrument under rapidly changing conditions is difficult, and no satisfactory technique is available. An approximation to the calibration factor under these conditions can be obtained when the mean value between the factor for direct solar radiation and for a completely overcast sky, is used. The latter factor has been shown above to depend on the change of the direct solar radiation constant with solar elevation. If this change is small, i.e., the deviation from a cosine response of the instrument is negligible, then the difference between the factor for clear sky and overcast sky is small. This does not mean, however, that there cannot be large differences between these two factors, particularly at low solar height.

Table 1.3.2 below shows all the calibration factors obtained for the Kipp solarimeter No. 1.

TABLE 1.3.2

CALIBRATION FACTORS FOR THE KIPP SOLARIMETER NO. 1
($mV\ mW^{-1}\ cm^{-2}$)

Clear sky	Overcast sky	Diffuse clear sky radiation	Broken cloud cover
Fig. 1.3.2	0·108	0·112	Mean between Fig. 1.3.2 and overcast sky

To show how the calibration factors change with season, the relationship between the daily noon height of the sun and the calibration factors from above

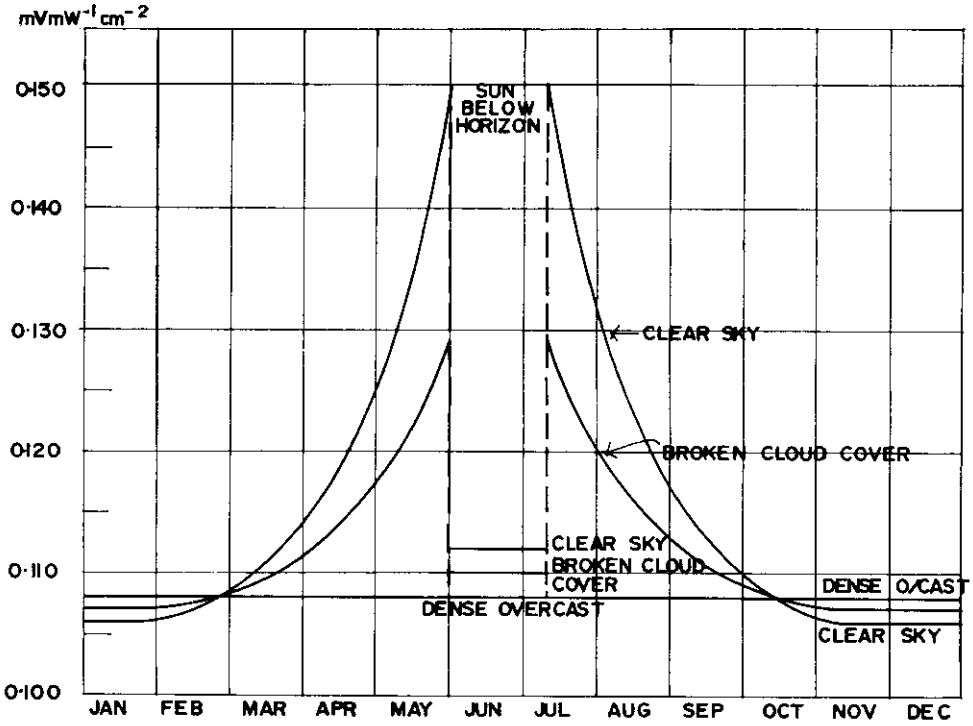

FIG. 1.3.4. The calibration factors of the Kipp solarimeter No. 1 at Mawson at noon for different cloud conditions of the sky throughout the year (reduced to 20°C).

was used. Fig. 1.3.4 shows the calibration factors with the sun above and below the horizon for clear sky, overcast sky and a broken cloud cover. For any of these conditions the calibration factor to be used with the Kipp solarimeter No. 1 can be read off directly for any day of the year.

1.3.3. The Kipp solarimeter No. 2

This instrument was calibrated against the Kipp solarimeter No. 1 during overcast conditions. The readings of the two solarimeters were compared under these conditions, and the corrections obtained due to the shade-ring are thus valid for isotropic radiation. The results of these comparisons are shown in the inset of Fig. 1.3.2. The corrected calibration values are also shown in Fig. 1.3.2. It can be seen that the error due to the shade-ring is a function of the noon elevation of the sun, i.e., the inclination of the shade ring to the horizontal. The point marked "theoretical" was obtained using the plotted function $k \sin 2h$ in Fig. 1.3.3 of the Liljequist integral for isotropic radiation, and assuming the shade-ring horizontal, half of its area screening the upper hemisphere. From the plotted distribution of the isotropic radiation the amount screened from the solarimeter element can be found to be approximately 2%.

It is obvious that due to a different sky radiation distribution with clear-sky conditions, the above factors are not valid for clear skies. Without having direct values, the problem of determining correct calibration values from available data seems fairly complex and an attempt at the solution is probably not justified here.

The above constants were therefore used also for clear-sky conditions. Schüepp, as quoted by Möller (1957), gives the error due to screening by a shade-ring as 8 to 10% with a clear sky and 5% with an overcast sky. The error due to the shade-ring would thus seem to be somewhat higher for clear sky conditions.

1.3.4. The net radiometer

The polythene domes of the net radiometer are transparent to radiation between 0·4 and 100 μ and have only narrow absorption bands at 3, 5, 6·9 and 13·7 μ. These coincide with the strong absorption bands of water vapour and carbon dioxide, where almost no radiation exchange exists between the atmosphere and the Earth's surface (Möller 1957). Polythene domes are thus ideally suited for use in all-wave net radiometers. Calibrations using both the diffuse long-wave and the mainly directional short-wave radiation are however necessary in all-wave instruments.

The long-wave calibration of the net radiometer used at Mawson was carried out by the CSIRO Division of Meteorological Physics, using cavity radiation (Funk 1959). It was found that the instrument was 4% less sensitive in the long-wave than in the short-wave region. This was attributed mainly to the lower absorption of the blackened element in the long-wave region. To obtain equal sensitivities for short and long-wave radiation, a later modification of the instrument has two diagonal white lines painted on the blackened element to reduce the short-wave absorption, but leaves the long-wave absorption unaltered.

The short-wave calibrations with direct solar radiation were carried out in the same fashion as for the Kipp solarimeter by shading and un-shading the element of the instrument.

In addition, calibrations at normal incidence of the solar radiation were also carried out by pointing the radiometer at the sun by means of a diopter. The results of these calibrations are shown in Fig. 1.3.5, reduced to 20°C by using a temperature co-efficient of sensitivity of $+0{\cdot}001/°C$.

Ambach (1963) has shown that in a similar instrument to the one used by the author, scattering of the incident direct solar radiation by the polythene shield changed the calibration factor considerably at different incidence angles. Due to a higher ratio of scattered to direct radiation at high incidence angles, an apparent increase in the sensitivity of the instrument resulted. The exact opposite of this effect was observed with the instrument used by the author, i.e., a decrease of sensitivity at high incidence angles, which is attributed to increased reflection of short-wave radiation due to the imperfection of the blackening of the surface. The scattering by the shield must thus produce a smaller effect than the reflection from the element at high incidence angles.

Scattering by the shield was, however, observed directly in another way. It was noticed that, after exposure of the instrument in heavy drifting snow and high winds, severe scratching of the polythene shield by the snow particles occurred.

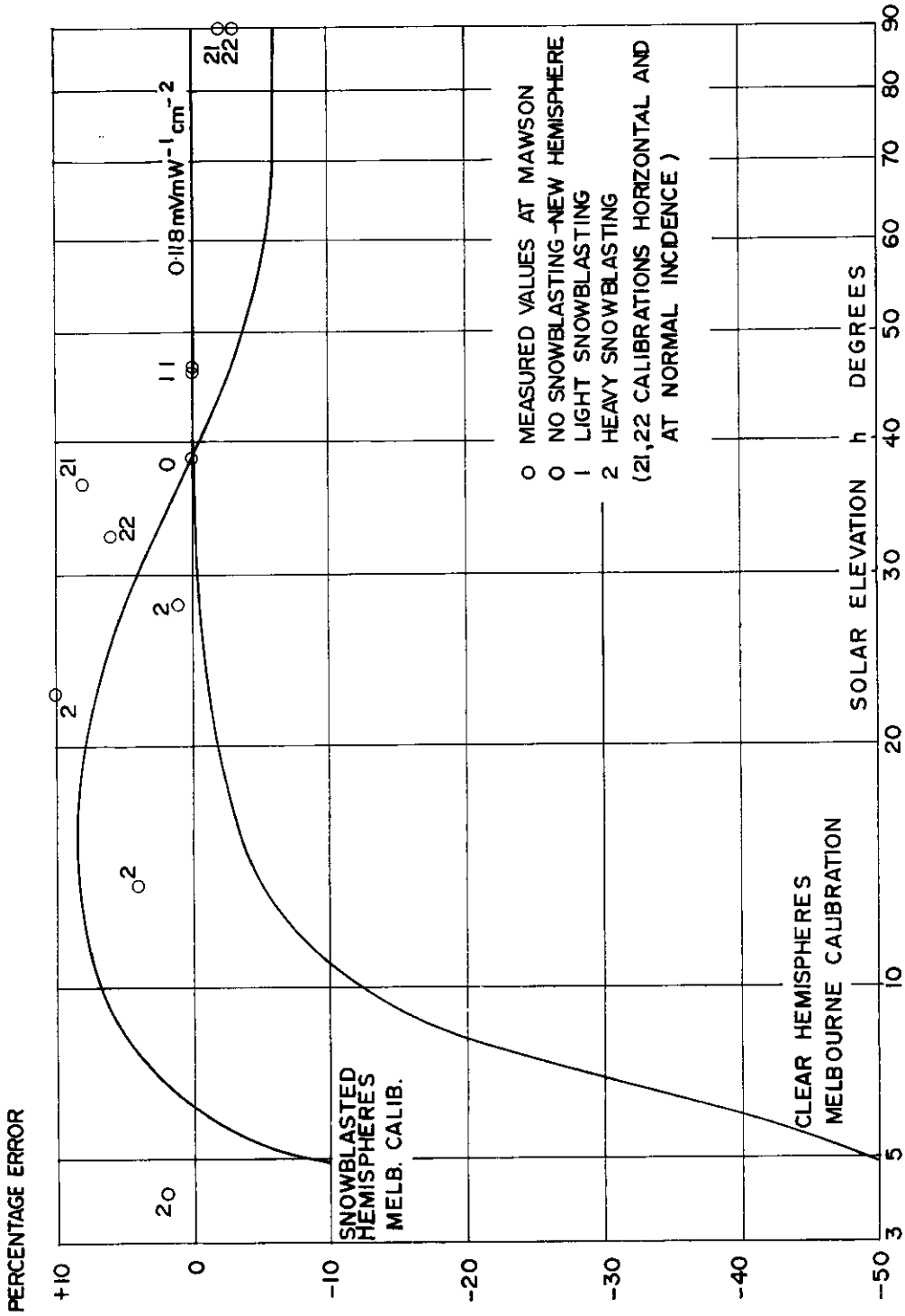

FIG. 1.3.5. Percentage error of a CSIRO net radiometer with the change of the incident angle of a direct beam.

This "snow-blasting" damaged both the upper and lower heimspherical shields over areas shown in Fig. 1.3.6.

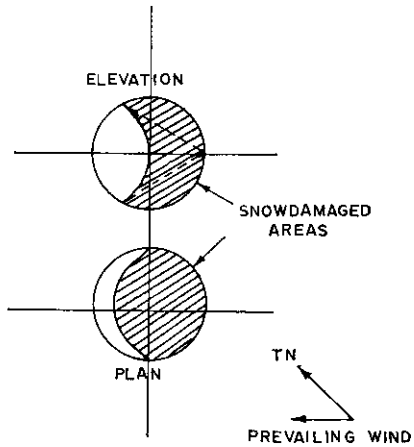

FIG. 1.3.6. Orientation of the net radiometer and extent of snow-blasting effect.

The alignment of the axis of the instrument i.e., the supporting rod of the radiometer, was parallel to the prevailing wind at Mawson, S.E.

Scattering from the inside of the upper hemisphere on to the blackened surface would occur when the solar elevation was less than 30° and give rise to an increased sensitivity. Alternatively, scattering from the outside of the shield would occur at normal incidence of the solar radiation, resulting in a decreased sensitivity.

This effect was clearly shown in a calibration carried out by the author at Melbourne University. Two radiometers, one fitted with clear, the other with snow-blasted hemispheres, were simultaneously shaded with small disks, then unshaded at regular intervals. The output emf's measured with a millivoltmeter were compared with the output emf from a Linke-Feussner actinometer pointed at the sun. The results are shown in Fig. 1.3.5 and can be seen to agree fairly well with the calibration points obtained at Mawson. These calibration points obtained at Mawson can in fact be interpreted to indicate the degree of snow-blasting which the hemispherical shields underwent. A visual, subjective comparison of the different degrees of snow-blasting incurred provided the labels "clear", "light" and "heavy" snow-blasting attached to all calibration points.

Using the integrals for isotropic and diffuse clear sky calibration factors from above, the following deviations from the clear sky constant with the sun in the zenith are obtained:

	Clear hemispheres	Snow-blasted hemispheres
Isotropic radiation	— 1·7%	—1·2%
Diffuse clear sky radiation	—10·5%	—4·2%

The functions of these integrals are shown in Fig. 1.3.7. The final calibration factors for clear sky, overcast sky and a broken cloud cover are given in Fig. 1.3.8.

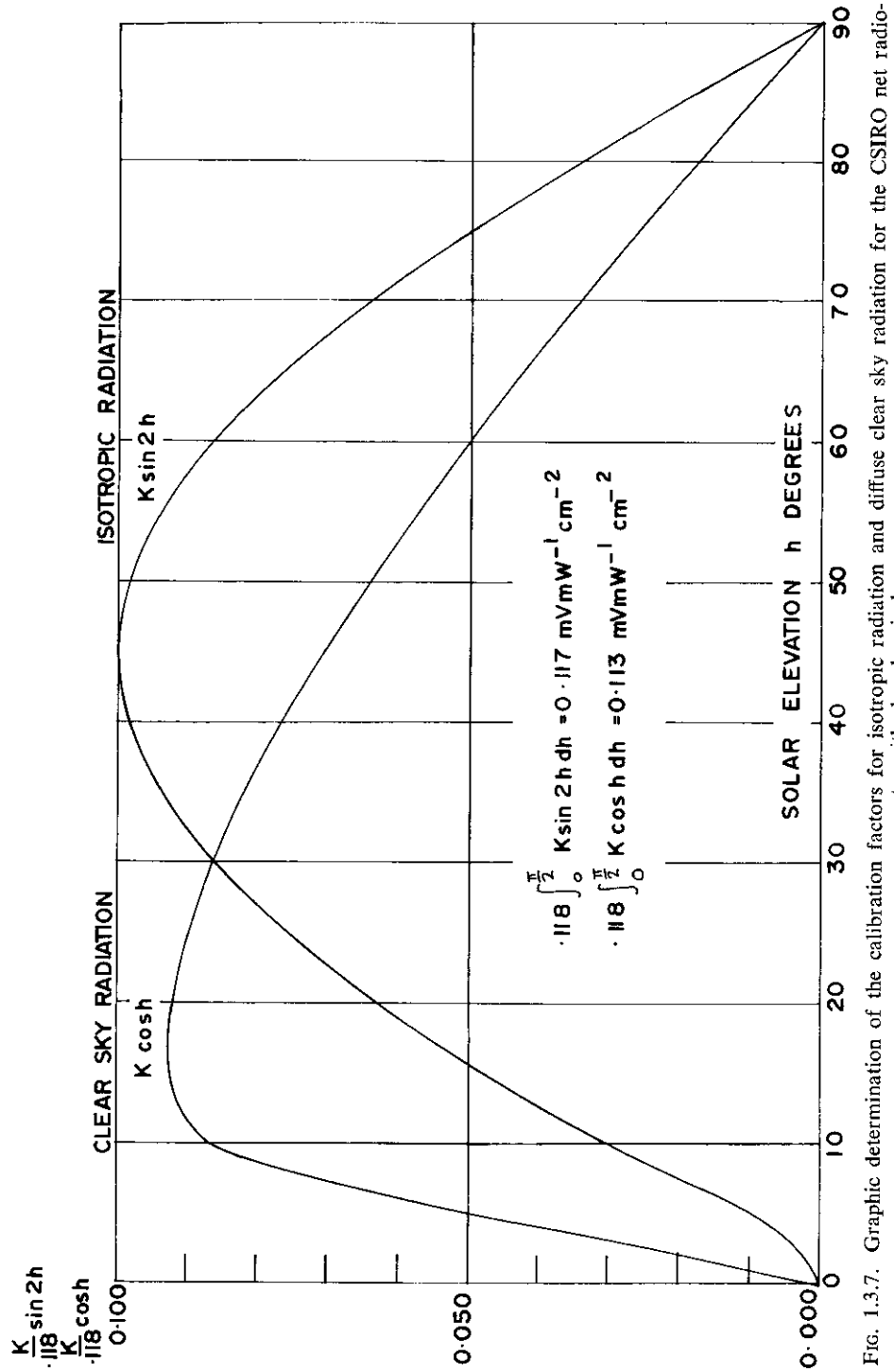

FIG. 1.3.7. Graphic determination of the calibration factors for isotropic radiation and diffuse clear sky radiation for the CSIRO net radiometer with clear hemispheres.

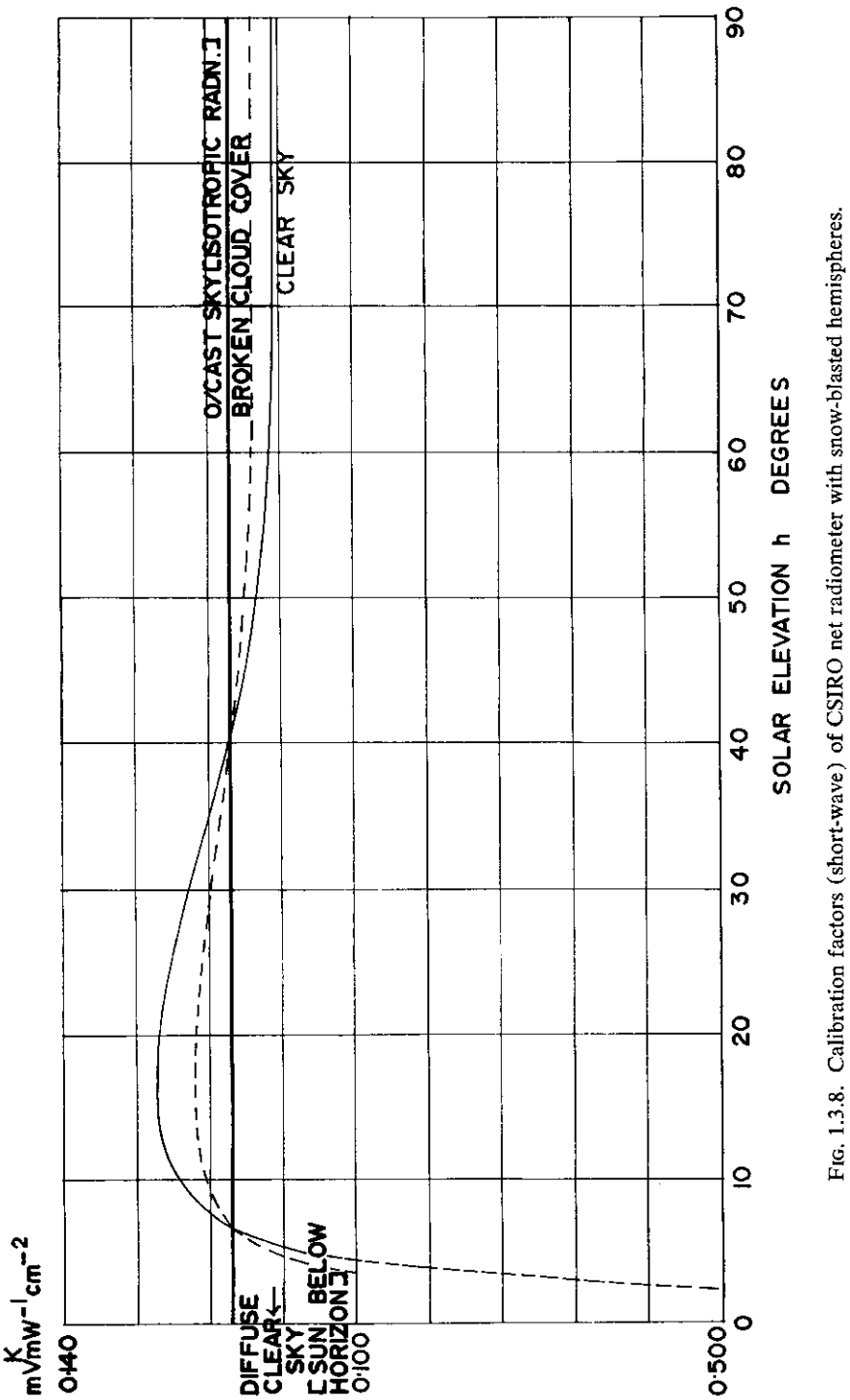

FIG. 1.3.8. Calibration factors (short-wave) of CSIRO net radiometer with snow-blasted hemispheres.

1.4. METHOD AND ACCURACY OF DATA REDUCTION

It is obvious that, with the multiplicity of correction factors that have to be used to obtain meaningful and correct data, the data reduction process must be very complex. Alternatively, if lower accuracy can be accepted, it can be rather more straightforward and brief. The problems involved in a correct reduction of the data, based on the calibration results from above, may be summarized as follows:

1. Direct integration by planimeter, or other means, of the solar radiation for periods of direct sunshine is not possible since this
   (a) neglects the dependence of the calibration factor on the solar elevation;
   (b) neglects the dependence of the calibration factor on the azimuth of the sun;
   (c) neglects the change in the calibration factor with the temperature.

2. The net flux of short-wave and long-wave radiation must be split up into a short-wave and long-wave component, since the calibration factors for the short-wave component is different from that of the long-wave component.

3. In principle, it is not possible to measure the net flux of radiation with the instrument used, since the calibration factor of the element facing upwards depends on the solar elevation, whereas the element facing downwards does not.

4. The calibration factor will change with the degree of damage to the instrument by drifting snow. This does not increase linearly with time but depends on the frequency of periods with drifting snow.

5. When measuring the albedo with direct sunshine, the calibration factor with the instrument facing upwards is different from the calibration factor with the instrument facing downwards.

a. Solarimeter No. 1. The reduction of the data obtained with the Kipp solarimeter No. 1 (without the shade ring) proceeded in the following way:

The calibration factor at solar noon (12 a.m. L.A.T. (local apparent time)) was taken from Fig. 1.3.4 for clear sky, overcast or broken cloud conditions as applicable. Clear sky values were used when the cloud cover was equal or less than one-eighth all day; overcast values when the cloud was equal or more than seven-eighths all day. Broken cloud values were used for all other days. A temperature correction using the mean monthly temperature was applied to the calibration factor. The integration of the global radiation using this corrected factor was carried out for each day.

A precise error estimate is difficult. The largest error will presumably be introduced when a broken cloud cover is assumed, and the calibration constant can be anywhere between that for isotropic radiation and direct clear sky solar radiation. Since the radiation intensity at low solar elevations is small, the effect of changes in the calibration factor, due to height and azimuth changes from solar noon, will also be small. The effect of diurnal temperature changes on the calibration factor will be negligible.

b. Solarimeter No. 2. The calibration constant of this instrument depended on the inclination of the shade ring to the horizontal. Since the ring was always carefully adjusted, the inclination was determination in relation to the solar elevation at noon L.A.T. The solar elevation at local apparent noon was determined from:

$$h = 90 - \phi + \delta$$

(h = solar elevation, ϕ = latitude, δ = declination)

The corresponding calibration factor was taken from Fig. 1.3.2, and a temperature correction using the mean monthly temperature was applied. Since the calibration factors of Fig. 1.3.2 were obtained with overcast skies, they obviously are not applicable for clear-sky conditions when the spatial distribution of the radiation flux will not be isotropic. The value of 2 to 3% quoted above gives an indication of the order of magnitude of the expected error.

c. Net radiometer. The change of the calibration factor with solar height was accounted for in the same fashion as with the solarimeter. Since the change of the calibration factor occurs at lower solar elevations than with the solarimeter, i.e., is negligible above $h = 20°$, the error introduced is smaller. An error is, however, introduced through the upward-facing element having a different calibration factor than the downward-facing element, since the first depends on solar elevation and the latter does not. The temperature correction is smaller, since the temperature coefficient of the radiometer is only half that of the solarimeter. No azimuth error occurs.

The difference between the calibration factor for short-wave and long-wave radiation, although only 5%, introduces a diurnal variation in the calibration factor for the all-wave measurement of the net flux of radiation. This is in addition to the variation of the calibration factor with solar altitude, and is based on the diurnal change of the ratio of short-wave to long-wave radiation. Since this ratio is zero at night, the long-wave calibration factor was used for all measurements of a net outgoing radiation from the snow surface. The change from net incoming to net outgoing radiation occurred between 0° and 15° solar elevation as shown in Section 7. The error introduced by this method is presumably small, since the short-wave incoming radiations must be small at zero net radiation and with a mean albedo of the ice surface of 70%. During the daytime, with net incoming radiation the short-wave calibration factor was used since the short-wave radiation is considerably larger than the long-wave radiation.

There is considerable difference between the calibration factors of the instrument with clear and snowdrift-damaged hemispheres, particularly at low solar elevations. The hemispheres must have been damaged as a rule soon after installation, since rarely a week passed at Mawson during 1961 without some snowdrift at the instrument level. In fact, under the circumstances it is advisable, rather than changing the hemispheres frequently, to change them only every two months, say, as it was done at Mawson in 1961. The calibration factor for snow-damaged hemispheres was used throughout.

An estimate of the final error in the deduced values of the radiation fluxes cannot thus be given readily. The errors inherent in the instruments used to measure the radiation fluxes have been indicated above. In addition, errors in the recording instruments such as an inaccurate time-scale, zero error of the galvanometer and a large time-constant may be present.

Finally, errors may occur in the integration. The 1961 data was digitized with a mechanical digitizer of the CSIRO Division of Meteorological Physics. Integration

of the daily values of the radiation fluxes was with the CSIRAC Electronic Computer of Melbourne University. The errors in the integration can be assumed to be small and mainly due to the digitizing process. The error due to the integration of the 1962 data was presumably higher, since the integration was done by means of a planimeter at Mawson during 1962.

Despite the care taken with the measurements and the data reduction, it cannot be claimed that the overall accuracy of the measured daily radiation totals is higher than the $\pm$ 5% quoted by Nicolet, at the beginning of this paper.

2. DURATION OF SUNSHINE

2.1. THEORETICAL DETERMINATION OF THE SOLAR ALTITUDE

Theoretical values of the time-solar elevation relationship throughout the year had to be deduced. This was done using the equation

$$\sin \nu = \sin \phi \sin \delta + \cos \phi \cos \delta \cos t$$

where ϕ = latitude
δ = declination
t = hour angle of the sun

A chart was constructed using cos t as abscissa and sin ν as ordinate, giving a linear relationship for these two parameters for a constant latitude and declination. Values of the declination were taken from the 1961 Nautical Almanac for 08 G.M.T., corresponding closest to solar noon at Mawson, and neglecting the change in declination during the day. Declination values were taken at five-day intervals throughout the year and a series of straight lines were drawn, giving the solar elevation at any time of the day and the year to 0·1° accuracy.

A correction for atmospheric refraction was applied, using a standard refraction table in Linke's Taschenbuch (Linke 1953) and extrapolating to zero degrees apparent solar elevation. The refraction there was taken to be 40′ at —15°C, 37′ at 0°C. This value may in actual fact be somewhat higher in the Antarctic, since pronounced inversions are generally present throughout the year. To calculate the duration of sunshine, a profile of azimuth and elevation of the horizon had to be measured and appropriate refraction values had to be applied. This profile is shown in Fig. 2.1.1 and also on the cos t vs sin ν chart, (Fig. 2.1.2) and its application is explained below.

2.2. DURATION OF SUNSHINE AT MAWSON, 1957-1963

The duration of sunshine was recorded as part of the routine metcorological observations to obtain climatological data. The duration of sunshine indicates the effective screening of the sun by clouds, and hence the depletion of the direct solar radiation incident on the surface of the earth. If a relationship between the daily insolation and the relative duration of sunshine can be established for a particular region, then the insolation in periods when only the duration of sunshine was recorded, can be obtained. This applies for example for Mawson, where the duration of sunshine has been recorded since 1957; accurate insolation values are, however, only available for the period between 1961 and the present date.

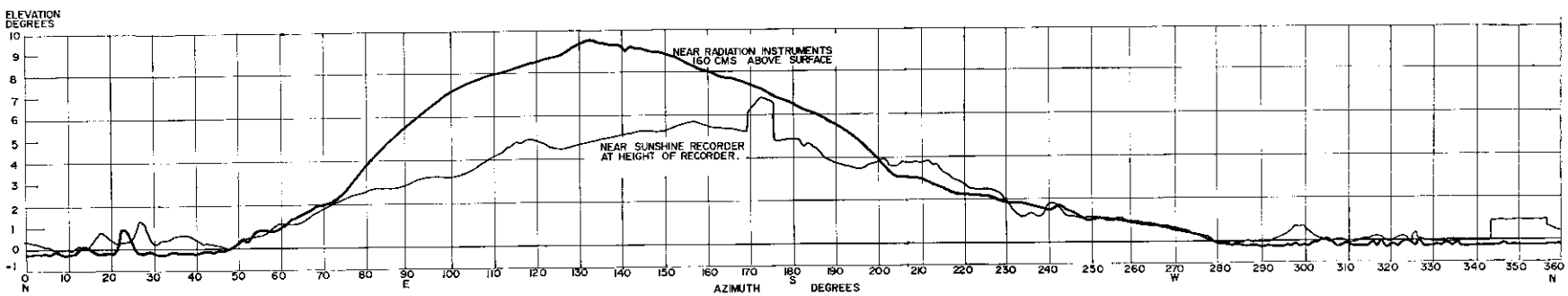

FIG. 2.1.1. Horizon at Mawson (measured on 24 November 1963).

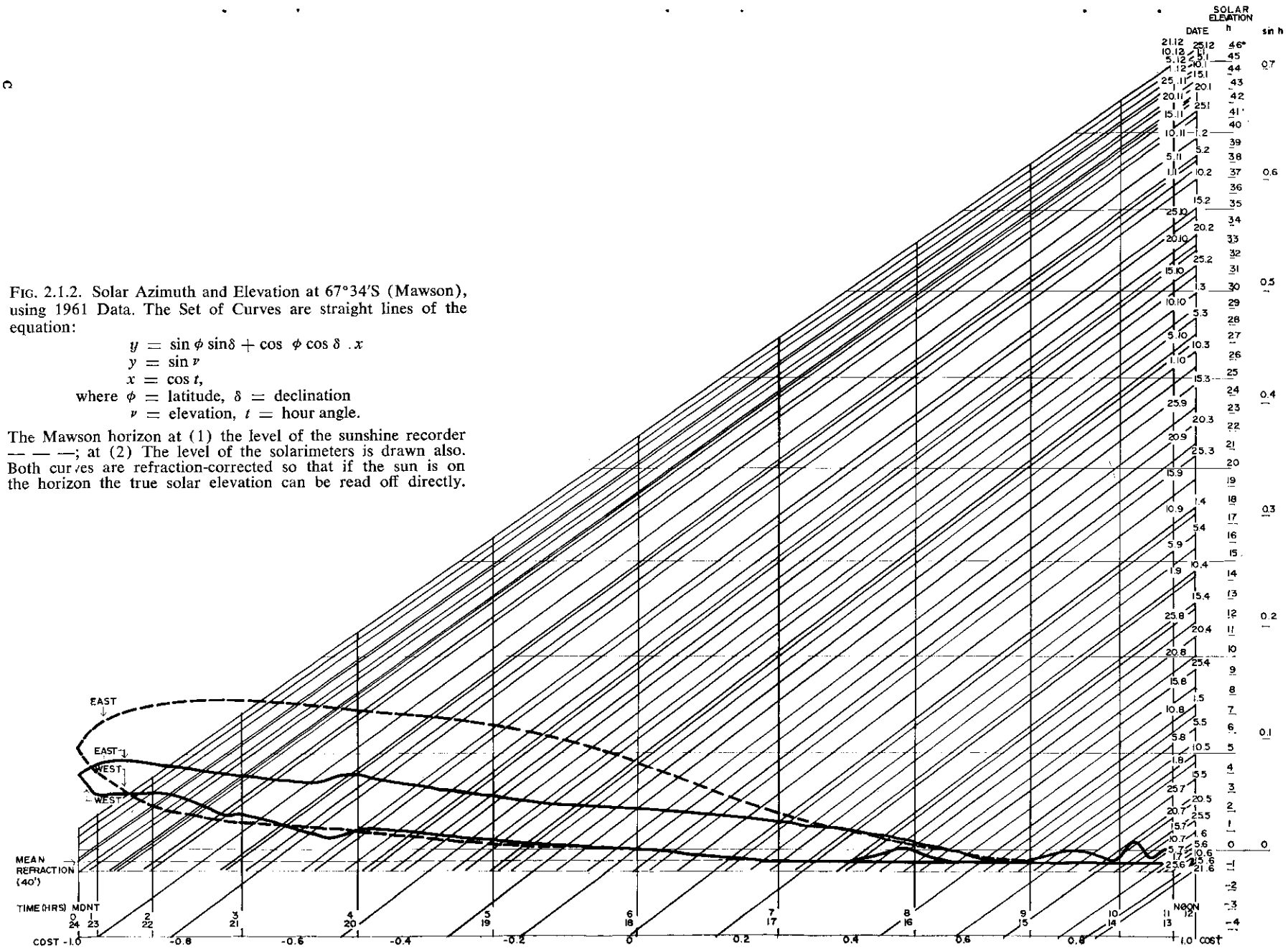

FIG. 2.1.2. Solar Azimuth and Elevation at 67°34′S (Mawson), using 1961 Data. The Set of Curves are straight lines of the equation:

$$y = \sin\phi \sin\delta + \cos\phi \cos\delta \, . x$$
$$y = \sin\nu$$
$$x = \cos t,$$

where ϕ = latitude, δ = declination
ν = elevation, t = hour angle.

The Mawson horizon at (1) the level of the sunshine recorder — — —; at (2) The level of the solarimeters is drawn also. Both curves are refraction-corrected so that if the sun is on the horizon the true solar elevation can be read off directly.

The duration of bright sunshine was recorded by an unmodified Campbell-Stokes glass-sphere sunshine recorder. Due to the shading effect of the ice plateau which has an elevation of approximately 8° south of the instrument, the duration of sunshine recorded is the correct value of the instrument site, but not necessarily that of its surroundings. The maximum duration of sunshine measured was 18·7 hours in midsummer. Due to screening of the sun's path by the elevated horizon, the expected 24 hours of sunshine for a flat horizon in midsummer were thus not recorded and modification to the instrument to record 24 hours of sunshine was unnecessary. The cards were read in the standard manner set out by the Commonwealth Bureau of Meteorology (1954) to 0·1 hours.

The instrument performed satisfactorily; hoar-frost deposition on the glass ball was not observed.

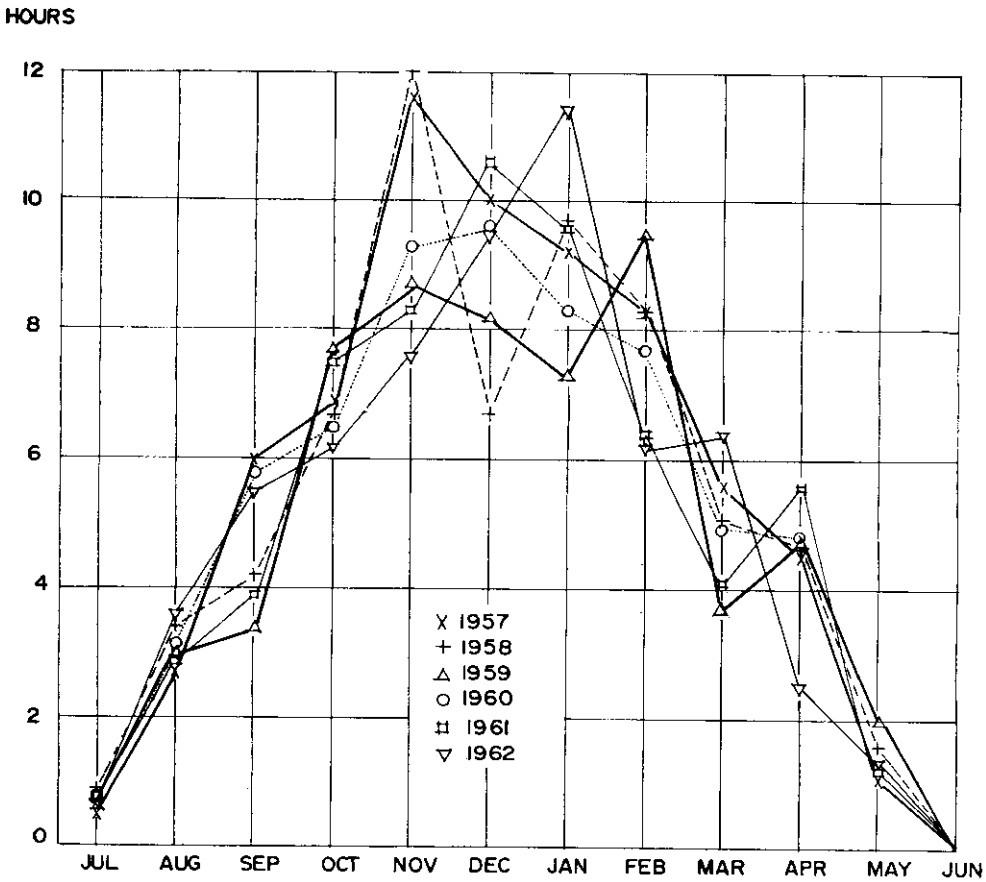

FIG. 2.2.1. Average daily hours of sunshine at Mawson (monthly means).

Fig. 2.2.1 gives the average daily hours of bright sunshine for each month measured from January 1957 to January 1963. The possible number of hours of bright sunshine with an unobstructed horizon, represented as a smooth curve in Fig. 2.2.2, was calculated from

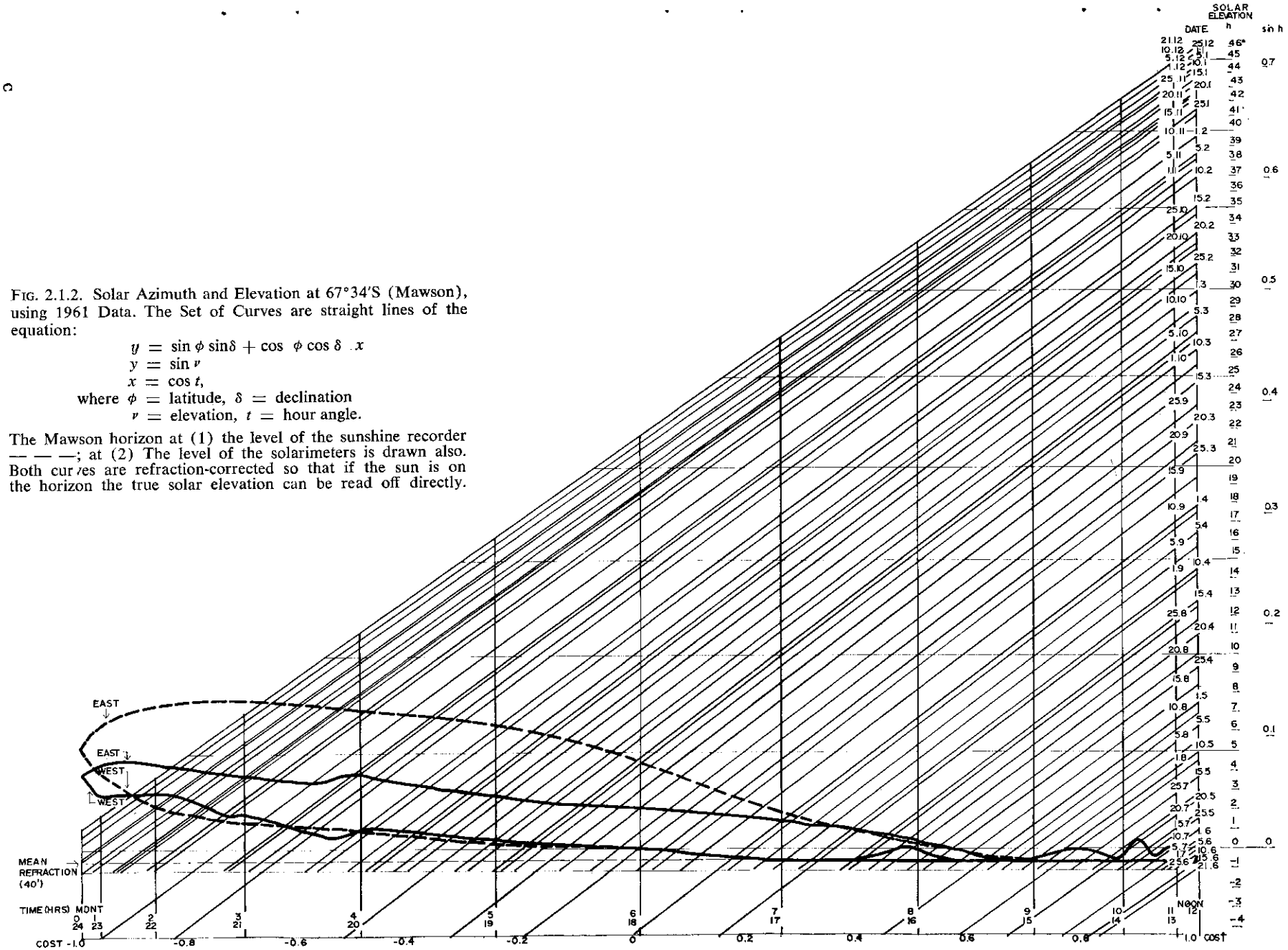

FIG. 2.1.2. Solar Azimuth and Elevation at 67°34'S (Mawson), using 1961 Data. The Set of Curves are straight lines of the equation:

$$y = \sin\phi \sin\delta + \cos\phi \cos\delta \, x$$
$$y = \sin\nu$$
$$x = \cos t,$$

where ϕ = latitude, δ = declination
ν = elevation, t = hour angle.

The Mawson horizon at (1) the level of the sunshine recorder — — —; at (2) The level of the solarimeters is drawn also. Both curves are refraction-corrected so that if the sun is on the horizon the true solar elevation can be read off directly.

The duration of bright sunshine was recorded by an unmodified Campbell-Stokes glass-sphere sunshine recorder. Due to the shading effect of the ice plateau which has an elevation of approximately 8° south of the instrument, the duration of sunshine recorded is the correct value of the instrument site, but not necessarily that of its surroundings. The maximum duration of sunshine measured was 18·7 hours in midsummer. Due to screening of the sun's path by the elevated horizon, the expected 24 hours of sunshine for a flat horizon in midsummer were thus not recorded and modification to the instrument to record 24 hours of sunshine was unnecessary. The cards were read in the standard manner set out by the Commonwealth Bureau of Meteorology (1954) to 0·1 hours.

The instrument performed satisfactorily; hoar-frost deposition on the glass ball was not observed.

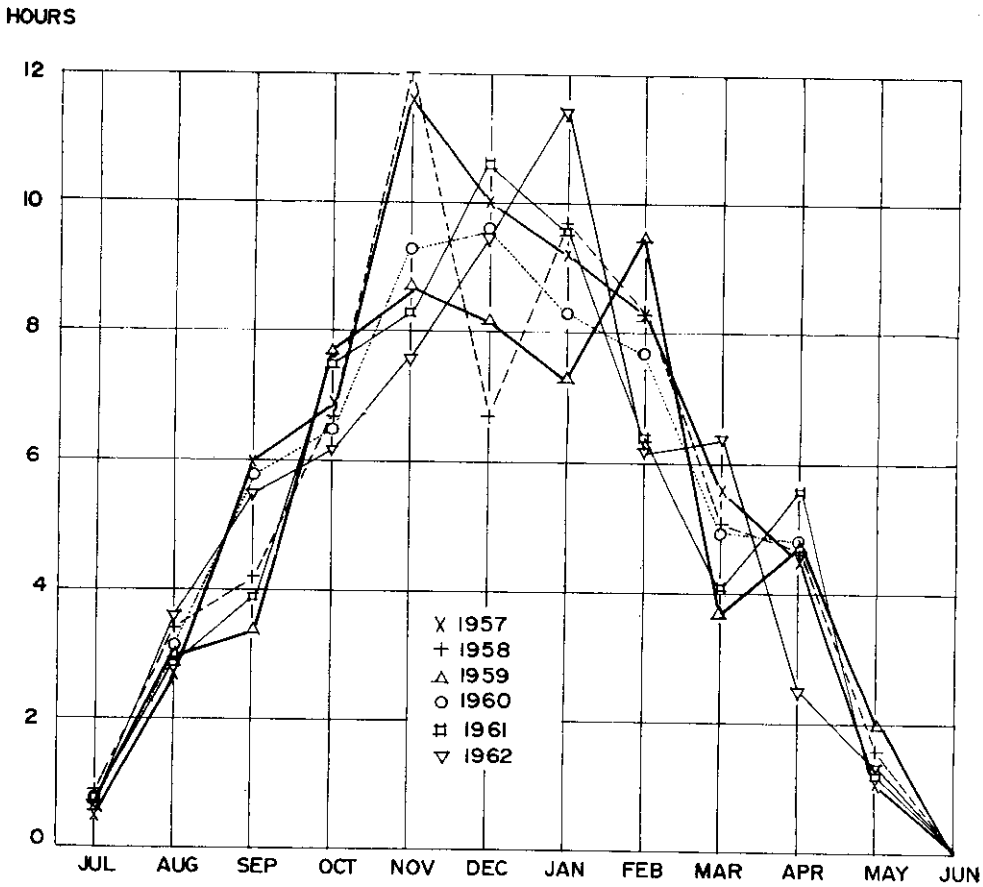

FIG. 2.2.1. Average daily hours of sunshine at Mawson (monthly means).

Fig. 2.2.1 gives the average daily hours of bright sunshine for each month measured from January 1957 to January 1963. The possible number of hours of bright sunshine with an unobstructed horizon, represented as a smooth curve in Fig. 2.2.2, was calculated from

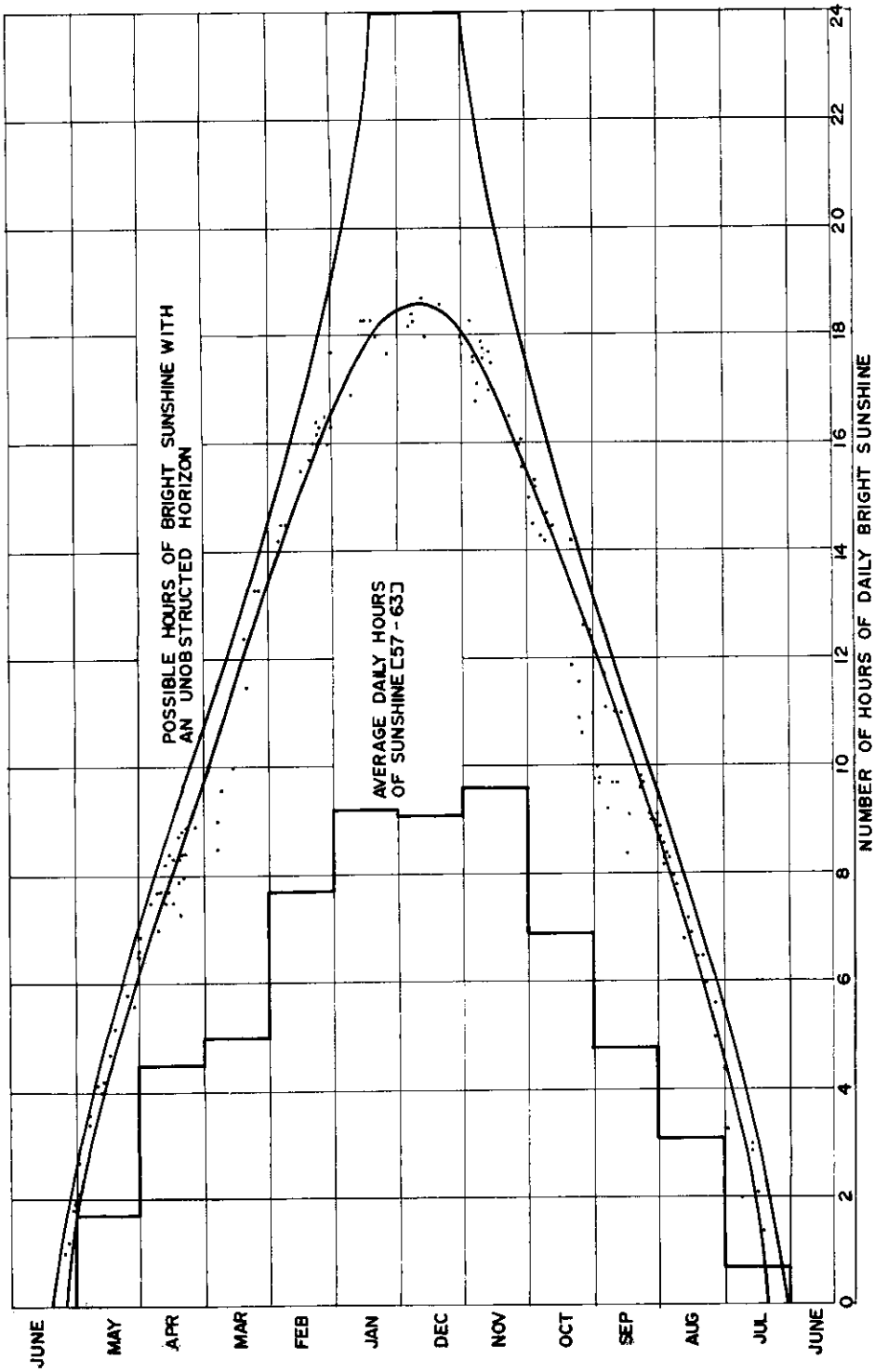

FIG. 2.2.2. Observed values of hours of bright sunshine on days with less than one-eighth cloud all day (January 1957 to January 1963), shown as dots, and average daily hours of sunshine.

$$\cos t_o = -\tan \phi \tan \delta$$

A correction for atmospheric refraction was applied as discussed above. Table 2.2.1 below gives the average monthly values of the duration of sunshine.

TABLE 2.2.1

DURATION OF SUNSHINE AT MAWSON

Year	Jan.	Feb.	Mar.	Apr.	May	Jun.	Jul.	Aug.	Sep.	Oct.	Nov.	Dec.
1957	9·2	8·3	5·6	4·5	1·1	0	0·5	2·7	6·0	6·9	11·6	10·0
1958	9·7	8·3	5·1	4·7	1·6	0	0·9	3·4	4·2	6·7	12·0	6·7
1959	7·3	9·5	3·7	4·7	2·0	0·1	0·6	3·0	3·4	7·7	8·7	8·2
1960	8·3	7·7	5·0	4·8	2·0	0	0·6	3·3	5·8	6·5	9·3	9·6
1961	9·6	6·4	4·1	5·6	1·2	0·1	0·8	2·9	3·9	7·5	8·3	10·6
1962	11·4	6·2	6·4	2·5	1·3	0	0·7	3·6	5·5	6·2	7·6	9·5
1963	9·1											

The average number of hours of daily sunshine for the total period above is 5·2 hours.

Fig. 2.2.2 shows the number of hours of daily sunshine measured by the sunshine recorder on days when there was less than one-eighth of cloud all day. A smooth curve is drawn through these observation points and the relative sunshine, i.e., observed values divided by the smoothed observed values on days with no cloud is calculated for the period January 1957 to January 1963.

The values for the relative duration of sunshine give an idea of the extent of cloudiness shown below (Fig. 2.2.3 and table 2.2.2).

There are two peaks of high relative duration of sunshine: in November and April. November also has the highest duration of sunshine throughout the year and is, as has also been found in other parts of Antarctica, the climatically most pleasant time of the year. (Rusin (1961) has summarized the degree of cloudiness at 21 Antarctic stations; see also Table 2.2.3 below.) Before the winter commences, there is another period of high values of relative duration of sunshine in April. The

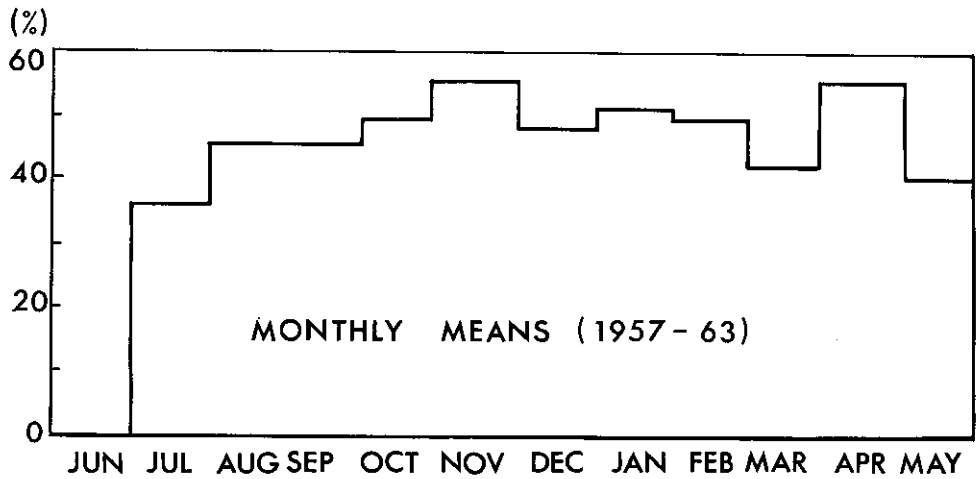

FIG. 2.2.3. Relative duration of sunshine (%) monthly means (January 1957 to January 1963).

TABLE 2.2.2

MONTHLY MEANS OF RELATIVE DURATION OF SUNSHINE (%) AT MAWSON
(Jan. '57—Jan. '63)

	Jan.	Feb.	Mar.	Apr.	May	Jun.	Jul.	Aug.	Sep.	Oct.	Nov.	Dec.
Duration of sunshine	17·8	15·1	11·7	7·9	4·1	0·2	1·9	6·8	10·5	13·8	16·9	18·5
Possible maximum duration of sunshine	9·2	7·7	5·0	4·5	1·7	0	0·7	3·1	4·8	6·9	9·6	9·1
Relative duration of sunshine (%)	52	51	43	57	42	0	37	46	46	50	57	49

distribution of sunshine is, however, fairly uniform throughout the year. The amount of direct sunshine received at Mawson is relatively high and the stretch of coast, on which Mawson lies, is perhaps justly referred to as the "Riviera of the Antarctic". Table 2.2.3 shows this best where the amount of cloudiness at various coastal stations in eastern Antarctica is given. The data for Mirny, Oazis, Wilkes and Lasarev is taken from Rusin (1961); the Davis data from the ANARE report on Meteorology (1961).

These values of the amount of cloudiness at various coastal stations (Table 2.2.3) compare with much smaller values (2 to 4-tenths mean annual) at the inland stations at Komsomolskaya, Vostok and Sovjetskaya (Rusin 1961) and high values (approximately 8-tenths at stations on the Graham Peninsula (Rusin 1961).

TABLE 2.2.3

AMOUNT OF CLOUDINESS AT VARIOUS COASTAL STATIONS IN EASTERN ANTARCTICA
(cloud amount in tenths)

	Jan.	Feb.	Mar.	Apr.	May	Jun.	Jul.	Aug.	Sep.	Oct.	Nov.	Dec.	Year
Mawson 1957-61	6·2	5·9	6·0	4·6	4·9	5·2	5·4	5·4	5·3	5·8	5·7	6·2	5·5
Mirny 1956-59	6·6	6·1	6·6	6·6	6·6	5·1	7·0	6·5	6·1	6·8	5·1	7·4	6·4
Oazis 1956-58	7·0	7·0	7·0	8·2	7·6	6·0	7·2	7·2	7·1	7·0	6·1	6·2	7·0
Wilkes 1958	—	7·7	6·5	7·2	7·6	4·5	7·8	7·2	6·8	8·0	8·3	7·5	(6·1)
Lazarev 1959-60	7·9	—	7·4	6·9	5·7	7·2	7·1	7·4	5·2	7·4	5·6	—	(6·8)
Davis 1958	6·3	6·6	6·7	5·5	6·2	6·8	7·7	6·9	7·6	7·0	5·1	7·6	6·7

2.3. LIMITING FACTORS OF THE SUNSHINE RECORDER

To assess the performance of the instrument numerically, the limiting height of recording, and also the limiting intensity of solar radiation, were determined. The data are set out in Table 2.3.1 below. The hour angle, t_o when the sun disappears below the horizon is given by

$$\cos t_o = -\tan \phi \tan \delta.$$

The maximum duration of sunshine is then 2 t_o. A correction for atmospheric refraction must be applied as discussed in Section 2.1. The values of the duration of sunshine actually observed are the mean values with a clear sky for the period January 1957-January 1963 taken from Fig. 2.2.2. To determine the amount of sunshine screened from the sunshine recorder by the elevated horizon, the azimuth and elevation of the horizon at the sunshine recorder site was determined to 1′ at 1° intervals azimuthally. In a similar fashion, the horizon seen from the plane of the

solarimeters on the ice plateau was measured. Both skylines are shown in Fig. 2.1.1. The horizon seen from the sunshine recorder was drawn on the cos t versus sin ν diagram (Fig. 2.1.2) and the screening effect obtained from that diagram. The expected hours of sunshine are then the theoretical values for an unobstructed horizon, corrected for refraction, as calculated in column 2 of Table 3.2.1 minus the effect due to obstructions in column 4. The difference between expected and actually observed values is 3 to 4% in autumn and spring and 6 to 8% and higher in summer and winter when the sun is close to the horizon for long periods at a time. The apparent solar elevation at which the sunshine recorder stops recording can then be obtained from the cos t versus sin ν diagram, and is shown in the last column of Table 2.3.1.

TABLE 2.3.1
LIMITING HEIGHTS OF THE SUNSHINE RECORDER

Date	Hours of bright sunshine				per cent error between measured and expected values	h^+ Limiting height of sunshine recorder
	Theoretically possible with a flat horizon (refraction correct)	Number of hours lost due to screening by elevated horizon++	Expected values with an elevated horizon	Measured values (means) with an elevated horizon		
	a	b	$a-b$			
1·1	24·00	4·10	19·90	18·5	−7	2°20′
1·2	18·80	1·61	17·19	16·6	−3	1°20′
1·3	14·78	0·83	13·95	13·5	−3	1°10′
1·4	10·70	0·42	10·28	9·7	−6	1°40′
1·5	6·86	0·05	6·81	6·1	−10	1°20′
1·6	2·56	0	2·56	1·8	−30	30′
1·7	0	0	0	0	0	—
1·8	5·40	0·18	5·22	4·8	−8	40′
1·9	9·46	0·30	9·16	8·7	−5	1°15′
1·10	13·26	0·65	12·61	12·1	−4	1°20′
1·11	17·44	1·27	16·17	15·5	−4	1°50′
1·12	24·00	4·89	19·11	18·1	−5	1°40′

++ Obtained graphically from the cos t sin ν diagram with the Mawson horizon at the instrument level drawn on to it (Fig. 2.1.2).
+ h is the apparent solar elevation at which the sunshine recorder stops recording.

This limiting height is approximately 1·4° apparent elevation. Since the atmospheric refraction can be assumed to be approximately 0·7°, the sunshine recorder stops at 0·7°, true solar elevation. From the relationship between solar height and direct solar radiation (Section 3) the limiting intensity of solar radiation for the sunshine recorder can be found to be approximately 0·3 *ly* min^{-1}. This means that, even with a cloud cover, the sunshine recorder will record if the solar radiation exceeds 0·3 *ly* min^{-1}. This may be the case for a high cloud cover of cirrus, cirrostratus or cirro-cumulus.

The effect of overburning of the chemically prepared recorder strips at high solar elevations is described by Kleinschmidt (1935). Using the method of evaluation as set down by the Commonwealth Bureau of Meteorology (1954) it is taken into account and the errors due to it are reduced to a minimum.

3. DIRECT SOLAR RADIATION

3.1. INTRODUCTION

The intensity of the solar radiation falling on a unit area normal to the solar beam outside the atmosphere, at the earth's mean distance from the sun, is known as the solar constant. The latest accepted value for this constant is the value of 1·98 cal cm^{-2} min^{-1} put forward by Nicolet in 1951, in place of the earlier accepted value of 1·94 cal cm^{-2} min^{-1} determined at the Smithsonian Institution. This intensity of the solar radiation outside the atmosphere is diminished by the depletion of the solar beam in the atmosphere.

Ångström (1929, 1930) has explained the extinction of the solar radiation in the atmosphere in terms of three independent processes:

(1) Extinction by Rayleigh—scattering;

(2) Extinction through scattering by the suspended dust-particles in the air;

(3) Extinction through absorption of the radiation by the atmospheric gases.

The air molecules are smaller than the wave-lengths of the solar radiation and the scattering due to them is described by the formula of Rayleigh according to which the scattering is inversely proportional to the fourth power of the wave-length.

$$S_{a\lambda} = \beta\lambda^{-4} \tag{3.1}$$

The scattering due to dust and other small particles is not in accordance with Rayleigh's law, since these particles are generally larger than the wave-lengths of the solar radiation. According to Ångström, it is possible to describe the scattering due to dust with the formula,

$$S_{d\lambda} = \beta\lambda^{-\gamma} \tag{3.2}$$

where β = the Ångström turbidity coefficient, a constant representing the amount of scattering particles, γ is a function of the size of the particles ($\gamma = 4$ for Rayleigh scattering) and it decreases with increasing particle size. λ is the wave-length of the mono-chromatic radiation considered.

Ångström found 1·3 as an average value of γ by analysing a great number of solar radiation measurements. Schuepp (1949) gave an improved method of measuring the turbidity in which λ can be determined separately. Published values by Volz (1956), Foitzik and Hinzpeter (1958), and Walko (1960) show values of γ varying between 0·5 and 2·05. The Ångström value of $\gamma = 1{\cdot}3$ can thus only be considered as a mean value. The scattering by suspended dust particles is small compared with the total extinction when the turbidity is low, as it is in polar regions. The effect of γ on the total extinction is thus small there.

If m is the penetrated air mass, I_γ' the intensity of the monochromatic radiation in an absolutely dry atmosphere and $S_{a\lambda}$ the Rayleigh scattering, we have

$$dI_\lambda' = -I_\lambda'(S_{a\lambda} + S_{d\lambda})\,dm$$

and

$$I_\lambda' = I_{o\lambda}\exp[-(S_{a\lambda} + S_{d\lambda})m].$$

Integrating over all wave-lengths, we have

$$I' = \int_o^\infty I_{o\lambda} \exp\left[-(S_{a\lambda} + S_{d\lambda})m\right] d\lambda \qquad (3.3)$$

This is the intensity which would be measured at the surface of the earth if there were no absorption due to atmospheric gases. Absorption in the long-wave region is mainly due to the presence of the tri-atomic gases of water-vapour, carbon-dioxide and ozone in the atmosphere; the bi-atomic gases O_2 and N_2 absorb only in the short-wave region (Möller 1957).

For most practical purposes, however, it is only necessary to consider water-vapour absorption; the absorption due to the other gases can be considered as a small correction term in the evaluation. Elsasser (1942) and Möller (1943) have given numerical solutions of this. Elsasser's method is discussed in 6.2. Considering

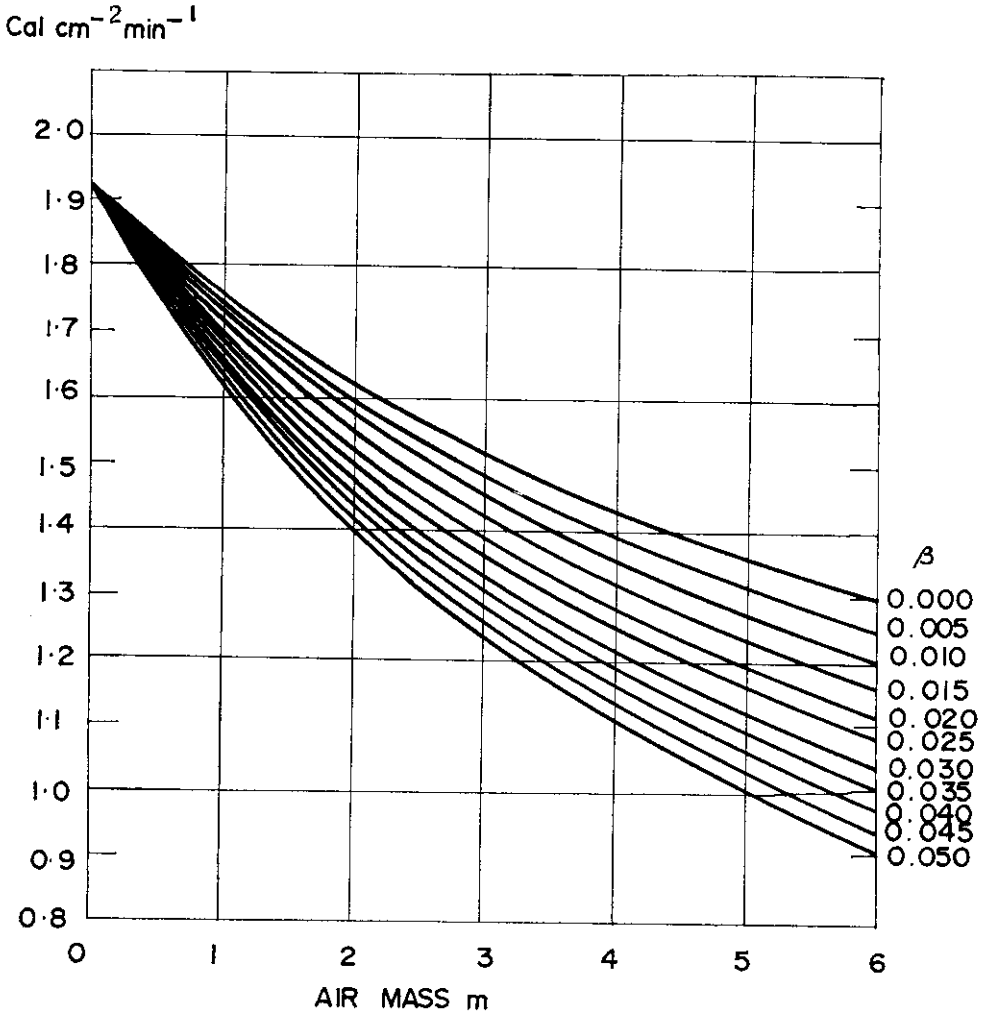

FIG. 3.1.1. The intensity of the direct solar radiation as a function of air mass (m) and turbidity (β) according to Ångström-Hoelper. The intensities refer to a completely dry atmosphere and the sun at middle distance.

that the absorption bands of water-vapour are in the infra-red part of the spectrum, where the depletion due to scattering is relatively small since λ is large, we can write the intensity I of a solar beam in an atmosphere containing water-vapour and other absorbing gases:

$$I = \int_o^\infty I_{o\lambda} \exp\left[-(S_{a\lambda} + \beta\lambda^{-\gamma})m\right]d\lambda - F - f \tag{3.4}$$

where F = absorption due to water-vapour,
and f = a small correction for absorption by other gases.

The integral has been computed by Hoelper (1937) for different values of the parameter β, using $I_o = 1{\cdot}94$ cal cm^{-2} min^{-1} and $\gamma = 1{\cdot}3$ and is shown in Fig. 3.1.1. Extensive use was made of this diagram in the reduction of the Mawson data.

The water-vapour absorption F and its variation with the penetrated air-mass, as well as the turbidity, can be determined directly with a method worked out by Ångström and Hoelper using filter measurements. If no filter measurements are available, F may be calculated using the formula given by Fowle (Fritz 1951) which uses the surface water-vapour pressure.

$$F = 0{\cdot}10 + 0{\cdot}0054\, \epsilon_o m \tag{3.5}$$

ϵ_o is the water-vapour pressure (in mm Hg).

This formula considers only average variations of the water-vapour with height and may thus not be quite applicable in polar regions where strong inversions exist near the surface. Hoelper (Fritz 1951) instead considers the total amount of water-vapour in the atmosphere at the point of observation, expressed as amount of precipitable water. This method by Hoelper was used to determine the water-vapour absorption F at Mawson.

The Ångström-Hoelper theory expressed in equation (3.4) was used in the study of the solar radiation at Mawson. The Hoelper relationship between absorbed radiation F and the penetrated air-mass was used to determine F. Absorption due to gases other than water-vapour was neglected. Since no filter measurements were available, values of β were obtained by comparing the measured values of the direct solar radiation and the integrated values of the Ångström-Hoelper theory. Mean values for the turbidity and its variation through the year were thus found. Mean values of the amount of water-vapour in the atmosphere were obtained from radio-sonde data. These mean values were used to compute "normal" values for the direct solar radiation. This procedure is similar to the method used by Liljequist (1956) to determine the direct solar radiation at Maudheim.

3.2. INTENSITY OF THE DIRECT SOLAR RADIATION AT NOON

The measured maximum daily values of the direct solar radiation, i.e. the noon values and their seasonal variations, will be presented first (Fig. 3.2.1). Due to the low turbidity, i.e., the small dust-particle content and low water-vapour content of the Antarctic air, the absorption of the solar radiation by the atmosphere can be expected to be small.

In fact, the values of the direct solar radiation observed in the Antarctic correspond to values measured at heights in excess of 2000 metres in lower latitudes.

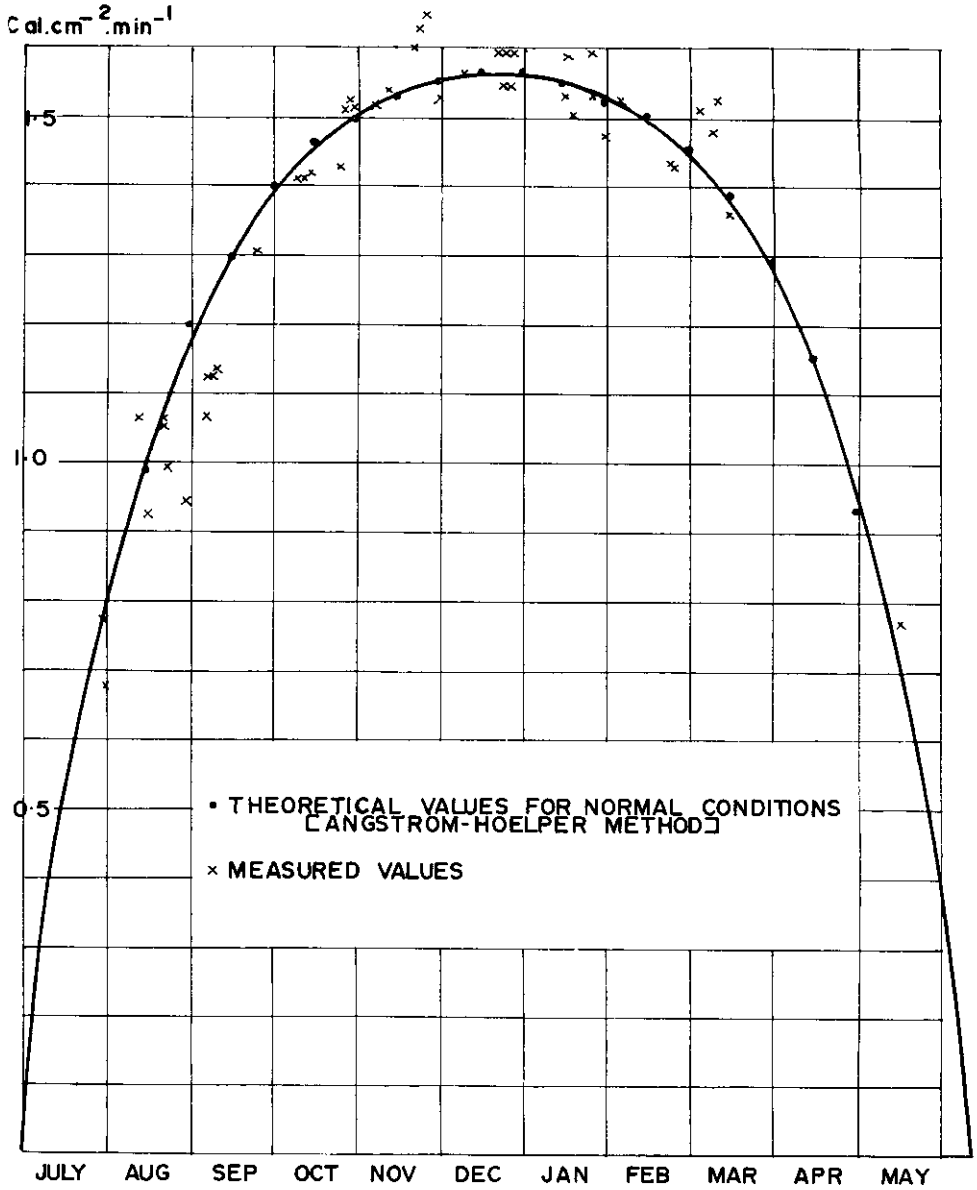

FIG. 3.2.1. Noon intensity of the direct solar radiation at Mawson 1961, on clear days.

Thus Hoinkes (1960), in a study at Little America V, practically at sea level found his measured intensities of the direct solar radiation to agree well with measurements made in the European Alps at 3000 metres altitude in summer. Values of the direct solar radiation measured by the author during summer in the Australian Alps at heights over 2000 metres exceed 1·6 *ly* min^{-1}. The maximum value of the direct solar radiation measured at sea level at Mawson was 1·65 *ly* min^{-1}. On three days towards the end of November, all the measured noon values exceeded 1·6 *ly* min^{-1}.

The noon values of the direct solar radiation on clear days are plotted in Fig. 3.2.1. Only days on which there was less than one-eighth of cloud all day have been included. The rings on the diagram represent theoretical values calculated from the normal conditions of turbidity and water-vapour content of the atmosphere above Mawson. The calculated values fit the observed values well; the Ångström-Hoelper method thus gives accurate results.

The sun was below the horizon for 22 days from 10 June to 2 July. After its return at the beginning of July, the direct solar radiation received at Mawson rose steeply to 1·0 *ly* min^{-1} in the middle of August and reached 1·5 *ly* min^{-1} on 1 November. It remained in excess of 1·5 *ly* min^{-1} for approximately 105 days to the middle of February and then decreased to zero on 10 June at the same rate at which it had increased after mid-winter.

Table 3.2.1 gives the noon values of the direct solar radiation calculated for normal conditions, i.e., the mean conditions of turbidity and water-vapour content of the atmosphere for each month. For comparison, the Maudheim values measured by Liljequist in 1950/51 are also given. All the calculated values are for actual solar distance.

The summer values at Maudheim are seen to be in good agreement with the

TABLE 3.2.1
NOON INTENSITY OF DIRECT SOLAR RADIATION ON CLEAR DAYS AT MAWSON (1961) AND MAUDHEIM (1950/51).
(Calculated by Hoelper's method for 'Normal' conditions)

	Mawson (67·5°S)		Maudheim (71°S)	
Date	Solar altitude (degrees)	Direct solar radiation (cal $cm^{-2}min^{-1}$)	Solar altitude (degrees)	Direct solar radiation (cal $cm^{-2}min^{-1}$)
1·1	45·4	1·56	42·0	1·54
15·1	43·5	1·55	40·2	1·52
1·2	39·5	1·52	36·4	1·51
15·2	35·1	1·50	32·4	1·48
1·3	30·0	1·45	27·0	1·45
15·3	24·6	1·38	21·6	1·39
1·4	17·9	1·29	14·9	1·24
15·4	12·7	1·15	9·7	1·04
1·5	7·5	0·93	4·4	0·78
15·5	—	—	—	—
1·6	—	—	—	—
15·6	—	—	—	—
1·7	—	—	—	—
15·7	—	—	—	—
1·8	—	—	—	—
15·8	8·4	0·99	4·7	0·36
1·9	14·1	1·20	10·4	0·83
15·9	19·3	1·30	15·5	1·09
1·10	25·5	1·40	21·6	1·22
15·10	30·9	1·46	27·0	1·35
1·11	36·8	1·50	33·1	1·43
15·11	40·9	1·53	37·2	1·49
1·12	44·2	1·55	40·5	1·52
15·12	45·7	1·56	42·1	1·54

values at Mawson. The difference between the values measured at the two stations increases towards winter when the solar elevation at Maudheim is lower, due to its higher latitude. Rusin (1961) shows the dependence of the direct solar radiation on latitude, solar elevation and elevation of the observing station above sea level in a summary of measurements made at several stations at the coast and in the interior of the continent. It appears that the direct solar radiation is very similar at sea level along the whole coast of Eastern Antarctica but increases rapidly with the elevation of the observing station.

3.3. ABSORPTION OF SOLAR RADIATION BY WATER-VAPOUR

In the following the absorption F of the direct solar radiation due to water-vapour and its variation with air-mass will be considered. The formula of Fowle, i.e.,

$$F = 0{\cdot}100 + 0{\cdot}0054\ \epsilon_o m,$$

gives the absorption, using surface data only, ϵ_o (mm Hg) being the surface vapour-pressure and m the air-mass. This formula assumes a mean variation with height of the water-vapour and may be rather in error for single observations when the mean conditions are not realized. This is particularly so in polar regions where the presence of surface inversions leads to surface conditions which are not representative of conditions in the free atmosphere.

Values at F obtained from radio-sonde data at Mawson and using Hoelper's method are compared with the Fowle equation in Fig. 3.3.1 below. A curve has been fitted to these measured points. The Fowle equation gives $F \neq 0$ for a dry atmosphere and cannot thus be considered to be correct for small $\epsilon_o m$ values. However, in summer when the vapour pressure is high and also surface inversions are weak or not present during the day, the Fowle equation can be used without much loss of accuracy.

More accurate values of F are obtained when the total amount of water-vapour above the observation site is considered rather than the surface water-vapour. The values of F may be obtained from the theoretical work by Hoelper. They have been tabulated by Linke (1953), Table 103, as a function of air-mass and amount of water-vapour and are reproduced in graphical form in Fig. 3.3.2. The total amount of water-vapour above the observation site is represented as the amount of precipitable water, and is obtained from radio-sonde ascents.

The Hoelper method cannot be used satisfactorily in all climatic regions (Schüepp 1949) and it must be determined first whether it can be used for Antarctic conditions. Liljequist, using results from filter measurements at Maudheim, could show that his measured values of F show the variation with air-mass as given by Hoelper. Since the atmospheric conditions at Mawson are probably not very different from those at Maudheim it must suffice to accept Liljequist's check of the Hoelper method. The good fit in Fig. 3.2.1 between the measured values and theoretical values determined from the Ångström-Hoelper equation (eq. (3.4)), which contains the term F due to Hoelper, also justifies the use of the Hoelper method.

For the evaluation of the Mawson data the "effective" amount of precipitable water was obtained from the once-daily early morning radiosonde flight at Mawson at 00 GMT. Only flights on clear days were considered when the weather was

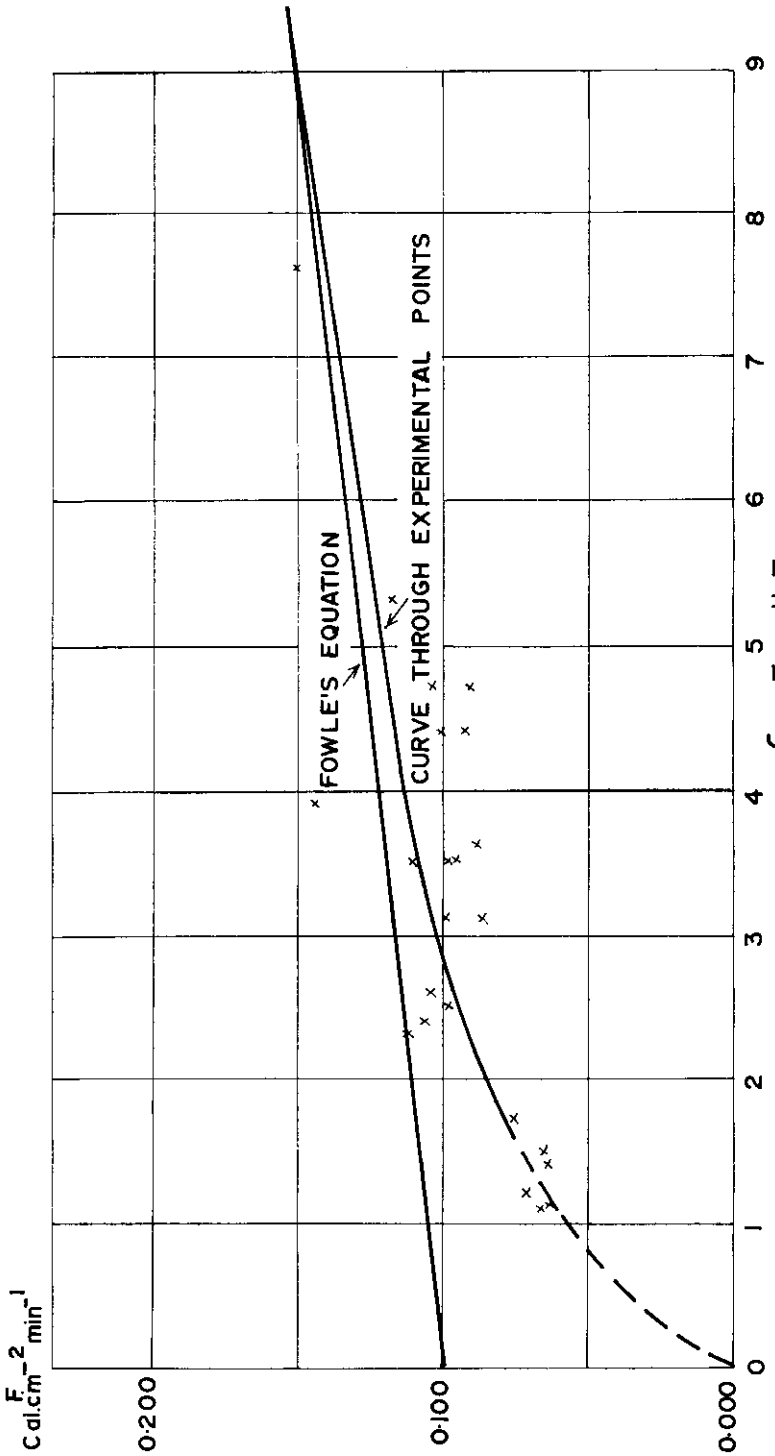

FIG. 3.3.1. Absorption (F) of solar radiation by water vapour (Mawson 1961).

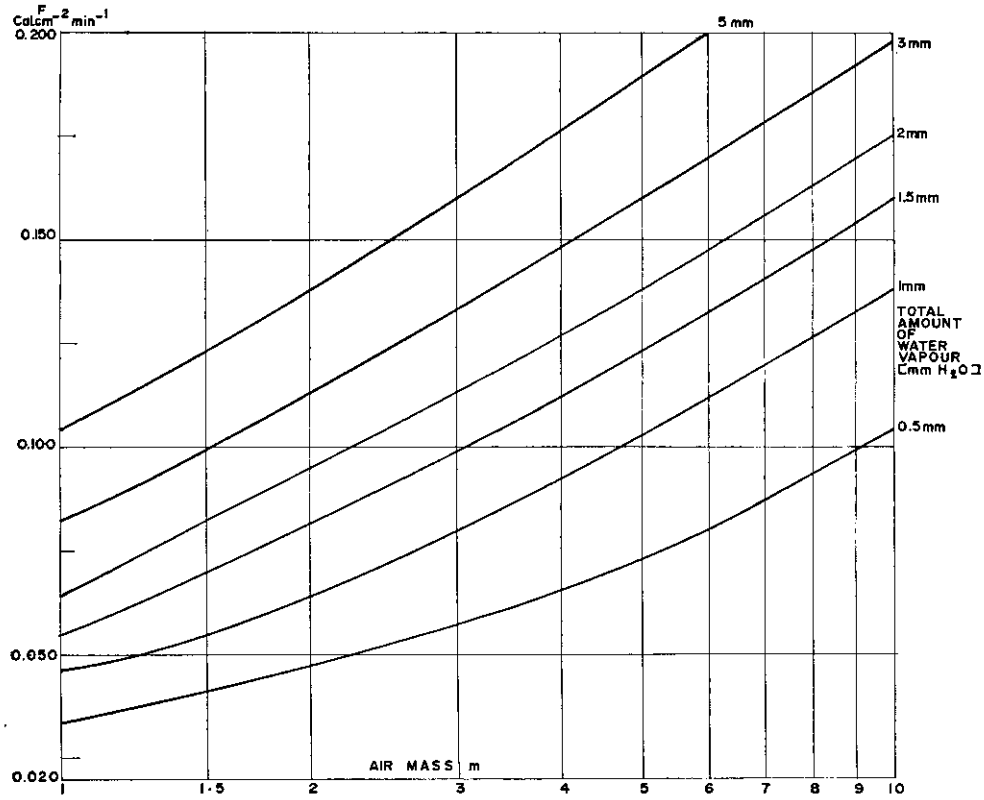

FIG. 3.3.2. Water vapour absorption (F) according to Hoelper.

stable and the amount of precipitable water could be assumed to remain constant all day. The effective amount of precipitable water is pressure-corrected by multiplying the mixing ratio at the different levels with the factor $\sqrt{\frac{P}{Ps}}$, where P is the pressure at the level in question and Ps (= 1000 mb); a standard pressure (Elsasser 1942), Table 3.3.1 gives the mean monthly values of the effective precipitable water and the number of radiosonde flights from which the monthly values were calculated. Flights were analysed individually and the monthly means obtained from them.

TABLE 3.3.1

EFFECTIVE PRECIPITABLE WATER (mm H_2O) MAWSON 1961

	Jan.	Feb.	Mar.	Apr.	May	Jun.	Jul.	Aug.	Sep.	Oct.	Nov.	Dec.
mm H_2O	2·8	3·2	1·9	1·5	1·4	1·0	0·8	1·0	1·4	1·3	2·7	3·1
No. of flights	11	7	5	5	1	3	4	7	6	11	9	10

The amount of water-vapour reaches a maximum in summer. In winter, the amount of precipitable water is only a quarter of the summer values.

At noon in the middle of each month the magnitudes of absorption due to water-vapour are as follows:

TABLE 3.3.2
EXTINCTION OF THE SOLAR RADIATION BY ABSORPTION IN WATER-VAPOUR AND TOTAL EXTINCTION.
Mawson 1961

Date	Solar height at noon (degrees)	Air-mass m_{760}	Amount of precipitable water mm H_2O	Water-vapour absorption cal $cm^{-2}min^{-1}$	Total extinction in atmosphere cal $cm^{-2}min^{-1}$*
15 Aug.	8·4	6·58	1·0	0·116	0·940
15 Sept.	19·4	3·004	1·4	0·095	0·640
15 Oct.	30·9	1·941	1·3	0·074	0·480
15 Nov.	40·9	1·525	2·7	0·094	0·410
15 Dec.	45·7	1·396	3·1	0·099	0·380
15 Jan.	43·5	1·451	2·8	0·093	0·390
15 Feb.	35·1	1·736	3·2	0·110	0·440
15 Mar.	24·6	2·392	1·9	0·100	0·560
15 Apr.	12·7	4·469	1·5	0·117	0·790

* From Fig. 3.2.1, using a solar constant of 1·94 cal $cm^{-2}min^{-1}$.

The water-vapour absorption is thus fairly constant throughout the year, the decrease in the water-vapour content of the atmosphere in winter balancing an increased air-mass to give similar magnitude of absorption. The extinction due to the absorption by water-vapour is in summer only approximately 25% of the total extinction and is approaching very small values in winter. Scattering processes are responsible for the remaining percentage, and the scattering due to suspended dust and hygroscopic particles in the atmosphere will be studied in the following section.

3.4. TURBIDITY

From the amount of precipitable water in the atmosphere above the point of observation, the atmospheric turbidity can now be derived. The Ångström turbidity coefficient β was discussed in 3.1 above. It can be takent to be approximately proportional to the amount of suspended dust and hygroscopic particles in the atmosphere. Since no direct filter measurements were made, the turbidity coefficient β was calculated in the following way:

1. The solar altitude at solar noon of each clear day was calculated and corrected for refraction.
2. From Linke (1953), Table 91, the corresponding air-mass m_{760} was obtained.
3. The air-mass m_{760} was corrected to actual atmospheric pressure to give the actual air-mass $m = \frac{P}{760}\, m_{760}$ where P is the actual atmospheric pressure in mm Hg.
4. With air-mass m and amount of precipitable water w obtained from radiosonde data for that day, the absorption F due to water-vapour was obtained from the Hoelper diagram (Fig. 3.3.2).

5. The measured noon values of the direct solar radiation, (i.e., global minus diffuse sky radiation divided by sin h, were multiplied by $\frac{1{\cdot}94}{\text{Sact}}$ where Sact is the actual solar constant given in Linke (1953) Table 8. This gives the direct solar radiation I with the sun at middle distance.
6. The sum $I + F = I'$ gives the intensity of the direct solar radiation with no water-vapour present. With intensity I' and air-mass m, the Ångström turbidity coefficient β was obtained from the Ångström-Hoelper diagram 3.1.1.

Monthly mean values of the turbidity coefficient β obtained at Mawson during 1961 in this way are shown in the table below.

TABLE 3.4.1

TURBIDITY COEFFICIENT β—MAWSON 1961

Month	Jan.	Feb.	Mar.	Apr.	May	Jun.	Jul.	Aug.	Sep.	Oct.	Nov.	Dec.
	·024	·025	·012	—	—	—	—	·012	·039	·033	·013	·026
No. of flights	10	3	4					4	6	11	8	9

The mean value for all the observations is ·025. The largest values occur in spring and summer. November, which is usually relatively clear at Mawson, and was so in 1961, shows a very small turbidity coefficient; this may be due to the small amount of hygroscopic particles present, in comparison with more cloudy months in spring and summer. Particularly, the September value of $\beta = 0{\cdot}039$ is high, coinciding with a higher than average cloud coverage. However, in view of the method that had to be used to determine values of β, no great significance can be attached to individual monthly values.

Generally it may be stated that the summer values of β are approximately ·025 as compared with the lower winter values of ·010 to ·015. These values then agree with values of β found by Liljequist at Maudheim, mainly 0·015 to 0·035 in summer, mean value 0·025. Ambach's Greenland values (Ambach 1963) in summer were in the range 0·011 to 0·030. Liljequist gives the β values of other investigators in polar regions which lie in approximately the same range.

3.5. DIRECT SOLAR RADIATION AT MAWSON

Summing up the discussion of direct solar radiation, the two factors mainly responsible for the depletion of the direct solar radiation in the atmosphere are:

1. the amount of precipitable water,
2. the turbidity.

The smoothed mean monthly values of these parameters determined at Mawson are given in the table below and were taken from Fig. 3.5.1.

TABLE 3.5.1

SMOOTHED MONTHLY MEANS OF AMOUNT OF PRECIPITABLE WATER W AND TURBIDITY β

		Jan.	Feb.	Mar.	Apr.	May	Jun.	Jul.	Aug.	Sep.	Oct.	Nov.	Dec.
w	$\frac{\text{mm}}{\overline{H_2O}}$	3·1	2·8	2·1	1·6	1·2	1·0	0·8	0·9	1·1	1·6	2·4	3·0
β		·025	·020	·020	·015	·015	·010	·010	·015	·020	·020	·025	·025

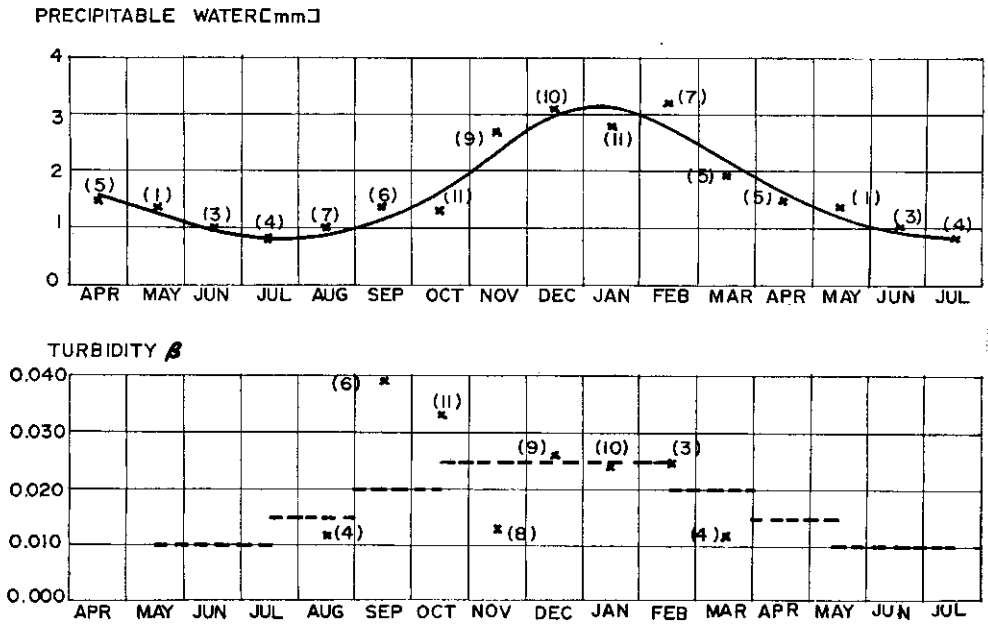

FIG. 3.5.1. Monthly means of amount of precipitable water and turbidity according to the Ångström-Hoelper method at Mawson. (The figures in brackets give the number of days from which the means have been computed.)

The smoothed mean monthly values of the two parameters are used to indicate normal conditions at Mawson, and with the aid of these values the normal values of the direct solar radiation can be obtained for any time at Mawson.

This is done in the following fashion:

1. The solar altitude at the time required is calculated and corrected for refraction.

2. From Linke (1953), Table 91, the corresponding air-mass m_{760} is obtained. (The correction to mean atmospheric pressure is omitted since it is very small.)

3. With the normal value of the turbidity and the air-mass m_{760} the intensity of the direct solar radiation I' with no water-vapour present is obtained from the Ångström-Hoelper diagram 3.1.1.

4. To correct for the presence of the "normal" amount of precipitable water, the absorption F due to water-vapour is obtained from the Hoelper diagram 3.3.2.

5. The quantity $I' - F$ represents the normal intensity of the direct solar radiation at the middle solar distance. Multiplying by $\frac{S_{act}}{1{\cdot}94}$ where S_{act} is the actual solar distance, gives the direct solar radiation for actual solar distance.

An example of the calculation is shown in Table 3.5.2.

A first check of the method will suffice here to indicate the magnitude of errors. Fig. 3.5.2 shows a check of the calculated data on 21 December. The curve shows

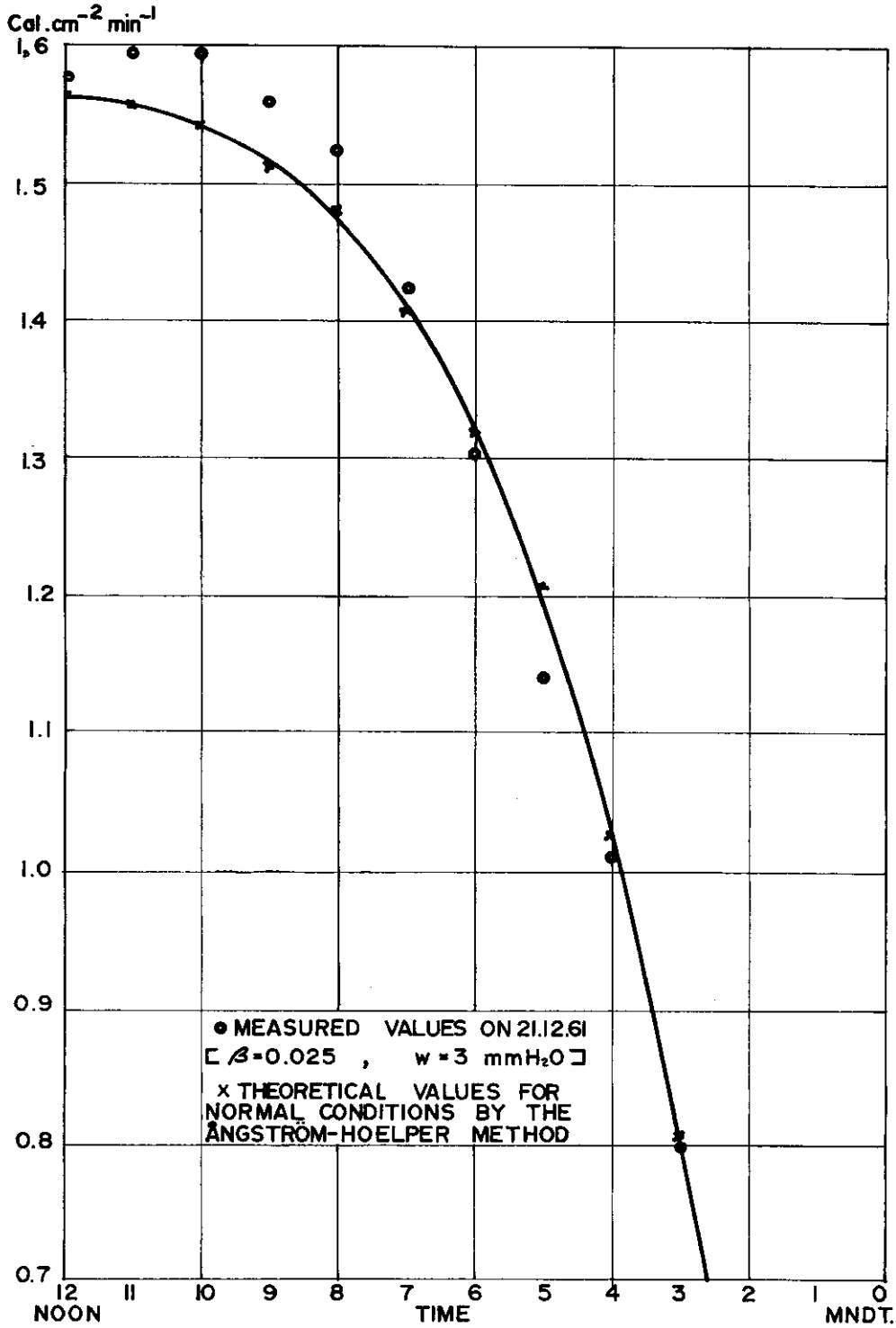

FIG. 3.5.2. Direct solar radiation, Mawson 1961.

theoretical values of direct solar radiation, using $\beta = 0{\cdot}025$, $w = 3$ mm H_2O, the circles are actually observed values. The agreement between the two sets of values is seen to be fairly good. The measured values of β and w were 0·025 and 2·6 mm H_2O. respectively.

TABLE 3.5.2

DIRECT SOLAR RADIATION BY THE ANGSTRÖM-HOELPER METHOD

Mawson 21.12.61, $\beta = 0{\cdot}025$, $w = 3{\cdot}0$ mm H_2O, $S_{act} = 2{\cdot}005$

Time (hrs)	$h°$	m_{760}	I'	F	$(I'-F)\frac{S_{act}}{1{\cdot}94}$
3	6·9	7·87	0·965	·185	·805
4	11·1	5·077	1·150	·160	1·022
5	16·1	3·567	1·297	·141	1·205
6	21·6	2·700	1·404	·127	1·320
7	27·3	2·172	1·478	·116	1·407
8	32·9	1·789	1·540	·107	1·480
9	38·0	1·621	1·569	·103	1·514
10	42·1	1·489	1·592	·099	1·543
11	44·9	1·413	1·605	·097	1·558
12	46·0	1·389	1·610	·096	1·564

The full results of calculations using the determined monthly magnitudes of w and β are shown in Fig. 3.5.3. From this, the direct solar radiation can thus be determined on a clear day at any time throughout the year. The curves have not been drawn for the period noon to midnight, but since they are symmetrical about noon, corresponding afternoon values of the direct solar radiation can be obtained from the morning curves. No irregularities of the horizon have been considered but the direct solar radiation is zero when the sun sets behind a flat horizon, taking the above-mentioned refraction correction into account.

Considering the similarity of the values of β and w between the Mawson and Maudheim results, it is not surprising that the curves of direct solar radiation obtained for both stations should show very similar maximum values: 1·56 cal cm^{-2} min^{-1} for Mawson and 1·54 cal cm^{-2} min^{-1} for Maudheim. It seems very likely that both β and w will not vary appreciably along the whole coastal fringe of eastern Antarctica and that only data on solar altitudes for any point along that coastal fringe are required, i.e., its latitude to enable one to determine the direct solar radiation at that point at any time with reasonable accuracy.

Finally, to support this argument, the Mawson values must be viewed in relation to measurements at other Antarctic stations. The values of the direct solar radiation according to data summarized by Rusin (1961) at Mirny, Maudheim and Little America (these stations lying between latitude 66 and 78°S at sea level), are within approximately 5% of each other for any given solar elevation. Thus the direct solar radiation appears to be very uniform in the whole coastal region of Eastern Antarctica. Rusin also shows that the direct solar radiation increases rapidly with the elevation of the observing station, values of over 1·7 cal cm^{-2} min^{-1} having been recorded at Sovjetskaya at 3600 metres altitude.

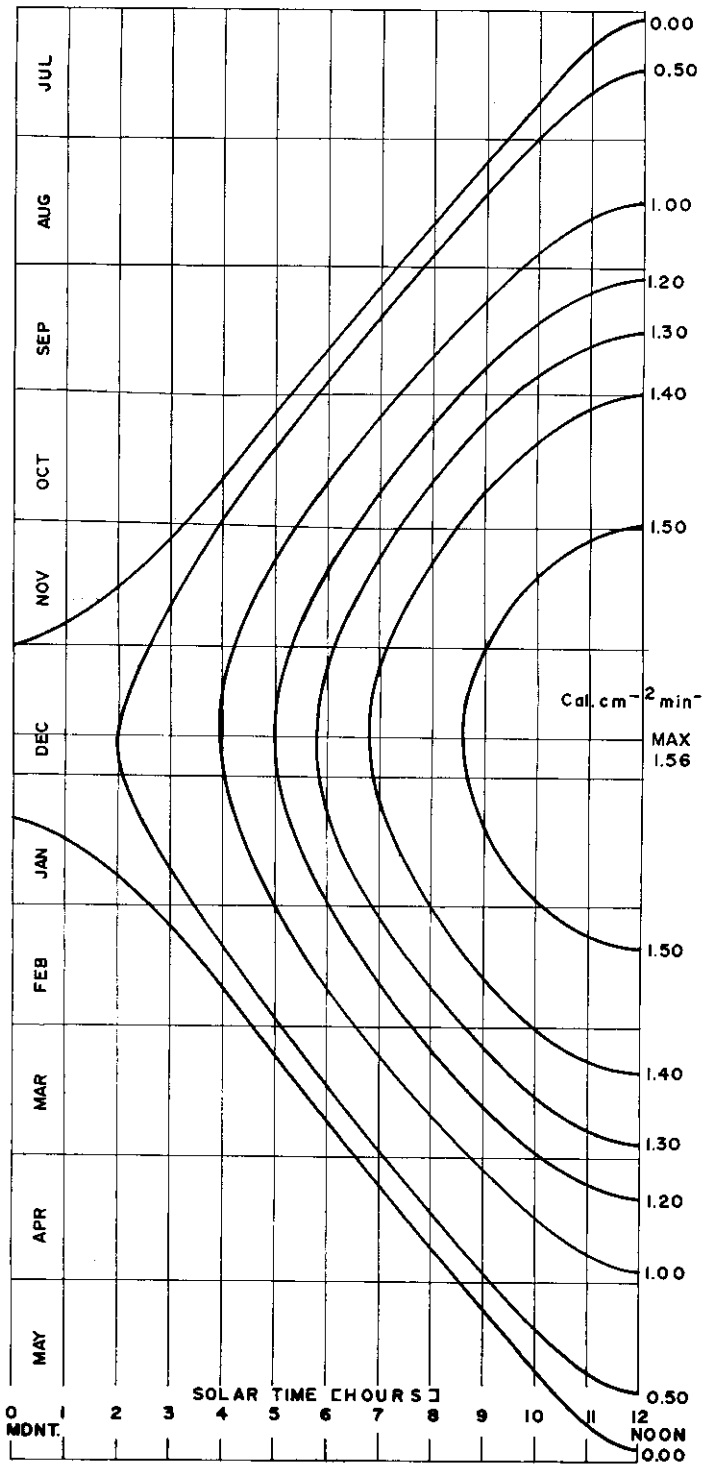

FIG. 3.5.3. "Normal" values of direct solar radiation at Mawson.
(Theoretical values using Ångström-Hoelper method.)

4. GLOBAL RADIATION

4.1. DIFFUSE CLEAR SKY RADIATION

The global radiation on clear days is the sum of two "short-wave" components of radiation falling on a horizontal surface:

(1) the direct solar radiation;

(2) the diffuse clear-sky radiation.

The values of the direct solar radiation were given in the preceding section.

Theoretical calculations of the diffuse clear sky radiation are difficult. Möller (1957) has discussed single and multiple scattering of the primary radiation in a Rayleigh atmosphere. The most complete and satisfactory treatment is given by Deirmendjian and Sekera (1954) who computed the clear sky radiation in a Rayleigh atmosphere and also took the scattering of the reflected radiation from the earth's surface into account. Their results are shown in Fig. 4.1.1. The effect of

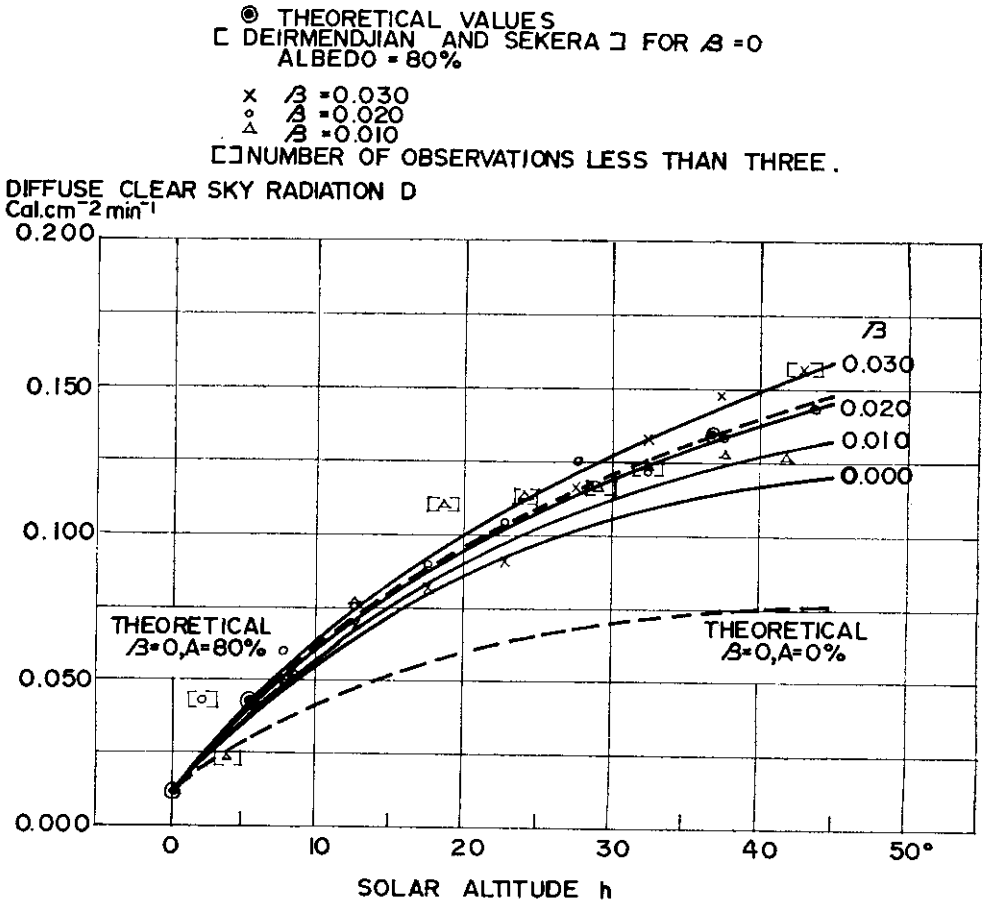

FIG. 4.1.1. The diffuse clear-sky radiation as a function of the solar altitude (h) and the turbidity (β).

turbidity on the diffuse sky radiation does not appear to have been satisfactorily determined yet.

The diffuse sky radiation was recorded continuously at Mawson by a Moll-Gorczinski solarimeter provided with a shade-ring. Corrections due to the screening of the sky as well as the sun were discussed in Section 1. To determine the dependence of the clear-sky radiation on the turbidity coefficient β, only data were used for days for which β had been calculated.

The 121 measurements of diffuse clear-sky radiation have been grouped in three ranges of the turbidity β; in each range the observed radiation is given as a function of solar elevation increasing in steps of 5°, n being the number of observations in each group. These results are given in Table 4.1.1.

TABLE 4.1.1
GROUP MEANS OF DIFFUSE CLEAR SKY RADIATION D, SOLAR ALTITUDE h AND TURBIDITY β.

Intervals of	$0 \leqslant \beta \leqslant 0{\cdot}015$				$0{\cdot}016 \leqslant \beta \leqslant 0{\cdot}025$				$0{\cdot}026 \leqslant \beta \leqslant 0{\cdot}036$			
				β				β				β
h	n	h	D	(mean)	n	h	D	(mean)	n	h	D	(mean)
0 – 5	2	3·9	·024		1	2·0	·044		—	—	—	
5·1–10	7	8·4	·051		4	7·6	·060		8	7·4	·049	
10·1–15	3	12·4	·077		3	12·3	·075		10	12·5	·068	
15·1–20	2	18·4	·111	·010	4	17·3	·090	·021	12	17·4	·082	·032
20·1–25	2	24·0	·114		4	22·7	·104		10	22·8	·091	
25·1–30	1	29·0	·117		3	27·5	·125		10	27·7	·116	
30·1–35	2	32·2	·122		5	32·4	·122		4	32·2	·133	
35·1–40	3	37·7	·127		7	37·6	·133		3	37·2	·148	
>40	4	41·9	·127		5	43·8	·143		2	43·0	·157	

The same results are plotted in Fig. 4.1.1. For comparison, the theoretical values of Deirmendjian and Sekera are also shown in Fig. 4.1.1. Since relatively few observations were made at Mawson for small turbidity values, the scatter in that region is accordingly larger. The curves have been drawn rounding off the values of β to 0·010, 0·020 and 0·030, extrapolating for $\beta = 0{\cdot}000$. At low solar elevations the curves were drawn to agree with the theoretical values.

The diffuse clear sky radiation appears to increase linearly with the turbidity β at a given solar altitude, at least in the range of turbidity investigated. This indicates that, since the air is very clear over the Antarctic continent, there should be little diffuse clear sky radiation. This is not so in comparison with results obtained by investigators quoted by Hann-Süring (1939) according to which the diffuse clear-sky radiation measured at temperate latitudes are of the order of, or smaller than, the Antarctic results. The high diffuse clear-sky radiation in the Antarctic seems to be due to the high albedo of the snow surface, the reflected radiation from the surface being scattered and contributing considerably to the diffuse clear sky radiation. This is apparent when considering the theoretical results of Deirmendjian and Sekera shown in Fig. 4.1.1 where the effect of a high albedo on D is clearly shown: i.e., an increase in albedo from 0 to 80% almost doubles the diffuse sky radiation.

The theoretical values for a surface albedo of 80% and Rayleigh scattering almost coincide with the measured diffuse clear-sky radiation for $\beta = 0{\cdot}020$. The difference between the observed and theoretical curves for scattering in a Rayleigh atmosphere is largely due to the fact that the surface albdo at Mawson was not 80% but only 64% (see Section 7). To a smaller extent, instrumental errors may be responsible for the difference.

Deirmendjian and Sekera only calculated the Rayleigh scattering for albedos of 0 and 80% and their involved calculations cannot be repeated here for an albedo of 64%. It can be concluded, however, that the Mawson measurements of the diffuse sky radiation agree with the theoretical expectations.

4.2. GLOBAL RADIATION WITH A CLEAR SKY

The global radiation with a clear sky will now be determined. The global radiation was measured continuously at Mawson with a Kipp solarimeter. The number of clear days at Mawson, however, were few and moreover unequally distributed throughout the year. To construct curves of global radiation with a clear sky it was decided to use the Ångström-Hoelper method rather than construct curves of normal values from the measured data. The measured data were only used to check the validity of the Ångström-Hoelper method.

Using the normal values of the water-vapour content of the atmosphere and the turbidity, the method of deriving normal values of the direct solar radiation is used as described in 3.5. Then the following steps are necessary to determine the global radiation:

1. After determining the direct solar radiation for actual solar distances as described, this quantity is multiplied by sin h to obtain the direct solar radiation falling on a horizontal surface.
2. The diffuse clear sky radiation D is then obtained from Fig. 4.1.1 using the normal value of the turbidity β and the solar altitude h.
3. The global radiation is obtained by adding D to I' sin h.

Tables 4.2.1 and 4.2.2 are examples of the calculations. Calculated values for all hours at intervals of 0·1 cal cm^{-2} min^{-1} throughout the year are shown in Fig. 4.2.1. The curves are symmetrical about 12 noon, and afternoon values can be read off from corresponding times in the morning.

The curve labelled "sun on the horizon" is for $h = 0$, where the direct solar radiation is zero and the diffuse sky radiation, and hence the global radiation, is 0·01 cal cm^{-2} min^{-1}.

Fig. 4.2.2 shows a test of the Ångström-Hoelper method for the noon values of the global radiation. The agreement between the theoretical and measured values is seen to be quite good. The measured values are based on an instrument constant using the mean monthly temperature. Since the diurnal variation of the temperature is highest in summer, this tends to over-estimate the noon values of the global radiation more in summer than in winter. If the difference between the mean monthly temperature and the summer noon temperature is 10°C, the measured values of the global radiation will have to be reduced by 2%. Some of the measured high summer values in Fig. 4.2.2 will be corrected by this procedure. The low

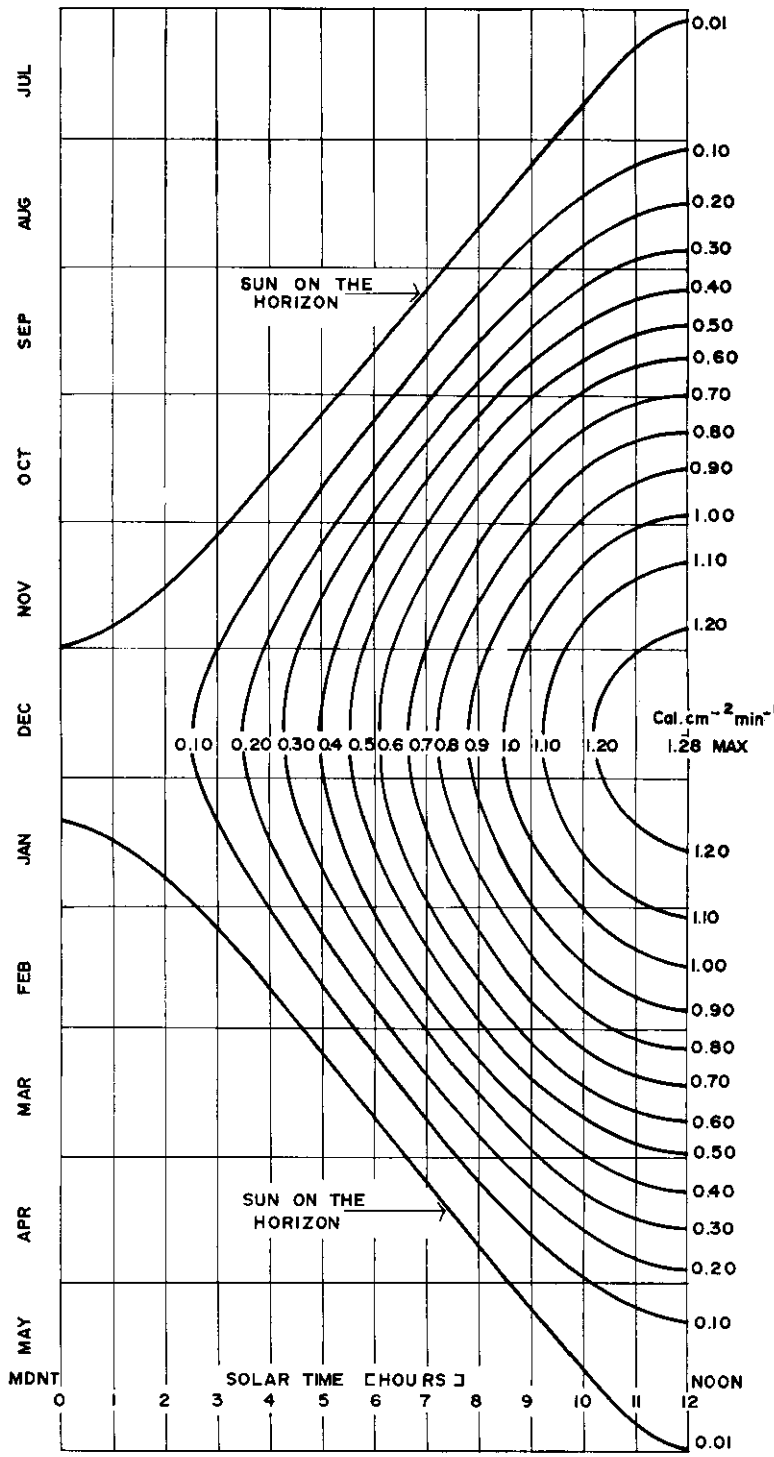

FIG. 4.2.1. "Normal" values of global radiation at Mawson.
(Theoretical values using Ångström-Hoelper method.)

TABLE 4.2.1

THEORECTICAL DETERMINATION OF THE GLOBAL RADIATION AT NOON AT HALF-MONTHLY INTERVALS THROUGHOUT THE YEAR, USING THE ÅNGSTRÖM-HOELPER METHOD AND NORMAL CONDITIONS AT MAWSON.

Date	h*	m_{760}	W (mm)	β	I'	F	$(I'-F)$	$\times \frac{\text{Sact}}{1{\cdot}94}$ (S)	Sact	sin h	S sin h	D	S sin h + D
1·7	0		0·9	·010									
15·7	1·2		0·8	·010									
1·8	4·5	11·33	0·8	·015									
15·8	8·4	6·58	0·9	·015	1·125	0·110	1·015	·990	1·892	·146	·144	·051	·195
1·9	14·1	4·047	1·0	·015	1·315	0·093	1·222	1·200	1·905	·243	·292	·075	·367
15·9	0·3	3·004	1·1	·020	1·395	0·084	1·311	1·297	1·919	·330	·428	·093	·521
1·10	25·5	2·314	1·3	·020	1·483	0·080	1·403	1·400	1·936	·430	·602	·110	·712
15·10	30·9	1·941	1·6	·020	1·538	0·082	1·456	1·465	1·952	·513	·751	·121	·872
1·11	36·8	1·666	2·0	·025	1·560	0·086	1·474	1·496	1·970	·598	·895	·136	1·031
15·11	40·9	1·525	2·4	·025	1·585	0·089	1·496	1·530	1·983	·655	1·002	·145	1·147
1·12	44·2	1·431	2·7	·025	1·600	0·091	1·509	1·552	1·996	·696	1·080	·150	1·230
15·12	45·7	1·396	3·0	·025	1·610	0·096	1·514	1·563	2·003	·715	1·120	·152	1·272
1·1	45·4	1·403	3·1	·025	1·610	0·097	1·513	1·565	2·007	·712	1·114	·151	1·265
15·1	43·5	1·451	3·1	·025	1·600	0·099	1·501	1·550	2·005	·687	1·064	·150	1·214
1·2	39·5	1·570	3·0	·025	1·578	0·101	1·477	1·522	1·999	·635	·966	·142	1·108
15·2	35·1	1·736	2·8	·020	1·570	0·102	1·468	1·504	1·988	·575	·865	·130	·995
1·3	30·0	1·995	2·4	·020	1·530	0·101	1·429	1·455	1·976	·500	·727	·119	·846
15·3	24·6	2·392	2·1	·020	1·473	0·103	1·370	1·385	1·961	·416	·576	·108	·684
1·4	17·9	3·226	1·8	·015	1·400	0·110	1·290	1·293	1·943	·307	·397	·086	·483
15·4	12·7	4·469	1·5	·015	1·275	0·117	1·158	1·150	1·927	·219	·252	·070	·322
1·5	7·5	7·30	1·4	·015	1·085	0·139	·946	0·932	1·910	·130	·121	·048	·169
15·5	3·8	12·44	1·2	·015									
1·6	1·0	27·0	1·1	·010									
15·6	0		1·0	·010									

* $h = 90 - \phi + \delta$ (refraction-corrected)

TABLE 4.2.2

THEORETICAL DETERMINATION OF THE DIURNAL GLOBAL RADIATION USING THE ÄNGSTRÖM-HOELPER METHOD AND NORMAL CONDITIONS AT MAWSON ON 21/12/61.

21/12/61 Time (hours)	m_{760}	I'	F	$(I' - F)$	$x \frac{\text{sact}}{1{\cdot}94}$ (s)	sin h	$S \sin h$	D	$S \sin h + D$	h
12 noon	1·389	1·610	·096	1·514	1·564	·720	1·125	·152	1·277	46·0
11	1·413	1·605	·097	1·508	1·558	·706	1·100	·151	1·251	44·9
10	1·489	1·592	·099	1·493	1·543	·607	1·033	·147	1·180	42·1
9	1·621	1·569	·103	1·466	1·514	·616	·933	·140	1·073	38·0
8	1·789	1·540	·107	1·433	1·480	·543	·805	·129	·934	32·9
7	2·172	1·478	·116	1·362	1·407	·458	·645	·118	·763	27·3
6	2·700	1·404	·127	1·277	1·320	·368	·486	·102	·588	21·6
5	3·567	1·297	·141	1·156	1·205	·278	·335	·085	·420	16·1
4	5·077	1·150	·160	·990	1·022	·193	·197	·066	·263	11·1
3	7·87	0·965	·185	·780	·805	·120	·097	·048	·145	6·9

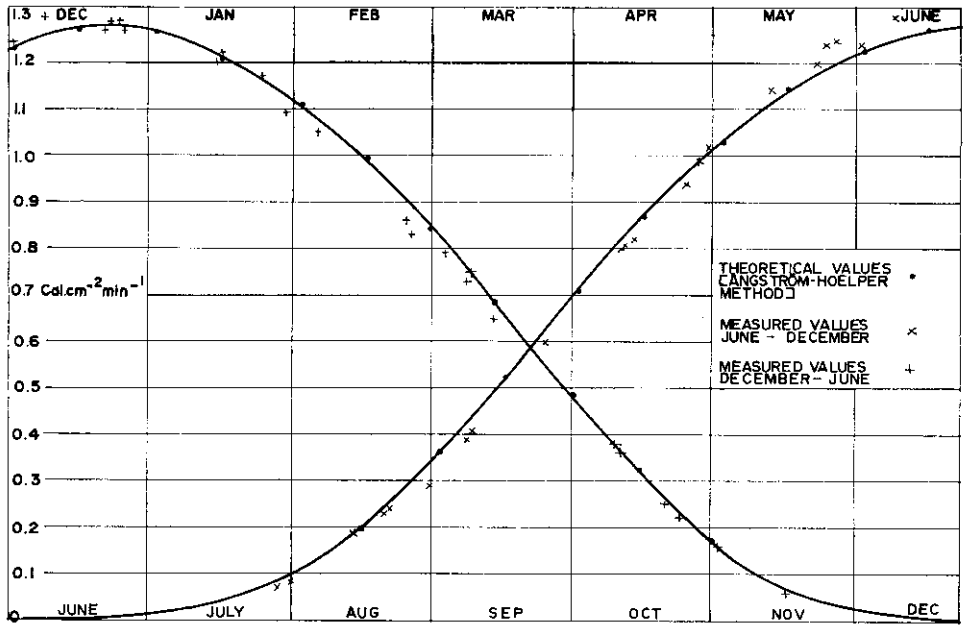

FIG. 4.2.2. Global radiation—noon values Mawson—clear sky.

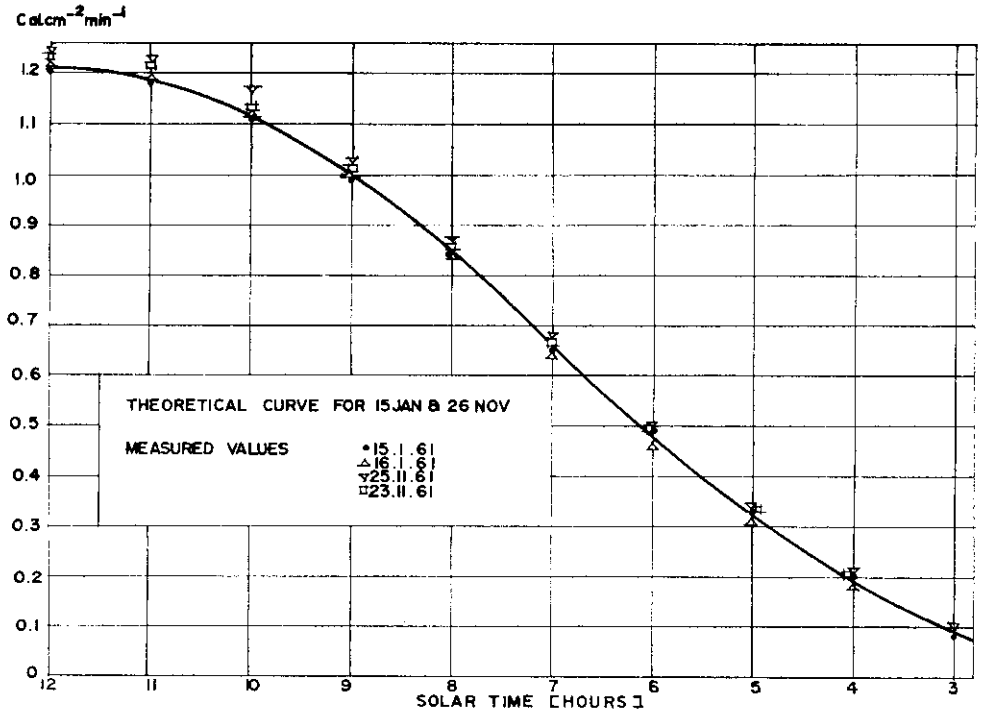

FIG. 4.2.3. Global radiation, Mawson. Test of the Ångström-Hoelper method.

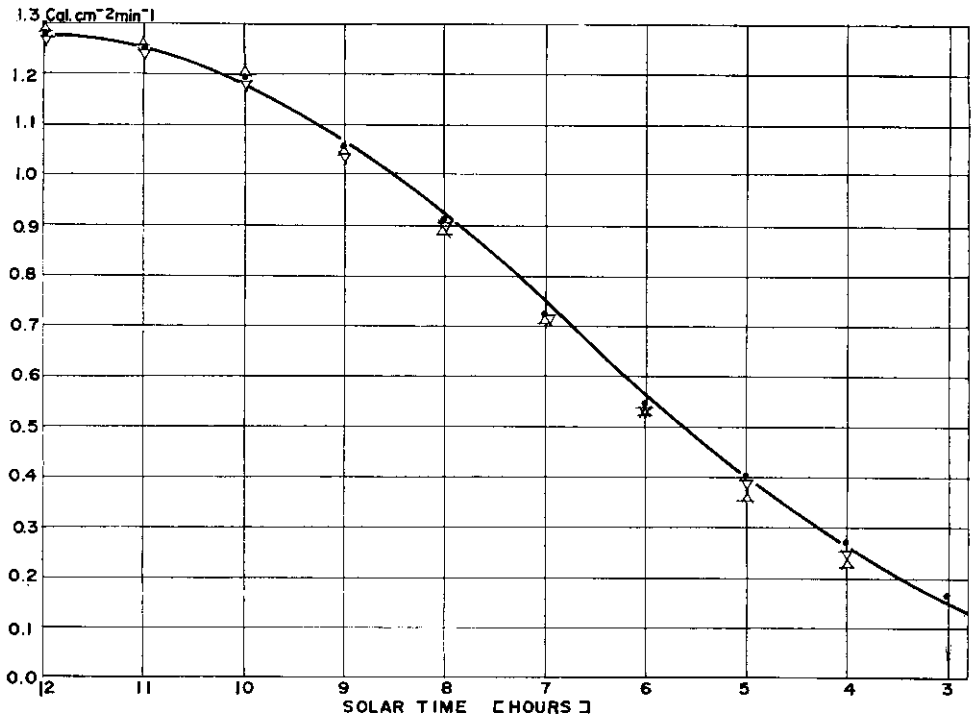

FIG. 4.2.4. Global radiation, Mawson. Test of the Ångström-Hoelper method. Theoretical curve for 21 December, 1961.

Measured values: • 21.12.61
△ 24.12.61
▽ 25.12.61.

September values are due to a high water-vapour content of the atmosphere, which was smoothed out when determining the normal values of the amount of precipitable water.

Figs. 4.2.3 to 4.2.5 show similar tests of the Ångström-Hoelper method for the diurnal changes of the global radiation. The agreement between theoretical and measured values is very good, particularly if the effect of the diurnal temperature change is considered to correct the measured values. The theoretical model thus seems to be correct.

The maximum value of the global radiation is 1·28 cal cm^{-2} min^{-1}. This compares with a maximum value of 1·197 cal cm^{-2} min^{-1} calculated for Maudheim under similar conditions of water-vapour and turbidity. The means of measurements at some other coastal stations (Rusin 1961) are very similar: Mirny 1·20 cal cm^{-2} min^{-1}, Oazis 1·24 cal cm^{-2} min^{-1}.

4.3. DAILY INSOLATION WITH A CLEAR SKY AND AN OVERCAST SKY

As shown above, with a clear sky, the global radiation can be relatively easily computed. With a cloudy sky this is not so, since the change of the incoming radiation due to the cloud depends on many factors. The cloud reflects and absorbs, and both reflection and absorption depend on factors such as cloud thickness,

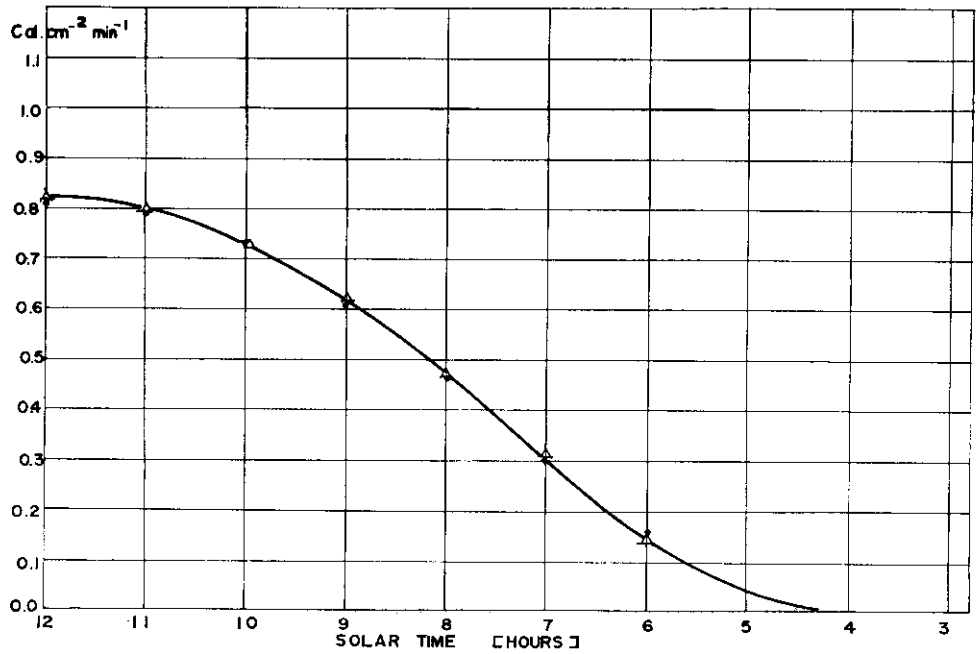

FIG. 4.2.5. Global radiation, Mawson. Test of the Ångström-Hoelper method. Theoretical curve for 11 October, 1961.
Measured values: • 11.10.61
△ 13.10.61.

density and the size of water droplets. Also, multiple reflection within the cloud (Möller 1957) and below it (Loewe 1961, 1962) complicates the problem.

The albedo of various types of cloud as a function of the thickness of the cloud is given by Möller (1957). The radiation transparency as determined by Haurwitz (1945-48) and Atkins (1951) is as follows for different types of cloud:

fog 0·14; stratus 0·25; stratocumulus 0·33;

middle clouds 0·4 to 0·5; cirrus 0·80. Variation between the different cloud types are seen to be very large.

The effect of cloud on the global radiation can be demonstrated by comparing the global radiation values for clear and overcast sky (G_o and G_1 respectively). These are shown in Fig. 4.3.1, together with values of the diffuse sky radiation (D_o) and the daily radiation total (B_o) or insolation received by a horizontal unit area outside the atmosphere, where

$$B_o = 2S^{(r)} \int_o^{t_o} [\sin \phi \sin \delta - \cos \phi \cos \delta \cos t]\, dt.$$

(Alisov, Drosdow and Rubinstein, 1956); where t_o is the hour-angle at sunset given by

$$\cos t_o = -\tan \phi \tan \delta$$

$S^{(r)}$ is the solar constant

Clear sky values of global and diffuse radiation, on all days on which

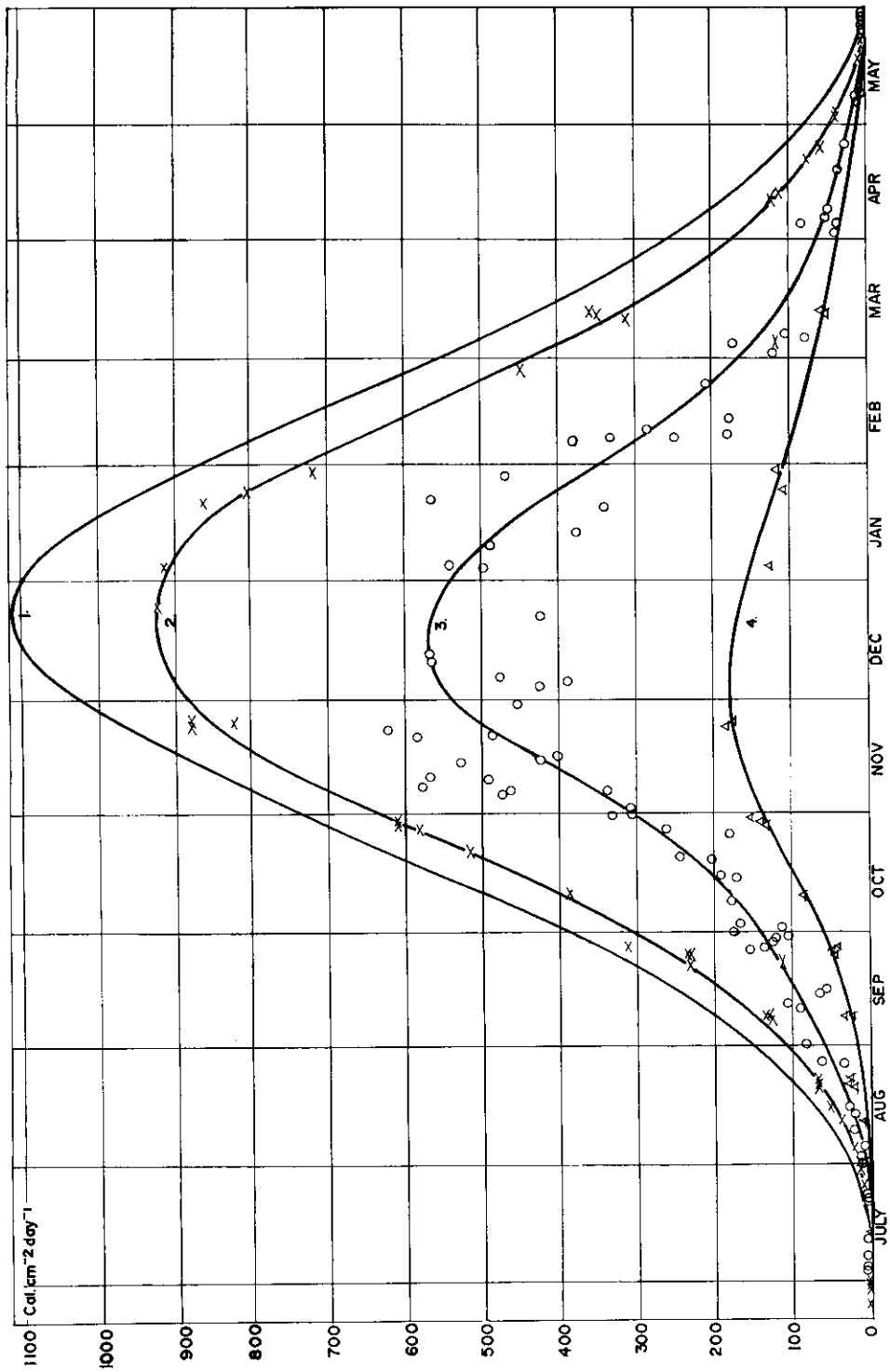

FIG. 4.3.1. Daily insolation at Mawson.

1. Horizontal surface outside atmosphere, B_o.
2. Daily insolation—clear sky all day, $\times$ G_o.
3. Daily insolation—overcast sky all day, o G_1.
4. Daily insolation from a clear sky, $\triangle$ D_o.

there was less than one-eighth of cloud all day during 1961 and 1962, were included; on overcast days global radiation was included on days on which there were more than seven-eighths of cloud all day during 1961 and 1962. Values of B_o were taken at approximately monthly intervals, as calculated in Alisov et al., and were corrected for actual solar distance, using solar constant values in Linke (1953).

The scatter of the values of the daily insolation with a clear sky, G_o (curve 2), is small as expected, but large for the values of the daily insolation with an overcast sky, G_1 (curve 3). This reflects the various factors mentioned earlier. Smoothed mean curves were drawn through the measured points. From these curves twice-monthly values of all quantities shown were read off and recorded in Table 4.3.1.

TABLE 4.3.1

Daily values of Global (G_0) and Diffuse radiation (D_0) with a clear sky and an overcast sky (G_1) and daily insolation with no atmosphere (B_0).

cal cm^{-2} day^{-1}

Date	B_0	G_0	G_1	D_0	$\frac{G_1}{G_0}$%	$\frac{G_0}{B_0}$%	$\frac{D_0}{G_0}$%
1·7	0	0	0	0	—	—	—
15·7	0	0	0	0	—	—	—
1·8	27	15	5	3	33	56	20·0
15·8	70	47	23	10	49	67	21·3
1·9	156	105	55	18	52	67	17·2
15·9	265	185	93	32	50	70	17·3
1·10	398	297	138	60	47	75	20·2
15·10	552	448	198	98	44	81	21·9
1·11	723	627	300	139	48	87	22·2
15·11	873	780	426	167	55	89	21·4
1·12	1015	880	535	180	61	87	20·5
15·12	1100	918	570	176	62	83	19·2
1·1	1098	914	547	158	60	83	17·3
15·1	1010	865	467	136	54	86	15·7
1·2	860	732	350	110	48	85	15·0
15·2	704	575	243	86	42	82	15·0
1·3	560	436	168	71	39	78	16·3
15·3	400	298	111	52	37	75	17·5
1·4	258	182	67	35	37	71	19·3
15·4	151	109	38	22	37	67	21·8
1·5	74	50	18	11	36	67	22·0
15·5	25	12	5	3	42	48	25·0
1·6	0	0	0	0	—	—	—
15·6	0	0	0	0	—	—	—

In addition the ratios $\frac{G_o}{B_o}$, $\frac{D_o}{G_o}$ and $\frac{G_1}{G_o}$ were calculated for these twice-monthly values and plotted in Fig. 4.3.2.

The ratio $\frac{G_o}{B_o}$ indicates the amount of radiation absorbed and scattered by a clear atmosphere. Up to 89% of the solar radiation incident on unit area of the atmosphere of the earth above Mawson reaches the ground in summer, with the highest peak in November, this month being the clearest period throughout the

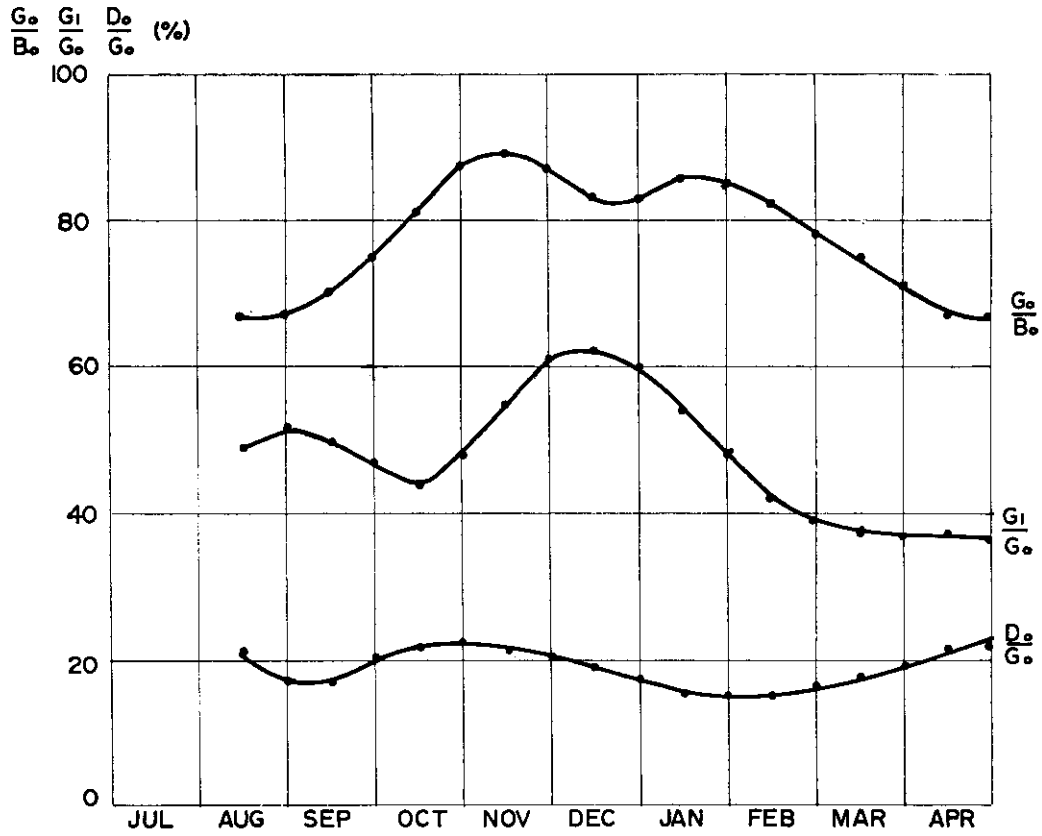

FIG. 4.3.2. Seasonal variations of the ratios of daily radiation totals (means).

year as discussed already in Section 2. In winter, only half of the incident solar radiation reaches the ground. The ratio $\frac{G_o}{B_o}$ is fairly constant throughout the summer, when a mean value of 85% can be taken.

The ratio $\frac{D_o}{G_o}$ is constant, too, over a long period. It reaches a minimum value of 15% in summer and approaches infinity in midwinter with the sun constantly below the horizon. This increase in the ratio $\frac{D_o}{G_o}$ towards winter is not shown very well in Fig. 4.3.2, due to lack of experimental data and increased inaccuracy of the ratio $\frac{D_o}{G_o}$ as this ratio decreases. It is nevertheless apparent.

The ratio $\frac{G_1}{G_o}$ (Fig. 4.3.2) has a maximum of 62% in December and a minimum of 36% in April. A number of polar observation stations both in the Northern and in the Southern Hemisphere show widely varying seasonal variation of the ratio

$\frac{G_1}{G_o}$ (results summarized by Möller (1957)). The values of $\frac{G_1}{G_o}$ in polar regions are, however, much larger than in temperate regions. Apart from a lower water content of the clouds in polar regions, Ångström and Tryselius (1934) explained the higher polar values to be due to multiple reflection between the snow surface and the cloud base, both having high albedos. The low values of $\frac{G_1}{G_o}$ in late summer and early autumn may thus be explained as being due to the fact that the ground albedo is least in that period, since there is much open water near the station. The rock around the station is exposed and no longer under a snow cover, and the ice surface has a lower albedo, due to melt water running on its surface. Absorption may also be higher due to an increased cloud thickness in the presence of more open water. In spring and early summer the albedo of the ground is highest, the sea ice extends far out to sea, cloud thickness is possibly smaller and hence the $\frac{G_1}{G_o}$ values are higher. Under these conditions multiple reflections between the ground and the cloud-base produce "white-out" conditions in which all the light is diffuse and scattered equally in all directions. Shadows disappear and navigation on a surface covered with sastrugi becomes very difficult. Hanson's (1960) photographs show white-out conditions well. Schulthess (1960) also gives excellent photos of the same phenomenon.

4.4. GLOBAL RADIATION WITH A BROKEN CLOUD-COVER

The global radiation at Mawson has so far been discussed under the conditions of clear sky and overcast sky. Typical curves of their diurnal variation are shown in Fig. 4.4.1. With a broken and rapidly changing cloud-cover (Fig. 4.4.1), no simple relation between radiation and cloud-cover can be expected to exist, apart from the obvious difficulty to measure the rapidly changing elements. A formula to estimate the global radiation under these conditions, although preferably to be used for mean conditions of cloud cover, has been put forward by Ångström (1934):

$$G = G_o [a - S (1 - a)],$$

where G = daily insolation with a relative duration of sunshine, S, G_o = daily insolation with a clear sky, $a = \frac{G_1}{G_o}$ with a dense overcast. In a diagram with abscissa S and ordinate $\frac{G}{G_o}$ this is a straight line.

To test this equation, all the measured values of G and S of the months October to March during 1961 and 1962 were used. The data were grouped for values of S = 0, 1-20, 21-40, 41-60, 61-80, 81-90 and > 90%. Values of G_o were taken from section 4.3, values of the maximum possible duration of sunshine from Section 2.2. The data are presented in Table 4.4.1. Graphical representation of the group mean values of the total period is given in Fig. 4.4.2.

The group means in Fig. 4.4.2 lie on a smooth curve, not on a straight line. However, a straight line could be drawn through the group means without much

FIG. 4.4.1. Diurnal variation of the global radiation (G) and diffuse sky radiation (D) in summer at Mawson on days with a clear, variable and overcast sky; typical curves.

TABLE 4.4.1

RELATIVE DAILY INSOLATION $\frac{G}{G_o}$ AS A FUNCTION OF THE RELATIVE DURATION OF SUNSHINE S

(October–March, 1961 and 1962 at Mawson)

Groups	January			February			March			October			November			December			Total		
S%	S	$\frac{G}{G_o}$	Freq	S	$\frac{G}{G_o}$	Freq	S	$\frac{G}{G_o}$	Freq	S	$\frac{G}{G_o}$	Freq	S	$\frac{G}{G_o}$	Freq	S	$\frac{G}{G_o}$	Freq	S	$\frac{G}{G_o}$	Freq
0	0	0·426	4	0	0·409	10	0	0·433	15	0	0·420	13	0	0·626	8	0	0·514	6	0	0·462	56
1–20	0·09	0·593	12	0·08	0·545	7	0·07	0·500	4	0·08	0·623	5	0·07	0·702	14	0·09	0·566	11	0·08	0·606	53
21–40	0·27	0·745	6	0·32	0·606	8	0·27	0·670	5	0·29	0·730	6	0·29	0·825	6	0·28	0·793	3	0·29	0·717	34
41–60	0·51	0·784	5	0·50	0·809	5	0·52	0·800	4	0·51	0·837	10	0·55	0·867	6	0·52	0·823	9	0·52	0·824	39
61–80	0·67	0·918	4	0·71	0·843	3	0·71	0·952	8	0·75	0·958	6	0·71	0·942	6	0·71	0·786	7	0·71	0·903	34
81–90	0·87	0·974	7	0·81	1·020	1	0·85	1·042	9	0·86	0·937	7	0·85	0·970	3	0·86	0·891	8	0·86	0·967	35
>90	0·98	0·984	20	0·99	0·964	9	1·00	1·033	9	0·97	0·975	13	0·97	0·988	12	0·98	0·933	14	0·98	0·976	76
TOTAL	—	—	58	—	—	43	—	—	53	—	—	60	—	—	54	—	—	58	—	—	326

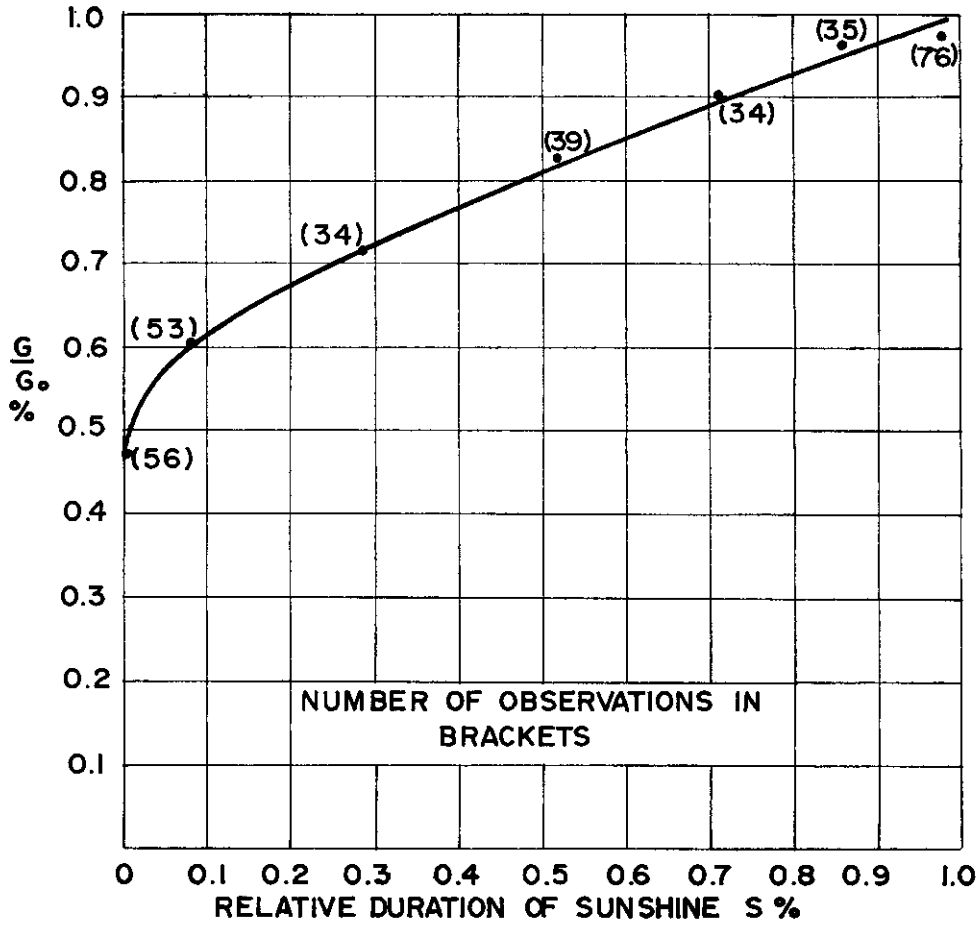

FIG. 4.4.2. Relative isolation (G/G_o) as a function of the relative duration of sunshine (S). October to March, 1961 and 1962, Mawson.

loss of accuracy, except for the group mean of $\frac{G}{G_o}$ for $S = 0$ which would be overestimated by approximately 10%. The Ångström formula could thus be used for all practical purposes. The curve shows that with an increase in cloud, the screening of the sun by the cloud is compensated for approximately by increased diffuse radiation from the cloud.

Strictly, due to the effect of strong forward scattering by thin clouds or from the cloud boundaries, the diffuse sky radiation increases with increased cloudiness. It reaches a maximum at 8/10 cloud-cover, then decreases rapidly until, at 10/10 cloud, it has approximately the same value as with a clear sky (Möller 1957). Correspondingly, the global radiation does not quite decrease linearly with an increase in cloud-cover as put forward by Ångström. Second or third order corrections must be applied. This is well shown by the Mawson results. At greater heights,

or also presumably at higher latitudes, the cloud thickness is usually smaller and the diffuse sky radiation increases with cloud cover up to 10/10.

If the duration of sunshine is known, it is thus possible to derive the global radiation for any cloud conditions using the curve in Fig. 4.4.2. This was the method used to derive data on days on which the global radiation was not measured, due to break-down of instruments, etc. The computation of the global radiation by this method for individual days rather than for means may, however, result in relatively large errors.

4.5. MONTHLY INSOLATION

To obtain an idea of the seasonal variation of the incoming radiation, the measured daily totals of the global radiation were added to give the monthly insolation. The measured daily values of the diffuse sky radiation were also added to give the monthly insolation from sky alone. The data are given in Table 4.5.1 below and in Fig. 4.5.1.

TABLE 4.5.1

MONTHLY INSOLATION G AT MAWSON (k cal cm^{-2}) AND MONTHLY INSOLATION FROM SKY (D)

						1961						
	Jan.	Feb.	Mar.	Apr.	May	Jun.	Jul.	Aug.	Sep.	Oct.	Nov.	Dec.
G		10·96	6·22	2·10	0·34	0·01	0·09	1·27	3·76	11·84	19·89	22·10
D		—	—	—	0·17	0	0·05	0·77	2·19	5·55	9·02	10·72
						1962						
G	21·56	11·16	6·99	2·21	0·28	0	0·10	1·35	4·44	10·70	19·27	21·47
D	7·62	5·60	3·21	1·30	0·20	0	0·05	0·66	2·17	5·22	8·09	10·25
						1963						
G	20·70											
D	7·86											

The summer values of the monthly insolation are high compared with values at lower latitudes (Rusin 1961). This is partly due to the clear and dry atmosphere of the Antarctic coastal region and also due to the high insolation with cloudy skies, owing to multiple reflection between ground and cloud. This is supported by a comparison of the mean Mawson values with values of monthly insolation at other Antarctic stations (Table 4.5.2 and Fig. 4.5.2) taken from Liljequist (1956), Rusin (1958), and Thomson and MacDonald (1962).

The first three stations listed in Table 4.5.2 show monthly totals which lie very close to one another. All these stations are within 5° of latitude, close to the coast, hence similar meteorological conditions probably exist for all of them. The last-mentioned station, Scott Base, lies further south. Its yearly total of the global radiation is not very different from the other stations but the monthly values in winter are much smaller.

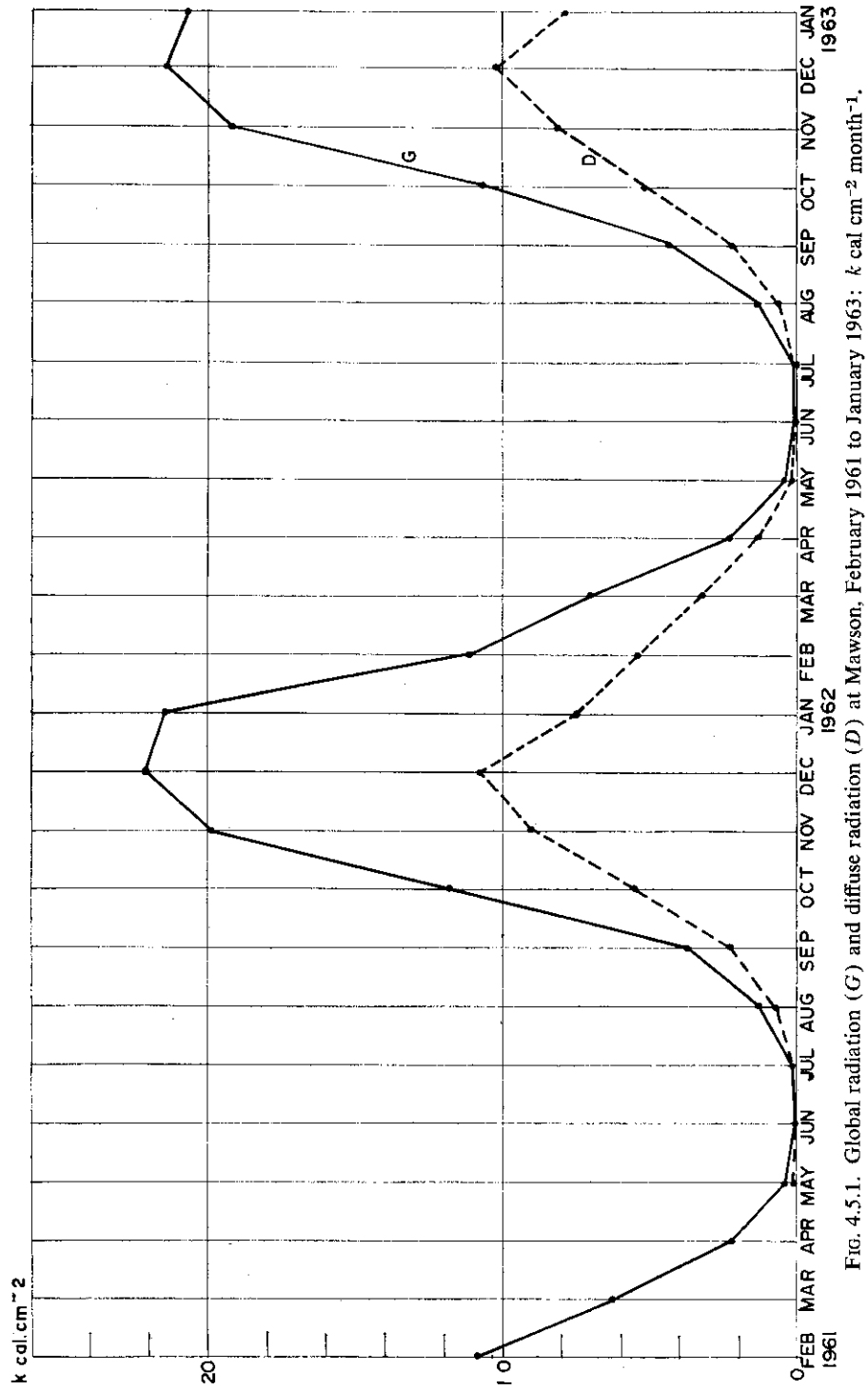

FIG. 4.5.1. Global radiation (G) and diffuse radiation (D) at Mawson, February 1961 to January 1963: k cal cm^{-2} month^{-1}.

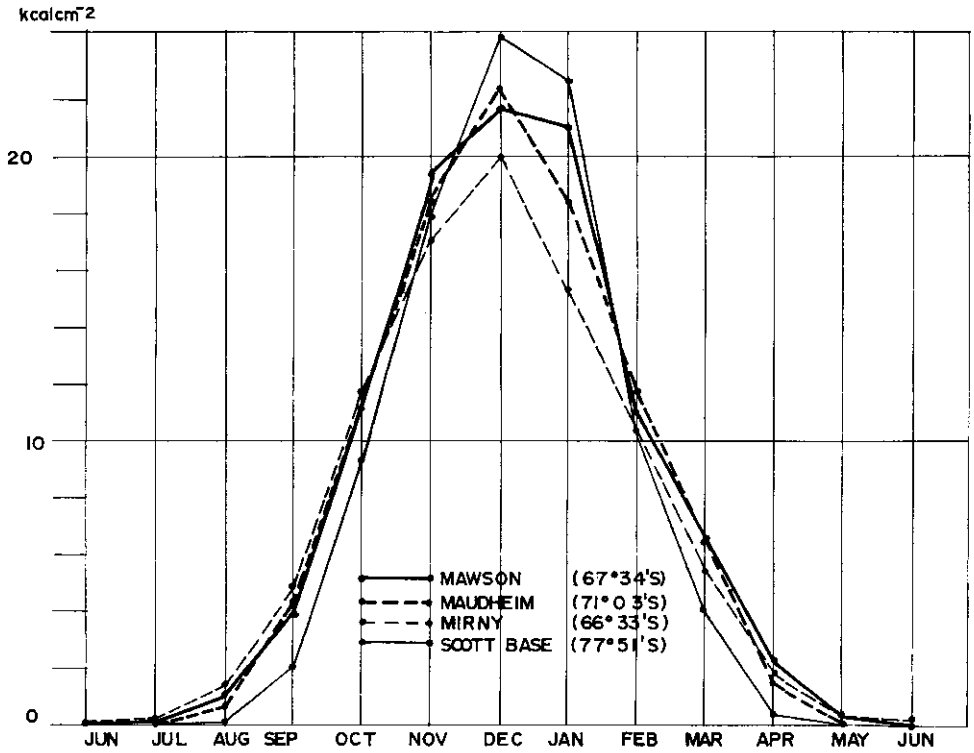

FIG. 4.5.2. Monthly totals of global radiation, k cal cm^{-2} month^{-1}.

TABLE 4.5.2

MONTHLY TOTALS OF THE GLOBAL RADIATION (k cal cm^{-2}) AT SEVERAL ANTARCTIC STATIONS

	Jan.	Feb.	Mar.	Apr.	May	Jun.	Jul.	Aug.	Sep.	Oct.	Nov.	Dec.	Year
Mawson	21·13	11·06	6·60	2·15	0·31	0	0·1	1·31	4·10	11·27	19·58	21·78	99·39
Maudheim	18·43	11·72	6·41	1·59	0·12	0	0	0·75	4·25	11·24	18·79	22·28	95·58
Mirny	15·40	—	5·6	1·8	0·4	0·1	0·2	1·5	4·9	11·9	17·2	20·0	90·7
Scott Base	22·69	10·24	3·97	0·38	0	0	0	0·07	2·06	9·50	18·21	24·22	91·34

Periods of observation:

Mawson	(67°34'S)	: Feb. '61-Jan. '63
Maudheim	(71°03'S)	: Feb. '50-Jan. '52
Mirny	(66°33'S)	: Jan. '56-Dec. '56
Scott Base	(77°51'S)	: Mar. '57-Feb. '59

The variation of the monthly global radiation of the coastal stations as a function of latitude is reflected in Fig. 4.5.3. This diagram shows the daily global radiation outside the Earth's atmosphere as a function of latitude. It was constructed using data from Allisow, Drosdow and Rubinstein (1956) and based on a mean solar constant of 2·0 cal cm^{-2} min^{-1}. If the turbidity and water-vapour content of the atmosphere at the various coastal stations are assumed as not varying greatly from one station to the next, then the variation of the global radiation with latitude is given by the shape of Fig. 4.5.3, although the magnitudes will be smaller. The assumption of very similar values of turbidity and water-vapour along

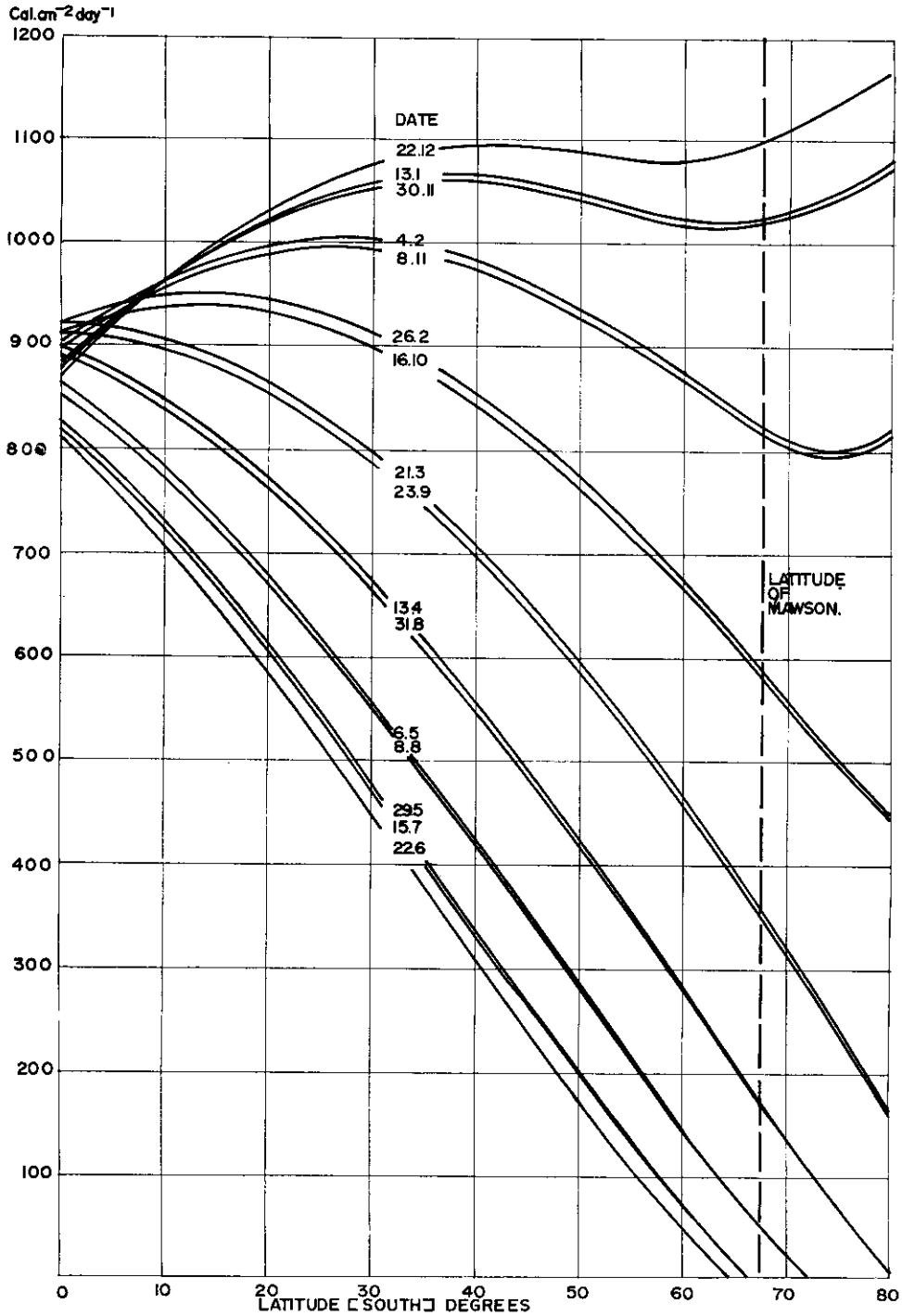

FIG. 4.5.3. Daily global radiation on a horizontal surface outside the Earth's atmosphere on a number of selected days (theoretical curves according to Allisow, Drosdow and Rubinstein).

the coast of eastern Antarctica, at least, has been shown to be justified in Section 3. Fig. 4.5.3 then shows the observed similarity of summer data and also the higher dependence on latitude in the winter months in Table 4.5.2.

Rusin (1961) constructed diagrams of the variation of the monthly global radiation with latitude from measurements at various coastal and plateau stations in Antarctica. The monthly variation of global radiation, according to this, is fairly constant between 65° and 75° south at coastal stations, only the winter values decrease somewhat with increasing latitude, as also demonstrated by the summarized measurements in Table 4.5.2 above. The curve of measurements at stations in the interior of the continent show large variation of the global radiation with latitude, i.e., in the case of the Antarctic continent with height. The highest values of the global radiation (approximately 31 k cal cm^{-2} $month^{-1}$) are recorded in summer at Komsomolskaya and Sovjetskaya which lie between latitude 74 and 80 at 3500 metres altitude, nearly the maximum height of the Antarctic plateau. Values at the South Pole at a lower height (2900 metres) are somewhat smaller (25 k cal cm^{-2} $month^{-1}$).

5. NET FLUX OF LONG-WAVE RADIATION

5.1. NET FLUX OF LONG-WAVE RADIATION WITH A CLEAR AND AN OVERCAST SKY

The problems associated with long-wave radiation in the region 4 μ to 100 μ are basically different from those in the short-wave region. According to Möller (1957) the extraterrestrial long-wave radiation is negligible and has been observed in the wave-length region 9 μ to 12 μ only. Scattering by gas molecules and dust particles is generally negligible, since these particles are small in comparison with the wave-lengths under consideration. In clouds, a majority of the water droplets have sizes of the order of the wave-lengths under discussion; however, scattering in this case is small compared with absorption. The absorption of the radiation by the atmospheric gases and therefore, also, the emission of the temperature radiation, are the most important processes; also, the emission from the surface and clouds. Finally, the long-wave radiation is not directional but diffuse and the emission of radiation by a gas is determined by the gas itself and its temperature only.

For the Earth's surface, empirical equations for the atmospheric long-wave radiation have been formulated after a great many measurements by Ångström (1915), Brunt (1932), Elsasser (1942) and others, (see Section 6.3). All these equations are based on observations of temperature and humidity at the surface. Lönnquist (1959) has modified these equations, introducing the total water content of the atmosphere, which is usually obtained from radiosonde data. A recent equation by Swinbank (1963) is based on temperature observations only.

The most elaborate and ambitious studies have produced radiation charts based on spectroscopic data on water-vapour and carbon dioxide absorption (Elsasser 1942) and (Möller 1943). Reference should be made to Section 6.2.

At Mawson the instrument available for measuring long-wave radiation was an all-wave net radio-meter. The net flux of long-wave radiation could thus be measured only with the sun below the horizon, i.e., with zero net short-wave flux. This method provided almost continuous recording of the net flux of long-wave

radiation throughout the winter. For the summer values a theoretical procedure was used; this will be discussed in Section 5.3.

At the level of the instrument the outgoing net flux of long-wave radiation, assuming the ice surface to be a black body, is given by

$$N_L = \sigma T^4 - A,$$

where σ = the Stefan-Boltzmann const. $= 0{\cdot}826 \times 10^{-10}$ cal cm^{-2} min^{-1} deg^{-4};

T = temperature ($^\circ K$) of the instrument and surrounding air which are assumed to be in thermal equilibrium;

A = long-wave atmospheric radiation.

The net flux of long-wave radiation at the ice surface will be slightly different from that at the instrument level when a steep temperature gradient exists near the surface. The likelihood of a steep temperature gradient at Mawson, i.e., a strong inversion with the sun below -3° is, however, small, since strong, almost continuous katabatic winds with an annual mean windspeed of 10 m sec^{-1} at 10 metres height, will then give neutral stability, hence small temperature differences and negligible differences in σT^4 (see also Section 5.2).

The analysis makes it necessary to determine first the solar height at which the short-wave radiation becomes negligible in comparison with the long-wave radiation.

TABLE 5.1.1

FREQUENCY DISTRIBUTION OF THE LONG-WAVE RADIATION NET FLUX

	Net flux at the instrument level cal cm^{-2}min^{-1}	Overcast sky		Clear sky	
		Number of observations	%	Number of observations	%
Incoming net flux		n	frequency		frequency
	0·010–0	10	4·2		
	0 –0.010	57	23·9		
	0·011–0·020	67	28·2		
	0·021–0·030	42	17·6		
	0·031–0·040	23	9·7		
	0·041–0·050	17	7·2		
	0·051–0·060	12	5·0		
	0·061–0·070	4	1·7		
	0·071–0·080	6	2·5		
Outgoing net flux	0·081–0·090				
	0·091–0·100				
	0·101–0·110				
	0·111–0·120			31	18·4
	0·121–0·130			54	32·1
	0·131–0·140			49	29·2
	0·141–0·150			28	16·7
	0·151–0·160			5	3·0
	0·161–0·170			1	0·6
	TOTAL	238	100·0	168	100·0
	MEAN	0·022 cal cm^{-2}min^{-1}		0·130 cal cm^{-2}min^{-1}	

Bullrich (1948) determined the global radiation as a function of the solar height, with the sun below the horizon, and found the global radiation to decrease by an order of magnitude with a decrease in solar height of 2·5°. This compares well with Liljequist's (1956) measurements, which showed that the diffuse clear sky radiation amounted to 0·002 cal cm^{-2} min^{-1} with the sun 3° below the horizon. The short-wave net flux at these solar altitudes thus enters the total net flux only as a very small term which can be neglected.

From the continuous recording of the net long-wave radiation values at the synoptic hours at three-hour intervals and with the sun below —3° have been used. The air temperature measured at the synoptic hours in a Stevenson meteorological screen was taken to be the temperature at the instrument level.

Altogether 406 measurements of the net flux of long-wave radiation were analysed, 238 with an overcast sky and 168 with a clear sky. Table 5.1.1 shows the frequency distribution of the measurements.

It must be remembered that these measurements only refer to situations with the sun at least 3° below the horizon. Summer values are thus missing, and also the daytime values in spring and autumn. The analysis below cannot thus be considered to give average yearly values. Its main interest lies in the fact that it shows very markedly the different radiation conditions resulting from different states of the sky.

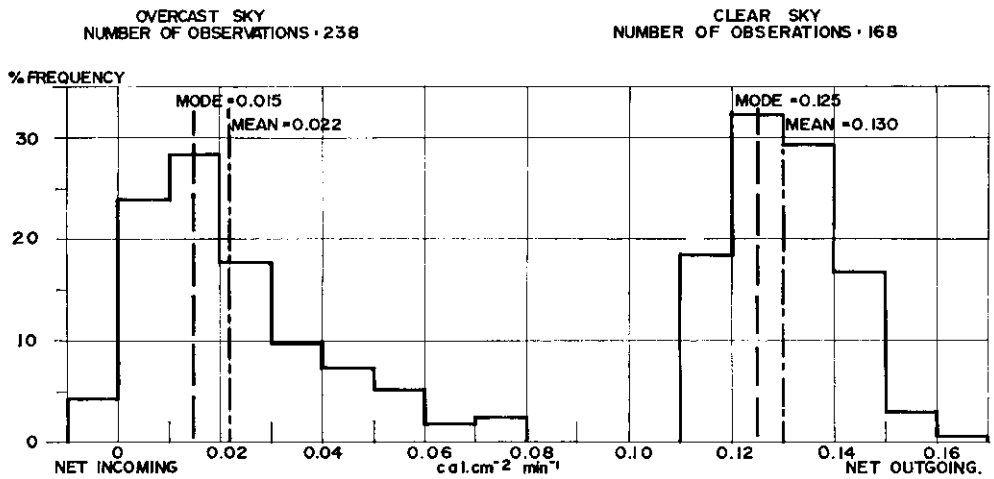

FIG. 5.1.1. Per cent frequencies of net flux of long-wave radiation on overcast days and clear days—sun $\leqslant$ 3° below horizon, Mawson 1961.

The general features of the frequency distributions are shown in the histograms in Fig. 5.1.1. Modes and means were determined from the histograms. The net flux of long-wave radiation with a clear sky has a mean value of 0·130 cal cm^{-2} min^{-1} and a mode of 0·125 cal cm^{-2} min^{-1}, the distribution curve being positively skewed. With an overcast sky the mean value is only 0·022 cal cm^{-2} min^{-1} and the mode 0·015 cal cm^{-2} min^{-1}, the curve also showing positive skewness. The distribution curves are well separated and do not overlap.

When a dense cloud cover is present, this cloud practically radiates as a black body with a temperature approximately the same as that of the cloud base. The back-radiation from the cloud thus decreases the net outgoing flux at the surface considerably. The different values in each of the two groups must be explained in terms of temperature and wind speed. This will be attempted in the next Section.

5.2. NET LONG-WAVE FLUX WITH A CLEAR SKY IN RELATION TO TEMPERATURE, WINDSPEED AND SURFACE INVERSION STRENGTH

Measurements of the net flux of long-wave radiation at Arctic and Antarctic stations have shown that the net long-wave flux decreases with temperature at the instrument level (Wexler 1941). The decrease with temperature varies for the different stations, but in most cases is fairly high and is attributed to the effects exercised by the presence of surface inversions. Wexler's summary of results is shown in Fig. 5.2.1.

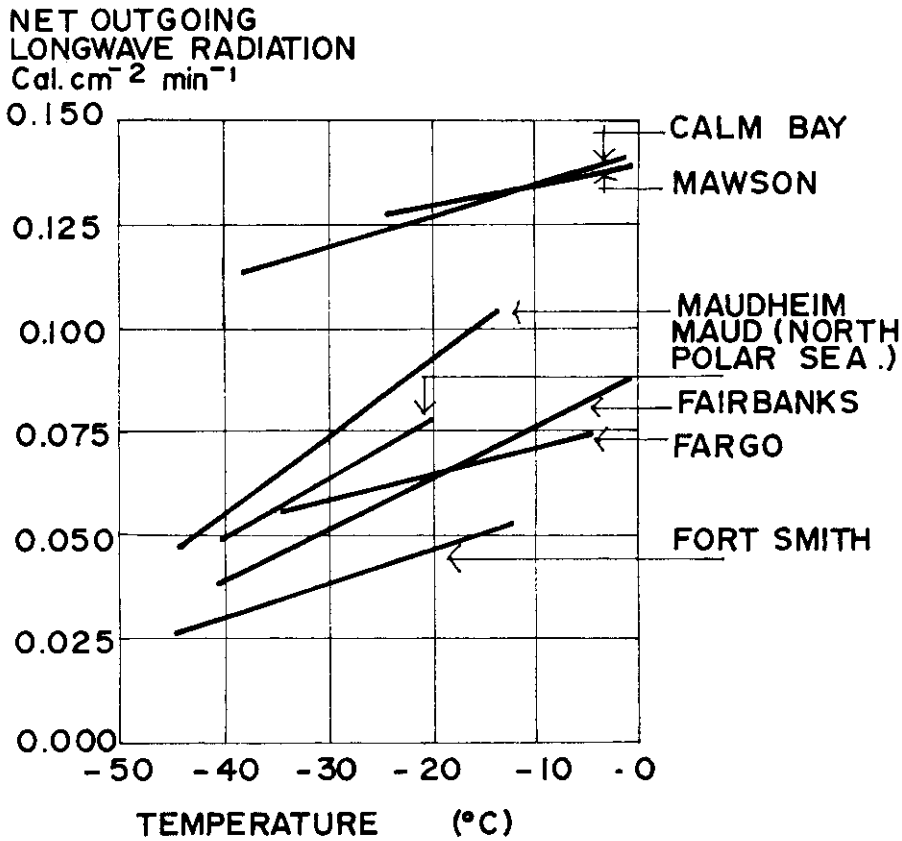

FIG. 5.2.1. Net long-wave radiation with a clear sky in relation to the temperature near the surface: comparison of some observation series from polar or continental stations.

The 168 clear-sky measurements of the long-wave flux at Mawson were compared with the air temperature at instrument level and are presented in Fig. 5.2.2.

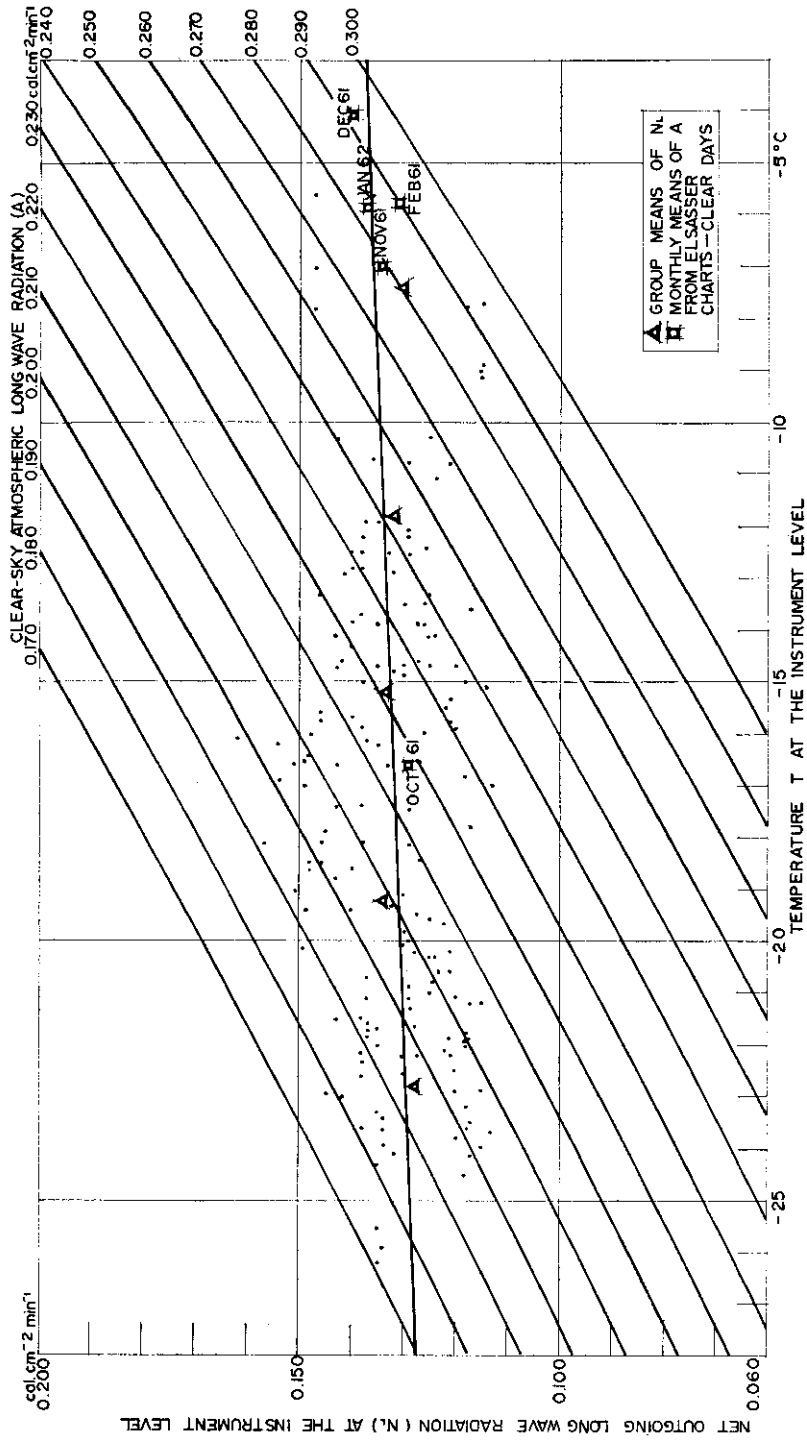

FIG. 5.2.2. Measured values of the net outgoing long-wave radiation with a clear sky at Mawson, 1961.

Isopleths of the atmospheric long-wave radiation calculated from the equation,

$$A = \sigma T^4 - N_L,$$

were also entered on the diagram. The rings represent the measured values of the long-wave flux N_L at temperature T. Group means for 4° intervals are shown as triangles. To be able to derive a relationship between N_L and T for the higher temperatures in summer, data derived for the summer months October to February from an Elsasser chart were also included (squares) (see Section 6.2). These data comprise the mean monthly atmospheric radiation on all clear days obtained from an Elsasser radiation chart.

The scatter in Fig. 5.2.2 is high but it can be seen that a straight line can be drawn through the group means and the points obtained by calculation from the Elsasser chart. There is remarkably good agreement where they overlap. The long-wave net flux can be seen to be dependent on the temperature at instrument level, although the difference is only 7% for the range of 0°C in summer to —25°C in winter, approximately the minimum temperature to be expected at Mawson.

The dependence of the long-wave flux on temperature seems to be somewhat less than for most of the stations quoted by Wexler. Also, the magnitude of the net outgoing flux is higher than for most of the other stations with exception of Calm Bay, in Franz Josef Land, where the net flux decrease with temperature is also very similar to that at Mawson.

To explain the relatively high Mawson values and also the small dependence on temperature, Liljequist's discussion of the Maudheim data will here be referred to. Liljequist has shown that the temperature inversion over a snow surface decreases with increased wind and that, with winds higher than 8 to 9 m/sec at the 10-metre level, no marked inversion could be maintained. He further showed that with winds higher than 8 to 9 m/sec the net outgoing long-wave flux is considerably higher than at wind speeds lower than 8 to 9 m/sec. Above 8 to 9 m/sec the air flow becomes fully rough over a snow surface and, since for winter conditions, with no solar radiation, the net long-wave flux N_L is

$$N_L = Q - C$$

(where Q = turbulent heat transfer, C = heat conduction in the snow towards the surface), the net long-wave flux increases rapidly at 8 to 9 m/sec if the conduction in the snow is considered to vary only little.

At Maudheim the average annual windspeed was approximately 7 m/sec and the average windspeed during long-wave net radiation measurements 5·6 m/sec. By contrast at Mawson at the 10 metre level, the average wind was 10·5 m/sec and almost the same value applied during long-wave net radiation measurements, i.e., 10·2 m/sec, since strong katabatic winds were blowing almost continuously at Mawson. In summer, during the afternoon at Mawson short diurnal lulls occur in the wind speed; but the frequency of calms and winds from directions other than the katabatic wind direction is only approximately 10%. In winter there is no diurnal change in the katabatic wind speed (Streten 1963; also unpublished data by the author).

This would explain the much higher values of the net long-wave radiation at

Mawson, assuming the Maudheim findings hold true for the similar conditions at Mawson, since the conditions of wind at the two stations result in a difference in the inversion strength near the surface.

To test the validity of this assumption, the magnitude of the temperature inversion at Mawson was determined. This magnitude was defined by the difference $(T_x - T_o)$ where T_x = maximum tropospheric temperature (°C) and T_o = surface temperature (°C). Thirty radiosonde flights and 107 corresponding measurements of the outgoing long-wave radiation flux on clear days were analysed. These are given in Table 5.2.1.

TABLE 5.2.1

THE EFFECT OF THE SURFACE INVERSION STRENGTH ON THE OUT-GOING LONG-WAVE RADIATION FLUX AT MAWSON ON CLEAR DAYS

Surface inversion $(T_x - T_o)$ °C			Outgoing long-wave flux (cal $cm^{-2}min^{-1}$)	Number of measurements of long-wave flux
Group	Mean	No. of flights		
0 -1·4	0·6	10	0·138	31
1·5-2·9	2·4	12	0·133	43
⩾3	3·5	8	0·130	33

The maximum inversion strength does not exceed 4°C. This is much lower than the very pronounced inversions of up to 25°C measured by Liljequist. The predicted tendency of the outgoing long-wave radiation to decrease with an increasing inversion strength is also clearly shown.

The magnitude of the temperature inversion thus affects the outgoing long-wave radiation. The inversion strength itself is controlled by the wind velocity, and the constancy and magnitude of the wind speed at Mawson produces small temperature inversions and fairly constant values of the outgoing long-wave radiation.

5.3. ANNUAL VARIATION OF THE NET LONG-WAVE RADIATION FLUX

In the two preceding sections the dependence of the net long-wave radiation on cloud, temperature and wind conditions has been shown. To determine the annual variation of all components of the radiation balance, it has been necessary to estimate average values of the long-wave net flux for the summer months for which there are no direct measurements.

For the conditions of clear sky the following method was adopted: in Fig. 5.2.2 the relationship between the temperature at instrument level and the net outgoing long-wave radiation was determined, including data from radiosonde flights on clear days in summer. All these radiosonde flights took place at 00 G.M.T., early in the morning at Mawson when the katabatic wind was still strong. The curve is thus applicable for typical conditions at Mawson with a clear sky and katabatic wind of approximately 10 m/sec. The monthly mean temperatures were next determined from the daily 3-hourly observations for all clear days. They are shown in Table 5.3.1, together with the monthly number of observations.

TABLE 5.3.1

MONTHLY MEAN TEMPERATURES WITH A CLEAR SKY (MAWSON 1961)

Month	Temp. (°C)	Number of observations	Month	Temp. (°C)	Number of observations
Jan.	−3·1	56	Jul.	−23·3	52
Feb.	−2·7	47	Aug.	−22·0	69
Mar.	−10·9	35	Sep.	−17·2	32
Apr.	−16·0	59	Oct.	−14·7	63
May	−14·4	37	Nov.	−3·2	47
Jun.	−19·8	54	Dec.	−0·6	51

The corresponding net long-wave flux was read off from Fig. 5.2.2. Also, all the measured winter values were averaged to give monthly means. The results are summarized in Table 5.3.2.

TABLE 5.3.2

OUTGOING LONGWAVE NET FLUX (N_L) ON CLEAR DAYS (MONTHLY MEANS)
cal cm^{-2} min^{-1}

Month	N_L (calculated from mean temp.)	N_L (measured)	Number of measurements
Jan.	·137		
Feb.	·138	·139	6
Mar.	·134	·133	8
Apr.	·132	·141	37
May	·133	·131	34
Jun.	·130	·130	16
Jul.	·129	·122	15
Aug.	·130	·120	18
Sep.	·131	·131	13
Oct.	·133	·133	21
Nov.	·137		
Dec.	·138		

The agreement between calculated and measured values is good. The values finally adopted are the values calculated from the mean temperatures, which lie on a smooth curve, Fig. 5.3.1. The seasonal variation of the net outgoing long-wave flux is seen to be remarkably small, since the range of temperature from which the values were derived was not large, i.e., less than 25°C.

At Maudheim, however, where the annual temperature range is much higher, the effects of the temperature variation will tend to produce larger changes in the net long-wave outgoing radiation compared with Mawson.

For overcast conditions, a higher number of actual measurements of the net long-wave flux were made than for clear-sky conditions. These measurements are given in Table 5.3.3.

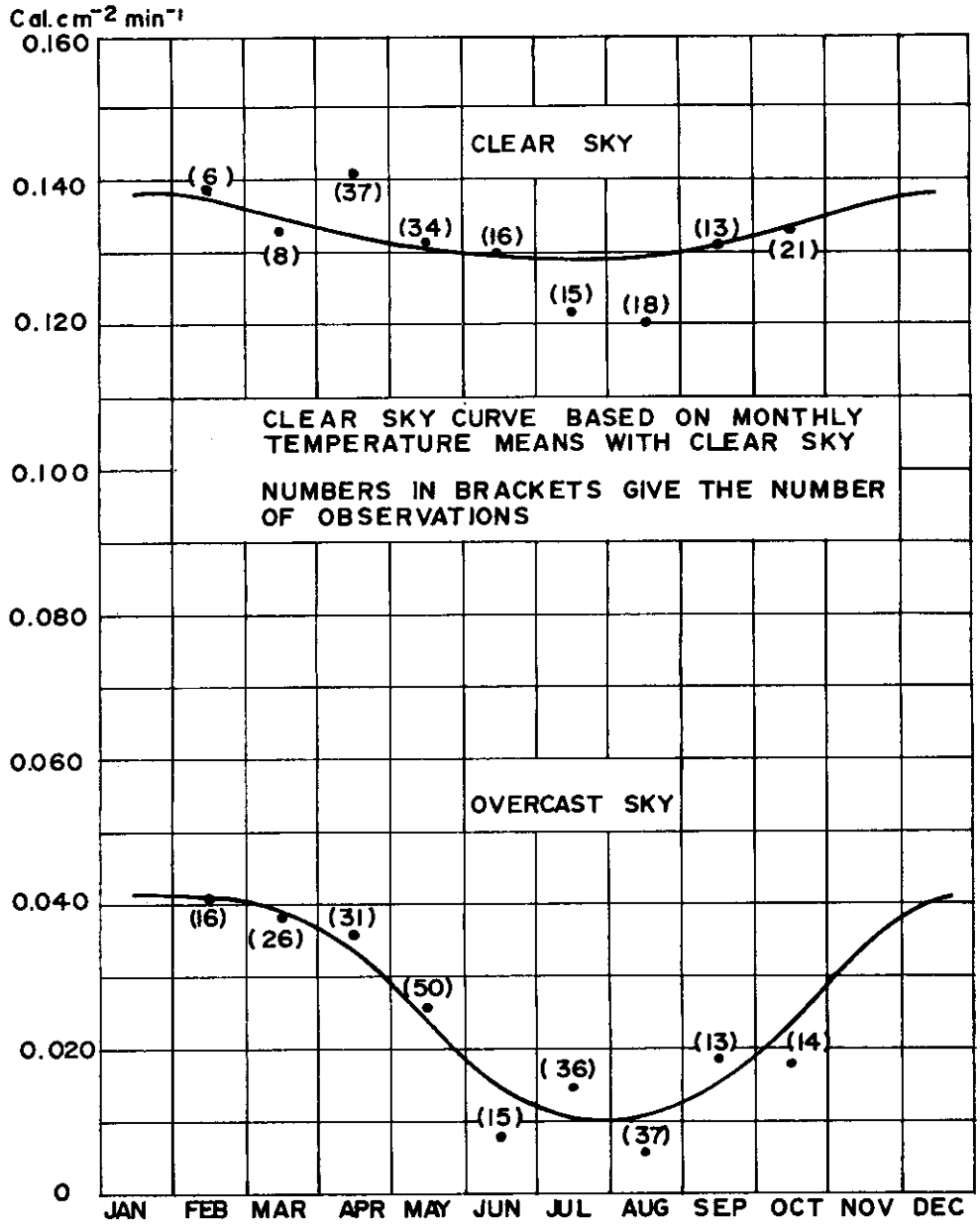

FIG. 5.3.1. Outgoing long-wave net flux (N_L) on clear days and overcast days (monthly means).

Drawn in Fig. 5.3.1, these values were connected by a smooth curve and the mean values for the summer months were extrapolated from this curve. The means for the summer months are thus somewhat doubtful for overcast conditions, but the systematic trend shown by the other months should make the possible error

small. In the absence of summer data, this procedure will suffice to give usable monthly mean values to calculate the monthly magnitudes of the components of the radiation balance. If the temperatures of cloud base and snow surface were available, the net flux could be calculated for the summer months as a difference of the black body radiation between the two surfaces, assuming that the radiation of the air layer between cloud and surface is negligible, or alternatively it could be calculated, using an Elsasser radiation chart.

TABLE 5.3.3

OUTGOING LONG-WAVE NET FLUX (N_L) ON OVERCAST DAYS (MAWSON 1961)
cal cm^{-2} min^{-1}

Month	N_L	Number of observations
Jan.	—	
Feb.	0·041	16
Mar.	0·038	26
Apr.	0·036	31
May	0·026	50
Jun.	0·008	15
Jul.	0·015	36
Aug.	0·006	37
Sep.	0·019	13
Oct.	0·018	14
Nov.	—	
Dec.	—	

The winter mean monthly values are almost zero and there is a high similarity throughout the year with the Maudheim values. Since, with an overcast sky, the difference in the surface inversions at both stations has disappeared, independent of wind conditions, one would expect this result. The values at Mawson are, however, consistently higher than the Maudheim values by 0·010 *ly* min^{-1}. This small difference can probably be attributed to small systematic errors in the two different methods of calculation. The final mean monthly values of the net flux of long-wave radiation for clear and overcast sky at Mawson are shown in Table 5.3.4 below:

TABLE 5.3.4

OUTGOING LONG-WAVE NET FLUX FROM THE SNOW SURFACE ON CLEAR DAYS AND OVERCAST DAYS. MONTHLY MEANS.
cal cm^{-2} min^{-1}

Month	Clear sky	Overcast sky
Jan.	·138	·041
Feb.	·138	·041
Mar.	·134	·039
Apr.	·132	·034
May	·131	·024
Jun.	·130	·014
Jul.	·129	·011
Aug.	·130	·011
Sep.	·131	·015
Oct.	·133	·023
Nov.	·137	·034
Dec.	·138	·041

6. ATMOSPHERIC LONG-WAVE RADIATION

6.1. ATMOSPHERIC RADIATION WITH A CLEAR SKY AND AN OVERCAST SKY

The measurements of the net long-wave flux (N_L) were discussed in Section 5. This net flux (N_L) applies to the level of the instrument which is in thermal equilibrium with the surrounding air at the temperature ($T°K$). From this temperature (T), using the Stefan-Boltzmann law, the atmospheric radiation can be calculated, i.e.,

$$A = \sigma T^4 - N_L,$$

where $\sigma = 0{\cdot}826 \times 10^{-10}$ cal cm^{-2} min^{-1} deg^{-4}.

The screen temperature at the time of the measurement of the net flux was used to calculate the atmospheric radiation. Table 6.1.1 shows the mean monthly values of the atmospheric radiation with a clear sky, averaged from individual calculations.

TABLE 6.1.1

MONTHLY VALUES OF THE ATMOSPHERIC RADIATION, A. (CLEAR SKY)
cal cm^{-2} min^{-1}

Month	A	Number of observations
Jan.	—	0
Feb.	·272	6
Mar.	·248	8
Ap.	·208	37
May	·241	34
Jun.	·189	16
Jul.	·209	15
Aug.	·207	18
Sep.	·214	13
Oct.	·233	21
Nov.	—	0
Dec.	—	0

With a clear sky, the long-wave radiation from the surface can pass through windows in the emission spectrum of the atmosphere into space. Möller (1957) gives a diagram, due to Sloan, Shaw and Williams, which shows these windows in the solar spectrum, i.e., with atmospheric absorption. The absorption in the largest window between the strong water-vapour absorption band at 6·3 μ and the equally strong carbon dioxide absorption band at 15 μ is so small, that even with the total depth of the atmosphere acting as an absorber, it could not be measured with sufficient accuracy. With an overcast sky, however, these windows are closed, since the cloud-base practically acts as a black body and the atmospheric radiation is in fact the black-body radiation from the cloud-base, neglecting the radiation of the air column between cloud and surface.

With increasing cloudiness from an initially clear sky, the windows in the atmospheric emission spectrum close and the net outgoing radiation should decrease if the surface temperature remains unchanged. If, however, there was initially a surface inversion, this inversion will decrease in magnitude when clouding over. The temperature and, therefore the black body radiation of the surface, will hence increase. This will give high values of the outgoing net radiation, even

though the atmospheric radiation has increased, i.e., with a cloudy sky, values of the net outgoing radiation may be similar to clear sky conditions with marked surface inversions. Only when the sky is completely overcast, and the surface inversion no longer present, does the net outgoing flux approach zero.

With a dense overcast sky, the atmospheric radiation must obviously be considerably higher than with a clear sky. To obtain mean monthly values of the atmospheric long-wave radiation, the same procedure was used as for calculating the clear-sky values, using the equation

$$A = \sigma T^4 - N_L$$

Results are shown in Table 6.1.2.

TABLE 6.1.2

MONTHLY VALUES OF THE ATMOSPHERIC RADIATION, A. (OVERCAST SKY)
cal cm^{-2} min^{-1}

Month	A	Number of observations
Jan.	—	—
Feb.	·404	16
Mar.	·372	26
Apr.	·364	31
May	·355	50
Jun.	·353	15
Jul.	·367	36
Aug.	·389	37
Sep.	·373	13
Oct.	·400	14
Nov.	—	—
Dec.	—	—

A comparison of Tables 6.1.1 and 6.1.2 shows that the atmospheric radiation with a clear sky is, in the monthly means, fairly consistently lower by 40% than the corresponding monthly means of the atmospheric radiation with an overcast sky. The effect of cloud on the effective radiation has been investigated by Ångström and Asklöf who found a linear relationship between the effective radiation and the cloud cover; by Bolz, Sauberer and Kreitz who found quadratic laws of the form $G_N = G_0\ (1 + 0{\cdot}27\ N^2)$ where $0 < N < 1$ is the cloud-cover; and by Raman who obtained from numerous measurements in India the following values for the ratio of the effective radiation with an overcast and a clear sky: low clouds 15 to 32% (mean 22%), middle clouds 43%, high clouds 56 to 75% (mean 68%). All the above are quoted by Möller (1957) and compare with ratios between 10 and 30% at Mawson with a cloud cover which is mostly low.

6.2. ATMOSPHERIC RADIATION FOR THE SUMMER, CALCULATED FROM AN ELSASSER CHART

During most of the summer the sun was above the horizon continuously and direct measurements of the net flux of long-wave radiation were impossible. Other

means of estimating the magnitude of the long-wave fluxes in the atmosphere had to be used, one of which was the method of the Elsasser radiation chart (Elsasser 1942).

This chart is based on the radiation properties of H_2O and CO_2. The most important of these is H_2O; the radiation and absorption of CO_2 can, however, not be neglected. Elsasser treats the CO_2 radiation by assuming CO_2 to emit as a black body in the wave-number region of 584 to 752 cm^{-1}.

To use the Elsasser chart, measured profiles of temperature and amount of water-vapour in the atmosphere were required, which were obtained from the daily radiosonde flights at Mawson. These flights took place at 00 G.M.T. early in the morning (6 a.m. Mawson time), with steady katabatic winds, i.e., typical wind conditions at Mawson. Only radiosonde ascents on clear days with stable conditions were analysed.

The humidities measured by the radiosondes are somewhat in doubt, since an accurate instrument for that purpose does not yet exist for use at very low temperatures. The humidity detector used in the sondes was a lithium chloride-coated strip, the standard detector of the Commonwealth Bureau of Meteorology.

In most cases, the humidity was too low to be measured above 500 mb. In all cases it was then extrapolated linearly between the 500 mb value and a hypothetical 0 mb value. This is obviously a very rough procedure but, since the actual amount of water vapour above 500 mb is very small, although not negligible compared with the amount of water-vapour below 500 mb, this procedure is justifiable, considering the uncertainty of the absolute humidity measurements in the first instance.

From the radiosonde ascents, temperature (T) and dewpoint temperature (Td) were available for the pressure levels 850, 700, 600 and 500 mb; also, for the surface and all significant levels where there was a change in either temperature or dewpoint temperature. The monthly mean values of T and Td were obtained at the surface and at the pressure levels 975, 965, 955, 940, 900, 850, 800, 700, 600 and 500 mb by meaning the data from all analysed flights at these levels, profiles of T and Td having been drawn for these flights.

The amount of effective water-vapour present was calculated as indicated by Elsasser, including a pressure correction $\left(\sqrt{\frac{P}{Ps}}\right)$ of the absorption, where P = pressure at respective levels, P_s = standard pressure at 1000 mb. The effective moisture u (gcm^{-2}) is given by

$$u = \frac{1}{g}\int_{P}^{P_o} w\sqrt{\frac{P}{Ps}}\,dP,$$

where g = the acceleration due to gravity, w = specific humidity (gm H_2O per kg air), P_o = atmospheric pressure at the surface.

The specific humidity was obtained from the aerological charts with the dewpoint temperature profiles. For the small pressure increments between levels used, the total water vapour u present was calculated in steps,

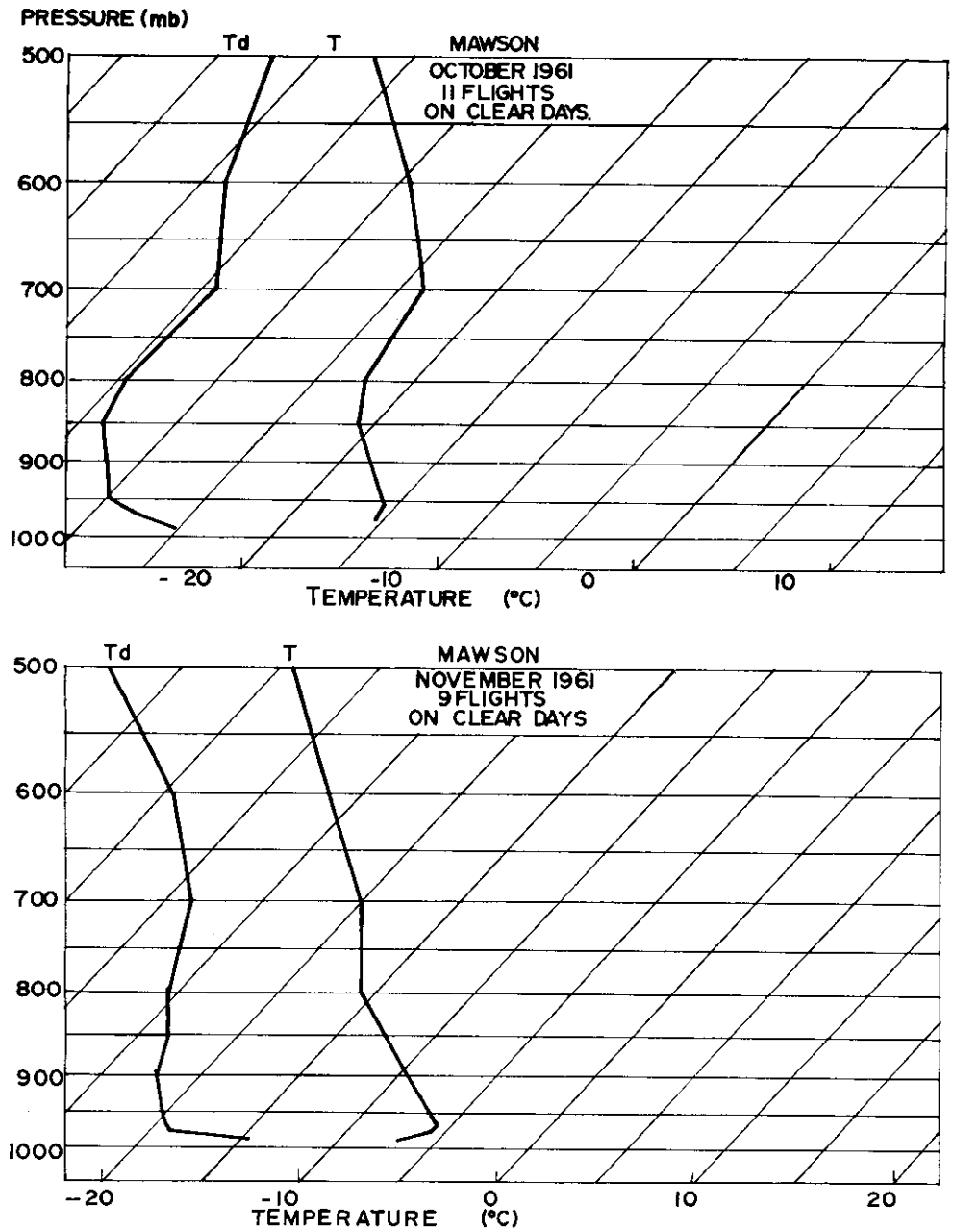

FIG. 6.2.1 (a & b). Temperature (T) and dewpoint temperature (Td) up to 500 mb from radiosonde ascents (monthly means, clear sky).

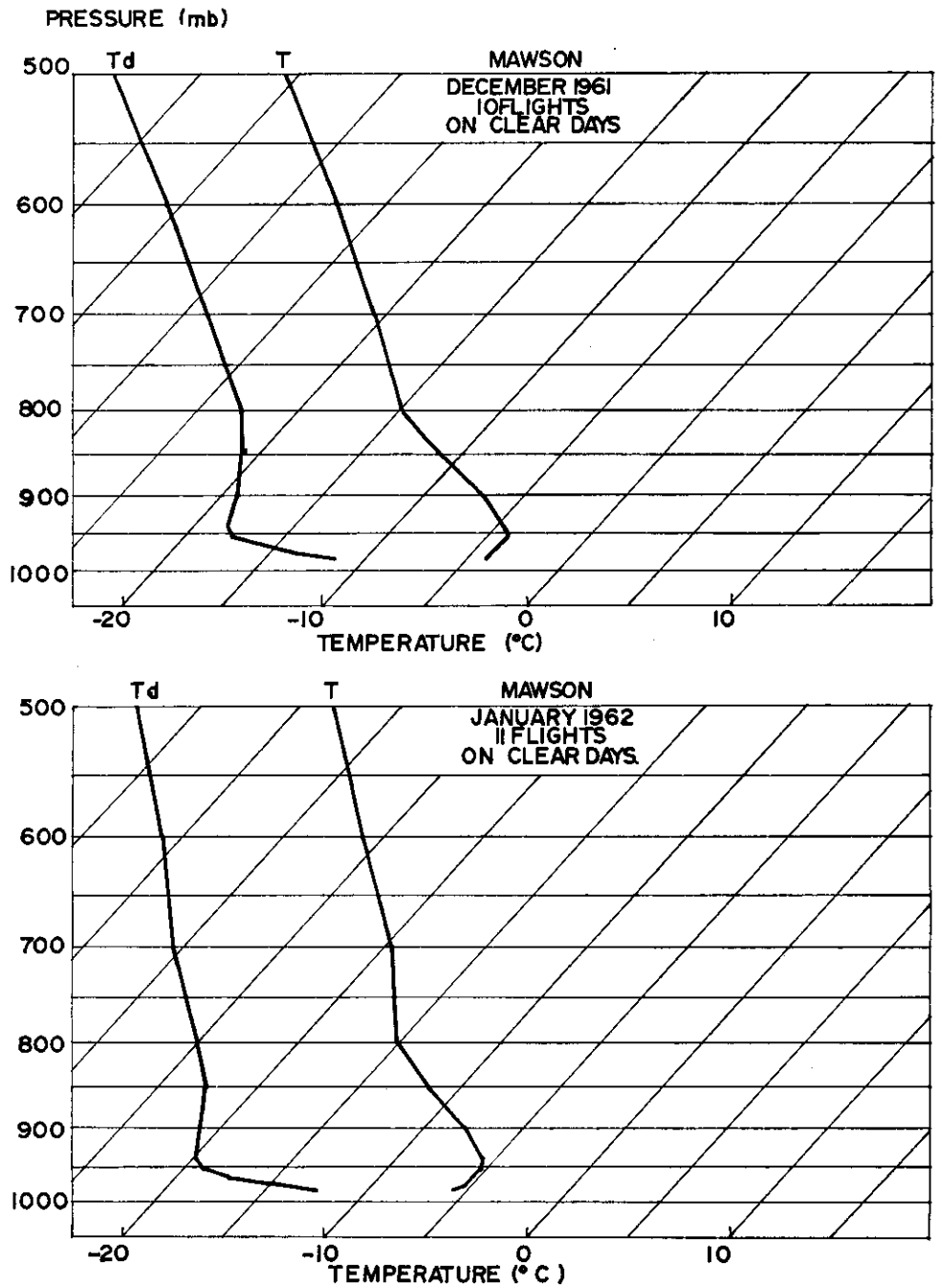

FIG. 6.2.1 (c & d). Temperature (T) and dewpoint temperature (Td) up to 500 mb from radiosonde ascents (monthly means, clear sky).

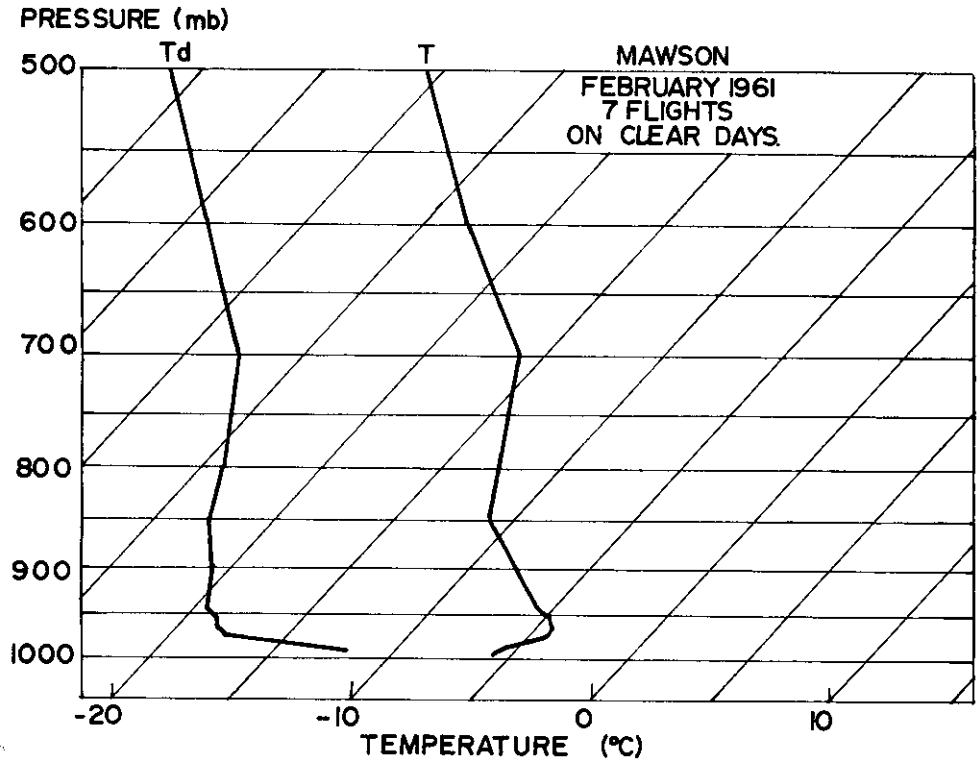

FIG. 6.2.1 (e). Temperature (T) and dewpoint temperature (Td) up to 500 mb from radiosonde ascents (monthly means, clear sky).

$$\Delta_i u = \frac{q_i}{g}\sqrt{\frac{P_i}{1000}}\,\Delta_i P,$$

where $\Delta_i u$ = the water vapour between the pressure levels with mean mixing ratio q_i, mean pressure P_i and pressure difference of the two levels = $\Delta_i P$.

Table 6.2.1 shows the results of the calculations.

Corresponding values of T and u are entered in the radiation chart and the atmospheric radiation is obtained as an area on the chart which is defined. The results obtained were:

ATMOSPHERIC LONG-WAVE RADIATION FROM THE ELSASSER RADIATION CHART (cal cm^{-2} min^{-1})

Month	Number of flights	Atmospheric radiation
Oct. 61	11	·228
Nov. 61	9	·279
Dec. 61	10	·292
Jan. 62	11	·283
Feb. 62	7	·290

As has already been shown in Section 5.2, there is remarkably good agreement between the measured values and values calculated from the Elsasser diagram.

TABLE 6.2.1

AMOUNTS OF WATER VAPOUR PRESENT WITH A CLEAR SKY
Monthly mean values

October 1961				November 1961			
P (mb)	T (°C)	T_d (°C)	u (gm cm^{-2})	P (mb)	T (°C)	T_d (°C)	u (gm cm^{-2})
988	−16·1	−25·2	0	989	−7·0	−14·6	0
975	−15·5	−27·0	·006	975	−5·7	−19·1	·015
965	−15·5	−28·1	·010	965	−5·7	−19·7	·024
955	−15·7	−29·1	·014	955	−6·2	−20·1	·032
940	−16·4	−30·1	·019	940	−7·1	−20·8	·044
900	−18·3	−31·8	·031	900	−9·4	−22·3	·074
850	−20·7	−33·8	·044	850	−12·6	−23·7	·107
800	−22·4	−34·7	·056	800	−15·9	−25·6	·137
700	−23·7	−34·2	·081	700	−20·0	−28·8	·187
600	−29·3	−38·9	·103	600	−26·8	−34·6	·223
500	−37·0	−42·1	·119	500	−34·4	−43·9	·242
(O)	—	—	·143	(O)	—	—	·262

December 1961				January 1962			
P (mb)	T (°C)	T_d (°C)	u (g cm^{-2})	P (mb)	T (°C)	T_d (°C)	u (g cm^{-2})
983	−4·1	−11·5	0	984	−5·9	−12·6	0
975	−4·0	−13·9	·012	975	−5·5	−14·8	·012
965	−4·0	−15·8	·025	965	−5·4	−17·4	·023
955	−4·0	−17·4	·036	955	−5·3	−19·0	·032
940	−4·7	−18·2	·051	940	−5·7	−19·9	·045
900	−7·1	−19·2	·088	900	−8·0	−21·1	·077
850	−11·2	−20·9	·131	850	−11·9	−22·7	·114
800	−15·0	−22·9	·169	800	−15·1	−25·0	·146
700	−20·6	−28·9	·226	700	−19·7	−30·5	·194
600	−27·5	−35·8	·260	600	−26·3	−36·0	·224
500	−35·9	−44·3	·277	500	−33·4	−43·1	·242
(O)	—	—	·296	(O)	—	—	·264

February 1961

P	T	T_d	u
993	−5.8	−12·0	0
975	−4·3	−17·5	·023
965	−4·5	−18·3	·033
955	−4·9	−18·8	·042
940	−5·8	−19·4	·055
900	−8·1	−20·7	·088
850	−11·0	−22·9	·125
800	−12·8	−24·1	·158
700	−16·0	−27·9	·214
600	−23·3	−34·1	·252
500	−30·9	−41·4	·274
(O)	—	—	·301

6.3. ATMOSPHERIC RADIATION AS COMPUTED FROM VARIOUS EMPIRICAL FORMULAE

It has been shown above how the atmospheric radiation can be obtained from the Elsasser chart, if radiosonde observations of temperature and humidity are

available. If there is no upper air data, a number of empirical equations have been proposed for the atmospheric radiation as a function of surface temperature and humidity. These equations will now be tested.

The first equation to be considered is the Ångström formula (Ångström 1915),

$$A = \sigma T^4 (a - b\, 10^{-\gamma\epsilon}),$$

where T = temperature near surface at instrument level (°K)
and ϵ = vapour pressure (surface).

One set of constants given by Ångström is: $a = 0{\cdot}804$, $b = 0{\cdot}236$, $\gamma = 0{\cdot}052$. Bolz and Falkenberg (1949) have made a redetermination of the constants and give the latter as: $a = 0{\cdot}820$, $b = 0{\cdot}250$, $\gamma = 0{\cdot}095$.

The second equation is the Brunt formula (Brunt 1932):

$$A = \sigma T^4 (a - b\sqrt{\epsilon}).$$

The constants, according to Brunt are: $a = 0{\cdot}440$, $b = 0{\cdot}080$; Möller (1951) gives $a = 0{\cdot}480$, $b = 0{\cdot}060$.

Other equations exist, based on humidity near the surface, such as the Elsasser logarithmic formula (Elsasser 1942) and the Robitzsch formula (Robitzsch 1926), but these will not be considered here.

Observations in different parts of the world have given different sets of constants and the equations cannot be expected to give great accuracy, especially when the air is stratified or when surface inversions exist as they do in the Antarctic. The equations, however, should indicate the order of magnitude of the atmospheric radiation.

To test the equations against the measured values of A with a clear sky, the latter values were grouped according to their corresponding vapour pressures, measured simultaneously with the atmospheric radiation. Table 6.3.1 presents the results.

TABLE 6.3.1

GROUP MEANS OF VAPOUR PRESSURE (ϵ), TEMPERATURE (T) AND MEASURED ATMOSPHERIC RADIATION (A)—CLEAR SKY

ϵ (mb)	0·3-0·6	0·7-1·0	1·1-1·4	1·5-1·8	1·9-2·2	2·3-2·6	2·7-3·0
ϵ (mb)	0·54	0·88	1·21	1·58	1·95	2·30	2·83
T(°C)	−22·4	−17·7	−14·3	−12·0	−9·1	−7·8	−6·1
A	·197	·216	·236	·256	·277	·261	·276
No. of observations	54	56	34	12	6	1	3

These results were compared with calculated values from the following equations:

(1) Observed values (from above, grouping the last three groups);

(2) Ångström formula—Ångström constants;

(3) Ångström formula—Bolz and Falckenberg constants;

(4) Brunt formula—Brunt constants;

(5) Brunt formula—Möller constants.

MEASURED AND CALCULATED VALUES OF THE ATMOSPHERIC RADIATION
(cal cm^{-2} min^{-1})

e (*mb*)	(1)	(2)	(3)	(4)	(5)
0·54	·197	·189	·194	·163	·170
0·88	·216	·207	·214	·180	·188
1·21	·236	·222	·232	·191	·202
1·58	·256	·232	·245	·207	·212
2·25	·275	·253	·270	·227	·231

It can be seen that the Ångström formula gives good agreement, especially when used with the Bolz and Falckenberg constants, but that the Brunt formula is seriously in error. When upper-air data are available, Lönnquist's revision (Lönnquist 1954) of the Ångström and Brunt equations, substituting the amount of water vapour u in the atmosphere instead of the surface vapour pressure, could probably be used. It will, however, be best in this case to use the Elsasser radiation chart which gives good results.

A more recent approach to calculate the atmospheric radiation from surface observations has been made by Swinbank (1962), who gives A in terms of temperature only:

$$A = 7{\cdot}63 \times 10^{-16} T^6 \text{ cal cm}^{-2} \text{ min}^{-1}.$$

To test this equation, the temperature at the instrument level (T) measured simultaneously with the atmospheric radiation (A) was grouped and A calculated using the above equation.

TABLE 6.3.2

MEASURED AND CALCULATED VALUES OF THE ATMOSPHERIC RADIATION
(cal cm^{-2} min^{-1}) using Swinbank's equation
Groups (°C)

	−5·0 to −9·0	−9·1 to −13·0	−13·1 to −17·0	−17·1 to −21·0	−21·1 to −26·0
T (°C) mean	−7·5	−11·8	−15·2	−19·2	−22·8
A (measured)	·281	·252	·231	·208	·195
No. of observations	8	21	50	37	49
A (calculated)	·267	·242	·223	·203	·187
A (calculated) new constant	·278	·252	·232	·211	·195

The agreement between theoretical and measured values is fairly good. Better agreement still is obtained, using a constant of 7·95 in the Swinbank equation. Since this value is empirical, it can be changed to fit the data. Values of A, using this new constant are shown in the last row of Table 6.3.2.

The dependence in the Swinbank equation, of the atmospheric radiation on the temperature at the instrument level only, is very convenient in radiation calculations. Swinbank explains that the dependence of A on T is due to the fact that the depth of the surface layer necessary to contain sufficient water vapour and CO_2, to provide effectively full radiation in the relevant wave bands, is always so shallow as to differ very little in temperature from the surface temperature (T). This is inferred from the sharpness and intensity of the absorption bands of both H_2O and CO_2. This equation seems better physicially founded than the previous empirical formulae and use will be made of it in the next section.

6.4. ANNUAL AND DAILY VARIATION OF THE ATMOSPHERIC RADIATION WITH A CLEAR SKY

Mean monthly values of the atmospheric radiation were determined above from direct measurements of the net flux radiation measured during the night. It was assumed that the net flux of long-wave radiation did not vary greatly during the day. Evidence supporting this assumption was found in the fact that the net flux of long-wave radiation hardly varied at all with temperature: thus the effect of the diurnal temperature variation would be negligible, providing cloud and wind conditions remained constant.

To determine the actual magnitude of the daily variation of the atmospheric radiation, an indirect method had to be used, since the long-wave radiation fluxes could not be measured during the day. In Section 6.3 it was shown that a simple relation between the screen temperature and the atmospheric radiation by Swinbank gave quite satisfactory correlation between calculated and measured values. Use of this relation was made to obtain an indication of the diurnal variation of the atmospheric radiation. Fig. 6.4.1 shows this relation in graphical form.

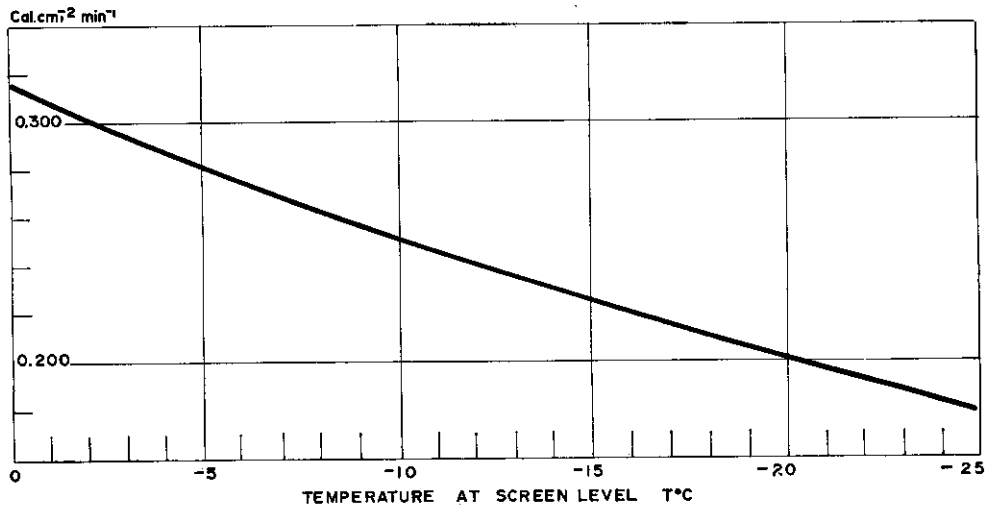

FIG. 6.4.1. Atmospheric radiation by the Swinbank equation, $A = 7{\cdot}63 \times 10^{-16} T^6$.

The basic data needed are thus only screen temperatures. To obtain an indication of the maximum possible monthly amplitude of the variation in atmospheric radiation, the maximum and minimum monthly temperatures with a clear sky were collected and are shown in Table 6.4.1. Also shown in the table are the screen temperatures on clear days at 00Z (6 a.m. Mawson time), generally the coldest synoptic observation time, and at 09Z (3 p.m. Mawson time) generally the warmest time of the day. The difference between the 00Z and 09Z temperature readings should give approximately the mean monthly amplitude of the diurnal temperature variation. This difference is shown as ΔT in the table.

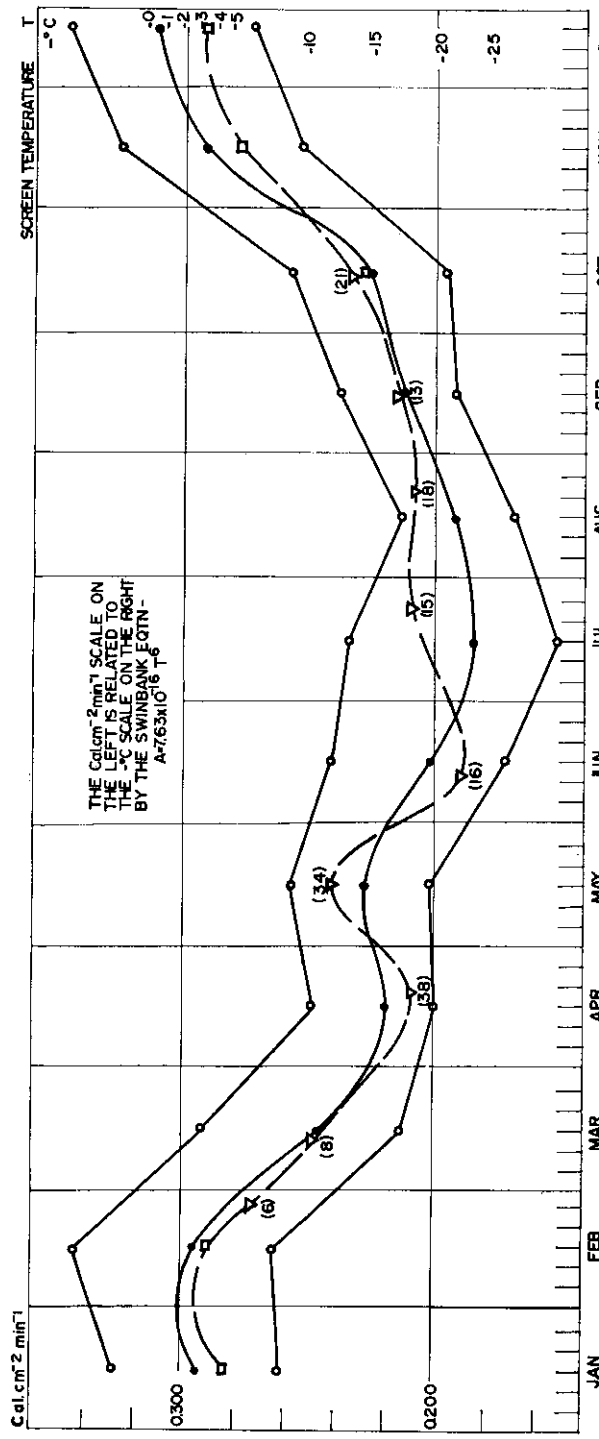

FIG. 6.4.2. Atmospheric radiation (A) on clear days at Mawson (monthly means). Observed values: brackets denote number of observations

□ From Elsasser chart
● From Swinbank equation: monthly temperature means, clear sky
○ From Swinbank equation: monthly temperature extremes.

Fig. 6.4.2 shows part of the data. The vertical scale shows the screen temperature at the right side of the graph and the corresponding values of the atmospheric radiation obtained from the Swinbank equation on the left side, the horizontal scale is a time scale. The mean monthly values of temperature are shown as full circles and are connected by a smooth curve. The temperature maxima and minima for each month are entered as circles. They should give the upper and lower limits between which the atmospheric radiation can vary in the respective months.

TABLE 6.4.1

MONTHLY MAXIMUM AND MINIMUM TEMPERATURES, ALSO MEAN MONTHLY TEMPERATURES AT 00*Z* AND 09*Z*.
Mawson 1961 — clear sky.
(°C)

Month	*T* max.	*T* min.	*T* 00*Z*	*T* 09*Z*	ΔT
Jan.	+1.4	−8·3	−6·3	−0·2	6·1
Feb.	+3·2	−7·8	−6·1	+0·7	6·8
Mar.	−3·4	−17·2	−13·1	−8·0	5·1
Apr.	−10·6	−20·0	−16·3	−14·5	1·8
May	−9·0	−19·5	−14·3	−13·0	1·3
Jun.	−11·9	−26·2	−21·8	−20·9	0·9
Jul.	−13·3	−31·5	−23·9	−23·2	0·7
Aug.	−17·2	−27·2	−22·3	−21·1	1·2
Sep.	−12·4	−21·8	−18·7	−14·9	3·8
Oct.	−8·9	−21·1	−17·0	−12·3	3·7
Nov.	+1·0	−9·7	−6·8	−1·4	5·4
Dec.	+3·5	−6·3	−4·0	+1·9	5·9

To compare the temperature data with measured values of the atmospheric radiation, the latter data were entered on the diagram. The triangles represent monthly means of measured values of the atmospheric radiation. Data derived from radiosonde ascents and using the Elsasser chart were also included (full squares) to extend the curve of measured atmospheric radiation into the summer months. The agreement between measured values and values from the Elsasser chart on the one hand, and the values derived from the Swinbank equation on the other hand, is fairly good.

Although the absolute range over which the atmospheric radiation can vary monthly is fairly high, i.e., approximately 40% of the mean values, the average daily variations are much smaller. Considering the mean amplitudes of the temperature variations in Table 6.4.1, it is seen that the daily temperature variation in summer is approximately 6°C and in winter 1°C. This gives rise to changes in the atmospheric radiation of 0·035 cal cm^{-2} min^{-1} and 0·005 cal cm^{-2} min^{-1} respectively, i.e., 12% and 3% changes of the mean monthly atmospheric radiation. In winter, the daily changes in the atmospheric radiation are thus not greater than the experimental error whereas, in summer, the daily changes are even smaller: since in summer the increase of the air temperature at screen level is accompanied by an increase in the ice temperature to 0°C, the net flux of long-wave radiation

from the ice surface will undergo only very small diurnal change. This was demonstrated by data presented in Section 5.

In this way the gap left by the difficulty of measuring atmospheric radiation during the day has now been bridged and the stage is set finally for discussion of the radiation balance as a whole in Section 7.

7. RADIATION BALANCE

7.1. ANNUAL AND DAILY VARIATION OF THE RADIATION BALANCE

The individual components of the radiation budget have been considered in turn. The balance will now be discussed, both for normal and for special conditions, such as clear or overcast sky and occasions of large and small surface albedo.

Monthly totals of the net incoming radiation (N^+) and net outgoing radiation (N^-) and the net radiation or radiation balance (N) are given in Table 7.1.1 and Fig. 7.1.1.

TABLE 7.1.1

MONTHLY TOTALS OF NET FLUX OF SHORT-WAVE AND LONG-WAVE RADIATION
(k cal cm^{-2})

1961

	Jan.	Feb.	Mar.	Apr.	May	Jun.
N^+	—	—	+1·14	+0·10	0	0
N^-	—	—	−1.84	−2·81	−3·19	−3·33
N	—	—	−0·70	−2·71	−3·19	−3·33
	Jul.	**Aug.**	**Sep.**	**Oct.**	**Nov.**	**Dec.**
N^+	0	+0·03	+0·76	+2·49	+4·03	+5·08
N^-	−2·74	−2·12	−2·05	−1·27	−1·10	−1·11
N	−2·74	−2·09	−1·29	+1·22	+2·93	+3·97

1962

	Jan.	Feb.	Mar.	Apr.	May	Jun.
N^+	+3·59	+1·96	+1·03	+0·13	+0·01	+0·01
N^-	−1·62	−1·09	−2·10	−1·85	−2·92	−2·78
N	+1·97	+0·87	−1·07	−1·72	−2·91	−2·77
	Jul.	**Aug.**	**Sep.**	**Oct.**	**Nov.**	**Dec.**
N^+	0	+0·02	+0·41	+1·55	+3·86	+5·12
N^-	−3·16	−2·81	−1·91	−1·33	−0·96	−0·92
N	−3·16	−2·79	−1·50	+0·22	+2·90	+4·20

Jan. 1963

N^+	+2·59
N^-	−1·04
N	+1·55

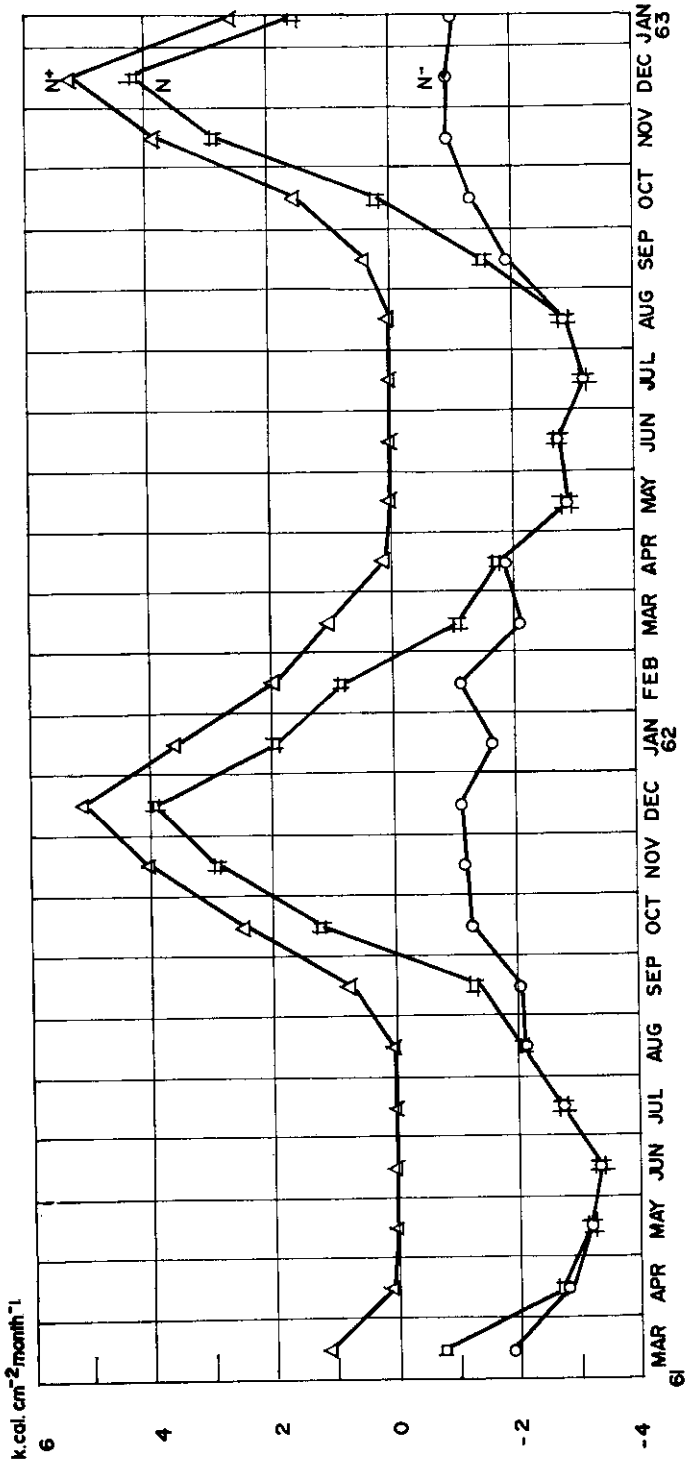

FIG. 7.1.1. Net flux of short-wave and long-wave radiation, Mawson.
N^+ is ingoing net flux
N^- is outgoing net flux
$N = N^+ + N^-$.

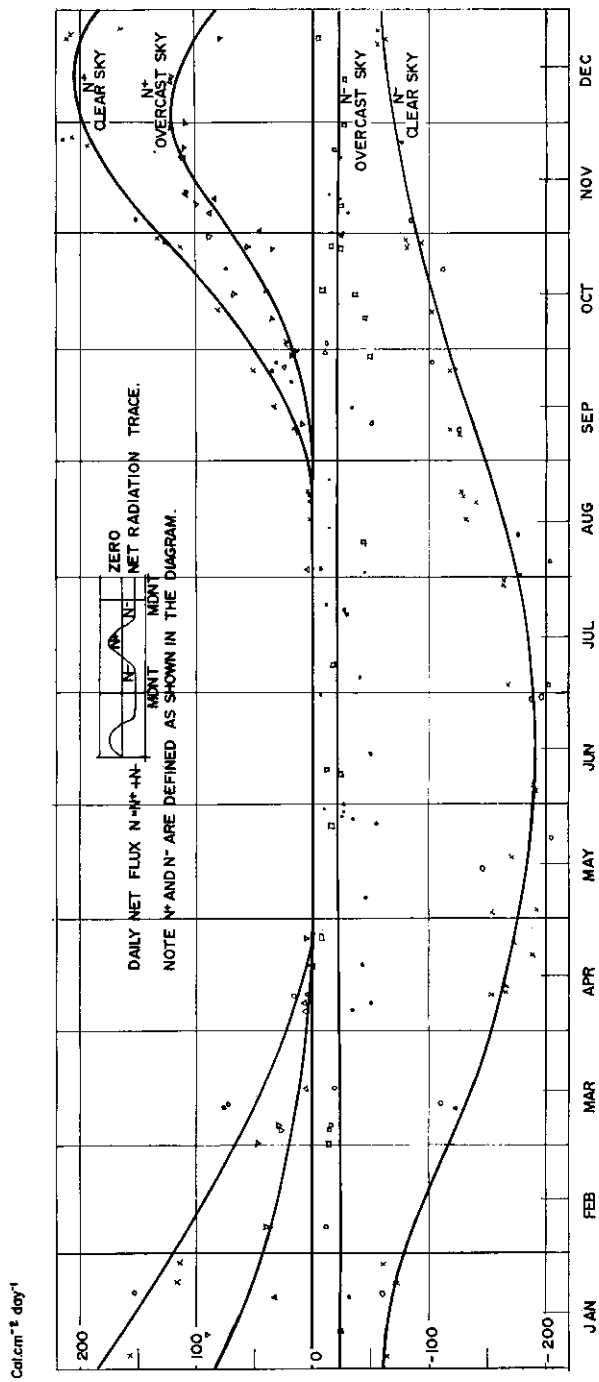

FIG. 7.1.2. Net flux of short-wave and long-wave radiation with a clear sky and overcast sky at Mawson, 1961/1962.

N^+ Clear sky × 1961 ○ 1962
Overcast sky △ 1961 ▽ 1962

N^- Clear sky × 1961 ○ 1962
Overcast sky ○ 1961 □ 1962.

The radiation balance for actual cloud conditions at Mawson is thus positive between October and February, i.e., during that period the snow surface receives more radiation than it loses. In winter there is practically not net incoming radiation, but the snow surface radiates strongly.

To determine the effect of cloud on the net flux of radiation, the values of the incoming and outgoing net flux of short-wave and long-wave radiation, on days with more than seven-eighth's cloud all day, were plotted in Fig. 7.1.2, together with the values of the net flux on days with a clear sky. It can be seen that, with a clear sky, the radiation balance is positive between 20 October and 14 February, reaching a maximum value of $+208$ cal cm^{-2} day^{-1} in December. In winter, the incoming net radiation is zero and the radiation balance has a maximum value of -187 cal cm^{-2} day^{-1}, i.e., the snow surface loses energy by radiation. The net outgoing radiation is fairly constant in winter and does not change as rapidly towards mid-summer as does the net incoming radiation in the summer months.

With an overcast sky, the magnitudes of both net incoming and net outgoing radiation are considerably reduced. The radiation balance is positive between 1 October and 25 February, a period which is a month longer than the corresponding period with a clear sky. The maximum value of the net incoming radiation is $+124$ cal cm^{-2} day^{-1}, i.e., only approximately two-thirds of the clear sky value. The net outgoing radiation shows practically no variation throughout the year and has a fairly constant value of -20 cal cm^{-2} day^{-1}. The radiation losses of the snow surface are thus reduced by a factor of almost 10 in winter, when there is a cloud-cover present.

The scatter of the points in Fig. 7.1.2 is moderately large and it must be remembered that the curve represents average conditions only. The albedo may vary daily when the air temperature is above 0°C, i.e., when the ice is melting, the density and temperature of the cloud layer varies considerably and hence also its radiation and absorption properties; finally the wind affects the net flux of radiation most markedly by controlling the degree of turbulent heat transfer to the surface (see Section 5.2).

Fig. 7.1.3 shows typical examples of the net flux of long-wave and short-wave radiation on days in summer with a clear sky, a variable sky and an overcast sky. Both net incoming radiation and net outgoing radiation are seen to be reduced in magnitude when the sky is overcast. On clear days, the change from net outgoing radiation to net incoming radiation coincides with sunrise as shown on the diagram for 25 December where the sunrise occurs at approximately 3 a.m. solar time. On days with cloud, the change from net outgoing to net incoming radiation is gradual and also later in time than on clear days. The maximum net incoming flux on clear days occurs 1 to 2 hours before solar noon. This is probably due to the fact that considerable heating of the surface takes place at and after noon in summer, and hence the radiation losses from the surface are high while the incoming radiation is fairly constant for a few hours around noon (see Fig. 4.2.1).

In winter, the diurnal change of the net flux of radiation shows little variation and there is no net incoming radiation at any moment. In the transition period between summer and winter there is only a brief period of net incoming radiation

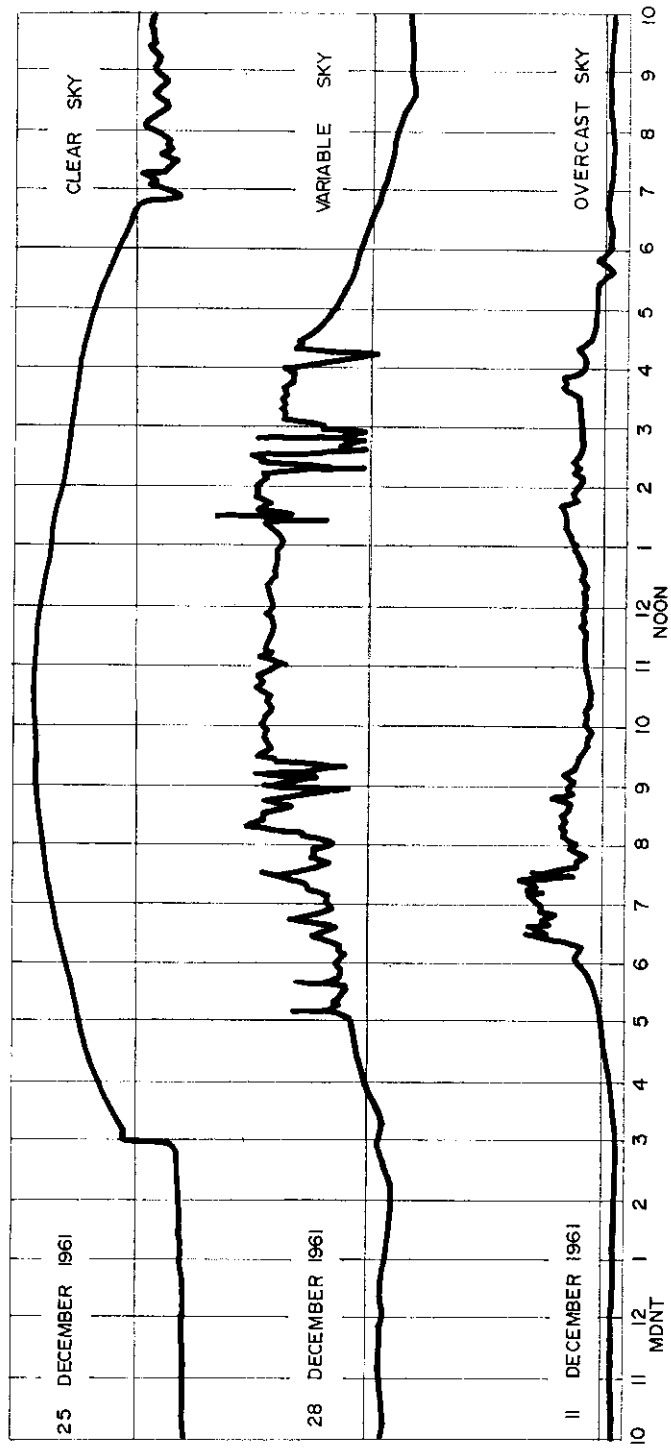

FIG. 7.1.3. Net flux of short-wave and long-wave radiation, Mawson, 1961: typical cases.

(see Fig. 7.1.4 for 8 September—not drawn on the same scale as for the December curves). The maximum value of the net incoming radiation occurs also somewhat before solar noon. At sunrise (approximately 7 a.m. on 8 September) the incoming short-wave radiation is not sufficiently high (as in summer) to change the net flux from net outgoing to net incoming. This occurs only 1½ hours after sunrise, after the short-wave net flux has increased gradually due to increased solar elevation. The effect of the direct solar radiation on the net flux can be seen in the sharp dip in the curve at approximately 8 a.m., which is due to the mast supporting the instrument shading the element of the instrument for some time, before unshading it again.

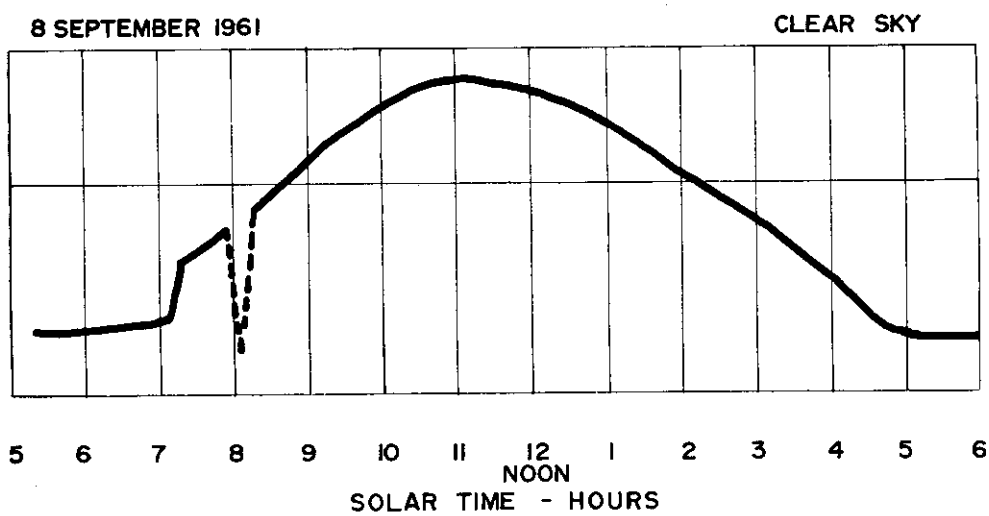

FIG. 7.1.4. Net flux of short-wave and long-wave radiation, Mawson, 1961: typical case.

Fig. 7.1.5 gives the solar elevation when the net flux is zero on clear days. The upper curve represents the afternoon values of the solar elevation for zero net flux, the lower curve the morning values. It can be seen that in summer the solar altitudes when the net flux is zero are considerably higher than in winter. Between 27 April and 15 August there is no net incoming radiation (see Fig. 7.1.2). The morning values of the solar altitudes when the net flux is zero are the same as the elevation angles of the horizon at sunrise, i.e., the net flux changes sign at sunrise as seen in Fig. 7.1.5. This is so for the period October to February. In spring and autumn, the net short-wave flux on sunrise is insufficient to change the sign of the net flux as seen from Fig. 7.1.2. The change of sign of the net flux occurs later at higher solar elevations, until finally the net flux is zero for an instant only on 15 August and 27 April. Just after 15 August and just before 27 April the change of sign of the net flux will occur close to the maximum of the solar elevation. These maxima are shown as curves (*A*) and give an upper limit to the values of solar elevation at which the net flux is zero. If the horizon would be flat at Mawson, by extrapolation from the curves of net radiation the morning values would lie on a curve similar to

curve (B), i.e., the net flux would presumably still change sign at sunrise in December.

The maximum value of the solar elevation when the net flux of radiation is zero is thus 17° at Mawson in summer, comparing with 15° at Scott Base, also in summer (Thomson and MacDonald 1961) and 27° at Port Martin (Loewe 1956).

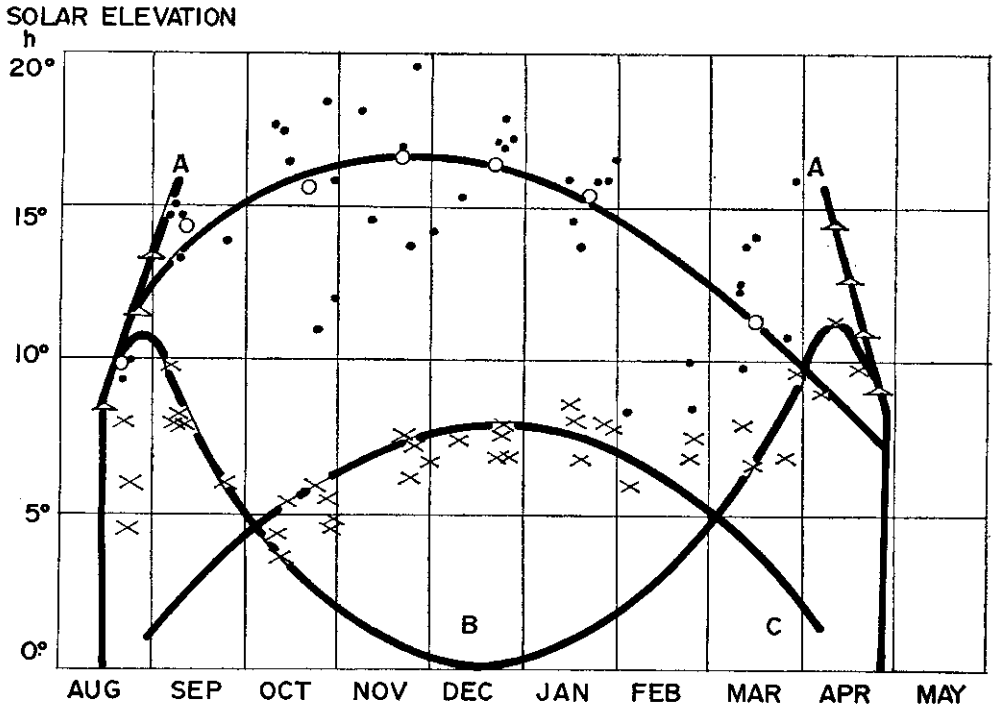

FIG. 7.1.5. Solar elevation when the net flux of radiation is zero on clear days at Mawson 1961.
• Measured values: afternoon
× „ „ : morning
○ „ „ : monthly means
Curves A: maximum possible solar elevation
Curves B: extrapolated curve of solar elevation when the net flux is zero, assuming that the horizon would be flat at Mawson (morning values)
Curve C: elevation of the sun when it is on the horizon at sunrise.

Fig. 7.1.6 shows the monthly values of the radiation balance at three Antarctic stations. The Mawson and Mirny values are similar, both stations being situated in regions of strong katabatic wind, at approximately the same latitude. The Mawson average yearly wind velocity at the 10-metre level is 10·5 m/sec, and the winter inversions are presumably not as pronounced as at Maudheim, hence Mawson shows higher radiation losses in winter. The Mawson radiation losses agree very well with the radiation losses of 100 cal cm^{-2} day^{-1} in winter, measured by Loewe at Port Martin, in Adélie Land (Loewe 1956). This region is characterized even more than Mawson by very strong winds.

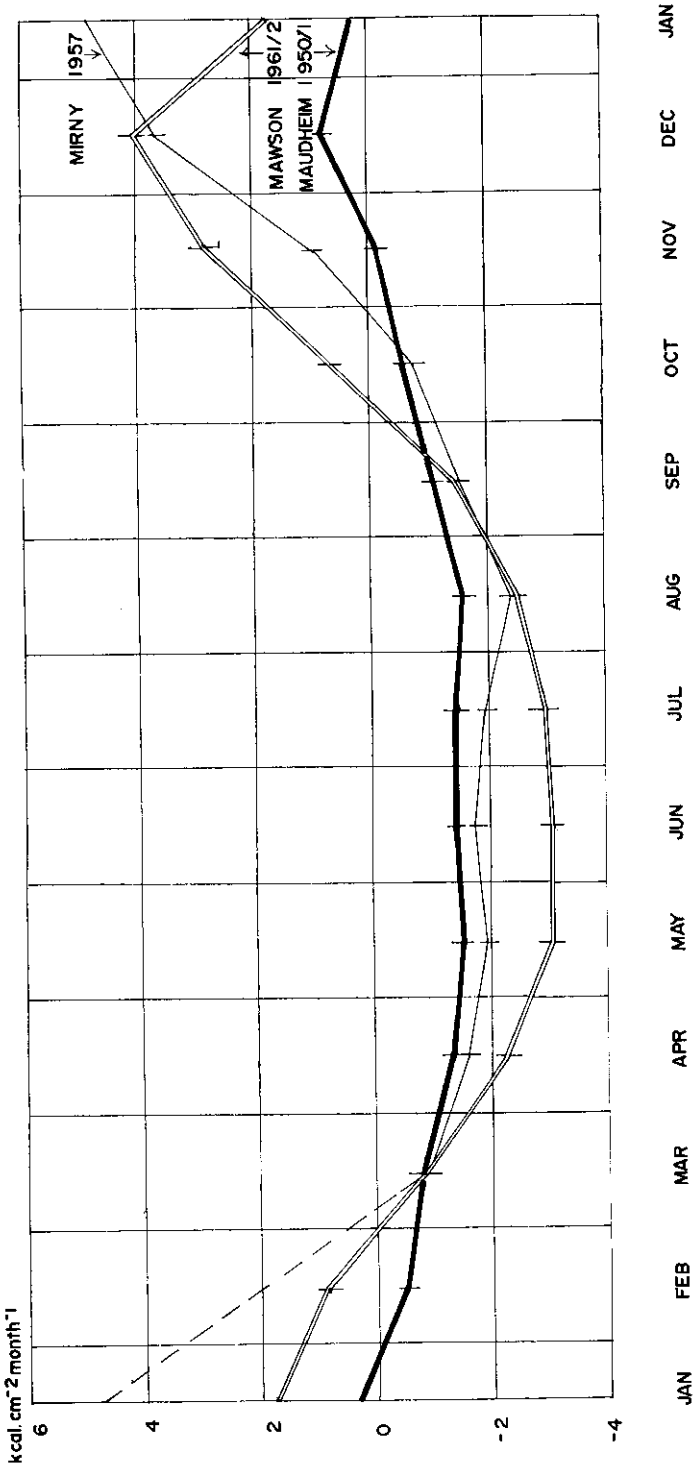

FIG. 7.1.6. The radiation balance at three Antarctic stations.

Next, is will be of interest to give the values of the radiation balance for the whole year for various Antarctic stations. This is done in Table 7.1.2.

TABLE 7.1.2

RADIATION BALANCE (k cal cm^{-2} $year^{-1}$) FOR ANTARCTIC STATIONS

Station	Latitude	Period of Observations	Radiation Balance	Investigator
Mirny	66° 33′	1956–57	−2·1	Rusin (1958)
Port Martin	66° 49′	1951	−5·3	Loewe (1956)
Mawson	67° 34′	1961–62	−5·6	Author
Pioneerskaya	69° 44′	1956–57	−7 to −8	Rusin (1958)
Maudheim	71° 03′	1950–51	−8·8	Liljequist (1956)
Scott	77° 51′	1957–59	+18·2	Thomson (1961)
South Pole	90° 00′		−12·8	Hanson (1960)*

* Estimate based on periodic instantaneous observations.

The high positive value at Scott Base is due to a low albedo in the summer months, when there was no permanent snow-cover beneath the instrument measuring the radiation balance. In winter, the stations in the interior of the Antarctic continent show a large negative radiation balance (Rusin 1958, 1961; Hanson 1960) due to the fact that the net short-wave incoming radiation is small or zero since the sun is below or close to the horizon.

The radiation balance figures make it possible to determine the one quantity which has not yet been discussed—the reflected short-wave radiation. This determines the albedo of the surface and is discussed in the next section.

7.2. ALBEDO OF THE ICE SURFACE

From the components of the radiation flux determined above, namely the global radiation, the net flux of long-wave radiation and the net flux of long-wave and short-wave radiation, the reflected short-wave radiation and hence the albedo can now be determined.

The albedo of a surface depends on a number of factors including the nature of the surface, the solar altitude and state of the sky. Liljequist (1956) has made a rather extensive study of the albedo of a snow surface under these varying conditions.

Further studies by Hoinkes (1960) at the South Pole and at Byrd, and by Shliahov (1957) and Rusin (1961) all give approximately the same values as Liljequist's for a snow surface, i.e., between 80 and 90%. Lower values than 75% were only measured on artificially contaminated surfaces. Data for ice surfaces are readily available. Geiger (1961) gives an albedo of 30 to 46% for clear glacier ice. Ambach (1963) shows clearly the variation of the albedo with the type of surface, determined from measurements in Greenland. His mean values for an ice surface are approximately 45%. Measurements in the European Alps (summarized by

Ambach 1963) show albedo values varying between 33% and 47% for an ice surface.

To derive estimates of the amount of short-wave radiation reflected by the ice surface and hence the amount of short-wave radiation absorbed by the surface at Mawson, the following method was used: From the individual components of the radiation flux the reflected short-wave radiation R was calculated by summing up the components,

$$-R = G + N_L - N,$$

where R = reflected short-wave radiation
G = global radiation
N_L = net flux of long-wave radiation
N = net flux of long-wave and short-wave radiation.

The albedo is then given by the ratio of the reflected short-wave radiation to the global radiation, i.e., $a = \frac{R}{G}$.

Results for clear sky conditions and overcast sky are given in Tables 7.2.2 and 7.2.3, respectively. Negative values are radiation fluxes from the surface; positive values are radiation fluxes towards the surface. Half-monthly values of N_L, G and N were obtained from Figs. 5.3.1, 4.3.1 and 7.1.2, respectively.

TABLE 7.2.2

RADIATION BALANCE AND ALBEDO FOR CLEAR SKY CONDITIONS AT MAWSON 1961/62
(cal cm^{-2} day^{-1})

Date	N_L	G	N	R	a%
1·7	−187	0	−187	0	—
15·7	−186	0	−186	0	—
1·8	−186	15	−176	−5	33
15·8	−187	47	−162	−22	47
1·9	−187	105	−140	−58	55
15·9	−189	185	−113	−109	59
1·10	−189	297	−67	−175	59
15·10	−192	448	−19	−275	61
1·11	−195	627	42	−390	62
15·11	−197	780	91	−492	63
1·12	−197	880	133	−550	62
15·12	−199	918	145	−574	62
1·1	−199	914	121	−594	65
15·1	−197	865	89	−579	67
1·2	−199	732	40	−493	67
15·2	−199	575	−3	−379	66
1·3	−196	436	−49	−289	66
15·3	−193	298	−88	−193	65
1·4	−192	182	−129	−119	65
15·4	−190	101	−155	−66	65
1·5	−190	50	−177	−37	74
15·5	−192	12	−185	−5	42
1·6	−189	0	−187	—	—
15·6	−187	0	−187	—	—

TABLE 7.2.3

RADIATION BALANCE AND ALBEDO FOR OVERCAST CONDITIONS AT MAWSON, 1961/62.
(cal cm^{-2} day^{-1})

Date	N_L	G	N	R	$a\%$
1·7	−17	0	−18	—	
15·7	−16	0	−18	—	
1·8	−16	5	−18	—	
15·8	−16	23	−18	—	
1·9	−19	55	−14	—	
15·9	−22	93	−10	−81	87
1·10	−27	138	1	−110	80
15·10	−33	198	22	−143	72
1·11	−42	300	49	−209	70
15·11	−49	426	84	−293	69
1·12	−56	535	101	−378	71
15·12	−59	570	93	−418	73
1·1	−59	547	62	−426	78
15·1	−59	467	37	−371	79
1·2	−59	350	17	−274	78
15·2	−59	243	7	−177	73
1·3	−58	168	−3	−113	67
15·3	−56	111	−11	−66	60
1·4	−53	67	−15	−29	43
15·4	−49	38	−18	—	
1·5	−42	18	−20	—	
15·5	−35	5	−20	—	
1·6	−26	0	−20	—	
15·6	−20	0	−20	—	

From these tables a number of facts are apparent. Firstly, the albedo values are numerically between the values of a snow surface and a clear ice surface. This is not surprising when one looks at the nature of the surface at Mawson (i.e., in Fig. 1.1.1).

The albedo would actually be expected to be somewhat lower in summer when the surface is covered with a thin film of melt water which is missing in winter when, moreover, the corrugations in the ice surface are filled with snow. The method used above is of course not sufficiently accurate to show these seasonal differences. In fact the albedo values are rather doubtful for the midwinter period when the reflected short-wave radiation is calculated as the small difference of large quantities. A small error in any of the radiation fluxes involved will thus give a large error in the albedo. This is shown in the two tables which give obviously erroneous albedo values towards winter. Excluding these values a mean albedo can be calculated for the year. With a clear sky, the mean albedo value for the period October to March is 64%. With an overcast sky the mean albedo value for the same period is 72%.

This difference in the albedo of a snow or ice surface with clear and overcast sky has been observed by other investigators. Hoinkes (1960), from readings at the South Pole, gives the albedo with a clear sky as 89%, with an overcast sky

88%. Most other investigators, however, give higher albedos with cloudy conditions. Thus Hanson (1960), also at the South Pole, gives the following values:

Period	Clear sky albedo	Cloudy sky albedo
Spring	77	84
Summer	74-83	80-88
Autumn	87	93

Liljequist gives the albedo with a dense overcast sky at about 90% and with a clear sky around 80% for moderate to high solar altitudes. He finds the albedo to be a function of the solar altitude, increasing when the latter decreases. Ambach (1963) also finds similar diurnal changes of the albedo, which he explains in terms of the spatial radiation distribution in the ice as a function of the solar height.

The difference between the albedo with a clear sky and an overcast sky is due to the multiple reflection between the cloud-base and the snow surface. Loewe (1961, 1963) discusses this in detail. Schwerdtfeger (1964) has suggested that the diurnal change of the albedo of a wind-deformed surface may partly be due to polarization of the incident light by the reflecting surface.

The Mawson values thus show the same tendency as observed elsewhere. The few measured albedo values will now be given to support this statement. Unfortunately the data are very limited, all the 1961 measurements having been lost in transit from Antarctica. The measurements were made by swinging the Kipp solarimeter, normally measuring global radiation, through 180° by a suitable fitting and comparing the reading obtained with the instrument facing upwards and downwards. Different calibration factors apply for the upward- and downward-facing instrument (see Section 1). The measurements are shown in Table 7.2.1.

TABLE 7.2.1

ALBEDO VALUES MEASURED AT MAWSON

Date	Time	Cloud	Albedo %	Nature of surface
17.9.60	—	nil	60	Ice surface with small patches of drift snow in the surface corrugations (approx. 20% of total area)
	—	nil	55	—
22.11.62	052	8/8 low cloud	66	—
	062	8/8 low cloud	67	—
24.11.62	082	nil	59	—

The measured values agree well with the computed mean values.

7.3. SHORT-WAVE RADIATION ABSORBED BY THE ICE

The high albedo of ice, and especially snow surfaces, reduces the energy available at the ice-air interface to values well below the high short-wave flux measured by the solarimeters in midsummer. Since the available energy (reduced by convection and evaporation) determines the temperature gradient in the ice and the amount of surface melting, attempts will be made to estimate it quantitatively.

If a mean albedo of 64% for clear sky conditions and 72% for overcast sky is assumed throughout the year, new values of the reflected short-wave radiation, and hence values for the short-wave radiation absorbed by the ice, can be determined from the global radiation. The short-wave radiation (Λ) absorbed by the ice will be simply

$$\Lambda = G - R,$$

where G = global radiation, R = reflected short-wave radiation. Using the values of G from tables 7.2.2 and 7.2.3 above, the following values of Λ are obtained (Table 7.3.1). (*—ve* values are outgoing radiation fluxes from the surface.)

TABLE 7.3.1

SHORT-WAVE RADIATION ABSORBED BY THE ICE AT MAWSON, 1961/62
(cal cm^{-2} day^{-1})

Date	Overcast sky			Clear sky		
	G	R	Λ	G	R	Λ
1·7	0	0	0	0	0	0
15·7	0	0	0	0	0	0
1·8	5	−4	1	15	−10	5
15·8	23	−17	6	47	−30	17
1·9	55	−40	15	105	−67	38
15·9	93	−67	26	185	−118	67
1·10	138	−99	39	297	−190	107
15·10	198	−143	55	448	−286	162
1·11	300	−216	84	627	−402	225
15·11	426	−307	119	780	−499	281
1·12	535	−385	150	880	−563	317
15·12	570	−410	160	918	−587	311
1·1	547	−394	153	914	−585	329
15·1	467	−336	131	865	−553	312
1·2	350	−252	98	732	−468	264
15·2	243	−175	68	575	−368	207
1·3	168	−121	47	436	−279	157
15·3	111	−80	31	298	−191	107
1·4	67	−48	19	182	−116	66
15·4	38	−27	11	101	−65	36
1·5	18	−13	5	50	−32	18
15·5	5	−4	1	12	−8	4
1·6	0	0	0	0	0	0
15·6	0	0	0	0	0	0

The maximum energy available at the ice surface due to short-wave radiation is thus approximately 160 cal cm^{-2} day^{-1} with overcast conditions, and 330 cal cm^{-2} day^{-1}, i.e., twice as much on clear days. The maximum energy available at the ice surface due to both short- and long-wave radiation is the value of N (i.e., net flux of short- and long-wave radiation) in summer, i.e., 100 and 150 cal cm^{-2} day^{-1} for overcast and clear sky respectively. These values are obviously much higher than for a corresponding snow surface, which has a higher albedo. Liljequist's values for a snow surface are given in Table 7.3.2, together with the Mawson values for an ice surface.

TABLE 7.3.2

MAXIMUM DAILY RADIATION ENERGIES AVAILABLE AT AN ICE-AIR AND SNOW-AIR INTERFACE (AT MAWSON AND MAUDHEIM RESPECTIVELY)
(cal cm^{-2} day^{-1})

Energy due to:	Ice-air		Snow-air	
	Clear sky	Overcast sky	Clear sky	Overcast sky
Short-wave flux	330	160	180	80
Net all-wave flux	150	100	30	40

The precise determination of the albedo is thus of some importance in the study of processes in the ice and at the surface which derive their energy from radiation.

7.4. MONTHLY TOTALS OF THE COMPONENTS OF THE RADIATION BALANCE

Finally, estimates of the total amount of radiant energy exchanged at an ice surface during the year will be derived. This will be done using the mean monthly values of the global radiation and net flux of short-wave and long-wave radiation measured during 1961 and 1962 at Mawson. A mean value of the albedo of 70% will be used, in view of the predominance of overcast conditions over clear sky conditions at Mawson. The quantities derived are thus based on a number of assumptions concerning the albedo and are expected to give only rough estimates of the magnitudes of the radiant energy fluxes. The values are shown in Table 7.4.1.

TABLE 7.4.1

MONTHLY TOTALS OF RADIANT ENERGY FLUXES (Mean 1961/1962).
(G = global radiation, N = net flux of all-wave radiation, R = reflected short-wave radiation, Λ = short-wave radiation absorbed by ice for an albedo of 70%).
k cal cm^{-2} $month^{-1}$

	Jan.	Feb.	Mar.	Apr.	May	Jun.
G	21·13	11·06	6·60	2·16	0·31	0
N	+1·76	+0·87	−0·88	−2·22	−3·05	−3·05
R	−14·79	−7·75	−4·62	−1·51	−0·22	0
Λ	6·34	3·31	1·98	0·65	0·09	0
	Jul.	**Aug.**	**Sep.**	**Oct.**	**Nov.**	**Dec.**
G	0·10	1·31	4·10	11·27	19·58	21·78
N	−2·95	−2·44	−1·39	+0·72	+2·92	+4·08
R	−0·07	−0.92	−2·87	−7·88	−13·70	−15·23
Λ	0·03	0·39	1·23	3·39	5·88	6·55

Year:	
G	99.40
N	−5·63
R	−69·56
Λ	29·84

This table sums up the previous detailed discussion and shows that the radiation balance of the ice surface at Mawson is mostly negative. In fact, it was shown in

Section 7.1 that even in summer the radiation balance at Mawson remains negative up to a solar altitude of 17° on clear days.

It remains finally to deal with the factors which compensate for the net radiation loss in the radiation balance. The geothermal heat contribution and the frictional heat created by the ice motion can be disregarded; in general they do not even reach the ice surface (Robin 1955). The seasonal storage of heat in the snow is also small. Latent heat supply, due to condensation and hoar frost formation, may replace some of the heat lost by radiation. The major energy transfer to the surface is, however, due to the turbulent heat exchange with the atmosphere. This has been demonstrated by Dalrymple et al. (1963) whose summary of midwinter energy fluxes at four Antarctic stations (average of June and July values) are reproduced in the final table. The Mawson values of the mean station temperature and net radiation have been added for comparison.

TABLE 7.4. 2

MEAN STATION TEMPERATURE (T_m, °C) AND SURFACE ENERGY BUDGET CONSTITUENTS (ly day^{-1}: net radiation (N), eddy heat flux (Q), using $k = 0{\cdot}428$, and snow heat flux (σ))

$E = N - Q - \sigma$ = remainder term (latent heat flux)

Mean of June and July values

Station (altitude)	Year	T_m	N	Q	σ	E
South Pole (2800 m)	1958	−58·1	−56·5	−51·0	−2·5	−3·0
Mirny (35 m)	1957	−16·4	−51·0	−97·7	−3·0	+49·7
Maudheim (37 m)	1950-51	−26·7	−46·0	−29·8	−7·5	−8·7
Little America (44 m)	1957	−21·6	−32·5	−13·1	−2·6	−16·8
Mawson (40 m)	1961-62	−15·3	−96·6	—	—	—

The values of all the surface heat budget constituents show large differences for the different stations depending on the location and climatic conditions at these stations. The radiation losses are high in all four cases and the compensating energy transfer to the surface is mostly by turbulent heat transfer, to a smaller extent by the release of latent heat in hoar frost formation and to an even lesser degree by heat flow to the surface from the ice. Only at Mirny is there a substantial heat loss through evaporation, which is compensated for by a high transfer of turbulent heat. The Mawson radiation loss is higher than at any of the other four stations, since Mawson is the only one of the listed stations which lies in the regime of strong katabatic winds. The values of the surface heat budget constituents, however, are expected to compare closest with the values for Mirny where, apart from weaker katabatic winds, similar climatic conditions are prevailing.

7.5. FINAL COMMENT

The discussion has been restricted to the radiation budget of the ice-air interface. The complete heat budget involves a number of other quantities. Foremost are the fluxes of sensible and latent heat already mentioned. In addition, the heat flux due to conduction in the ice, and transmission of radiation in the ice, play a significant role. Details remain to be established in a proposed elaborate study

involving the precise measurement of all the constituents of the surface heat budget, including the latent heat flux which up to date has only been determined as a remainder term at Antarctic stations. At the time of going to press this study has been completed and some of the results have been published: Schwerdtfeger and Weller (1967), or are in press: Weller and Schwerdtfeger (1967) and Weller (1967). Further papers are in preparation. The whole work has been submitted as a Ph.D. thesis in the Meteorology Department of the University of Melbourne.

8. ACKNOWLEDGEMENTS

It is a pleasure to acknowledge the help given by the following people in this project. In particular I wish to thank Dr. U. Radok, Head of the Meteorology Department, University of Melbourne, who encouraged this study and who offered extensive criticism of the manuscript. Dr. P. Schwerdtfeger, also of the Meteorology Department, gave valuable comments and advice. I would like to express my gratitude to the Director of the Bureau of Meteorology for making the material available and to the Chief of the C.S.I.R.O. Division of Meteorological Physics for the use of their calibration and computation facilities. Mr. N. Bacon, of the C.S.I.R.O. Division of Meteorological Physics, wrote the programme for the C.S.I.R.A.C. computer. I am also indebted to the ANARE meteorological observers of the Mawson wintering parties in 1961 and 1962, particularly to Mr O. Bode who supplied the 1962 data, and finally to Mr T. Wishart, glaciologist at Mawson in 1963 with the Australian National Antarctic Research Expeditions.

9. REFERENCES

ALBRECHT, F. H. W. (1956). Die Berechnung der Ångströmschen Trübungskonstanten aus Sonnenstrahlungsmessungen in verschiedenen Filtergebieten. *Geofisica Pura E Applicata* —Milano Bd. 33.

ALBRECHT, H. J., *and* DINGLE, R. (1957). Measurements of solar radiation at Mawson, Antarctica, 1954. *Geofisica Pura E Applicata*—Milano **33**: 222.

ALISSOW, B. P., DROSDOW, D. A., *and* RUBINSTEIN, E. S. (1956). Lehrbuch der Klimatologie (Transl.). Leningrad, 1952.

AMBACH, W. (1963). Untersuchungen zum Energieumsatz in der Ablationszone des Grönländischen Inlandeises. Expédition Glaciologique Internationale au Groenland E.G.I.G. 1957-1960 **4** (4).

ÅNGSTRÖM, A. (1915). A study of the radiation of the atmosphere. *Smith's Miscellaneous Collection* **65** (3).

ÅNGSTRÖM, A. (1929). On the atmospheric transmission of sun radiation and on dust in the air, I. *Geografisker Annaler* **11**: 156-166.

ÅNGSTRÖM, A. (1930). On the atmospheric transmission of sun radiation, II. *Geografisker Annaler* **12**: 130-159.

ÅNGSTRÖM, A. (1934). Uber den Zusammenhang zwischen Strahlung und Sonnenscheindauer. *Bioklimatische Beiblätter der Meteorologischen Zeitschrift* **1**.

ÅNGSTRÖM, A., *and* TRYSELIUS, O. (1934). Total radiation from sun and sky at Abisko. *Geografisker Annaler* **16** (1).

ATKINS, W. R. G. (1951). *Quarterly Journal of the Royal Meteorological Society* **77**: 659.

BOLZ, H. M., *and* FALCKENBERG, G. (1949). Neubestimmung der Konstanten der Ångströmschen Strahlungsformel. *Zeitschrift für Meteorologie* **3** (4).

BROOKS, D. L. (1950). A tabular method for the computation of temperature change by infra-red radiation in the free atmosphere. *Journal of Meteorology* **7**: 313.

BUDYKO, M. I. (1963). Atlas of the Heat Balance of the Earth. Geographical Committee, Academy of Science, USSR.

COMMONWEALTH OF AUSTRALIA. Department of the Interior. Bureau of Meteorology (1954). Australian Meteorological Observers' Handbook.

COMMONWEALTH OF AUSTRALIA. Department of the Interior. Bureau of Meteorology (1961). Meteorology: Mawson, Davis, Taylor and Macquarie Island. *ANARE Reports* (D) **10** (Publication No. 60).

COMMONWEALTH OF AUSTRALIA. Department of the Interior. Bureau of Meteorolgy (1963). Australian Radiation Records 1958-1961, and Monthly Means 1953-1961.

DALRYMPLE, P., LETTAU, H., *and* WOLLASTON, S. (1963). South Pole Micrometeorolgy Program, Part II: Data Analysis. Quartermaster Research and Engineering Center, Natick, Mass. Technical Report ES-7.

DEIRMENDJIAN, D. *and* SEKEDA, Z. (1954). Global radiation resulting from multiple scattering in a Rayleigh Atmosphere. *Tellus* **6**: 382.

DE Q. ROBIN, G. (1955). Ice movement and temperature distribution in glaciers and ice-sheets. *Journal of Glaciology* **2** (18).

ELSASSER, W. M. (1942). Heat transfer by infrared radiation in the atmosphere. Harvard Meteorological Studies (6).

FOITZIK, *and* HINZPETER (1958). Sonnenstrahlung und Lufttrübung S 270. Akadem. Verlagsgesellschaft Geest und Portig, Leipzig.

FRITZ, S. (1951). Solar radiant energy and its modification by the earth and its atmosphere. Compendium of Meteorology. American Meteorological Society: Boston.

FUNK, J. P. (1963). Improvements in polythene-shielded net radiometers. Proceedings of Symposium on Engineering Aspects of Environment Control for Plant Growth, 1962. CSIRO: Melbourne.

FUNK, J. P. (1959). Improved polythene-shielded net radiometer. *Journal of Scientific Instruments* **36**: 267.

GEIGER, R. (1961). Das Klima der bodennahen Luftschicht. Vierte Auflage. Braunschweig.

HANN, J., *and* SÜRING, R. (1939). Lehrbuch der Meteorologie, Vierte Auflage: Leipzig.

HANSON, K. J. (1960). Radiation measurements on the Antarctic snowfield, a preliminary report. *Journal of Geophysical Research* **65** (3).

HAURWITZ, B. (1945-1948). *Journal of Meteorology* **2**: 154 (1945); **3**: 123 (1946); **5**: 110 (1948).

HOELPER, O. (1937). Uber die Bestimmung des Atmosphärischen Trübungs-und Wasserdampfgehalts aus Strahlungsmessungen. *Meteorologische Zeitschrift* **54** (12).

HOINKES, H. C. (1960). Studies of solar radiation and albedo in the Antarctic. *Archiv. für Meteorologie, Geophysik und Bioklimatologie*, Series B. Band **10** (2).

IGY INSTRUMENT MANUAL (1958). Radiation Instruments and Measurements. Annals of the IGY **5** (6).

KLEINSCHMIDT, E. (1935). Handbuch der Meteorologischen Instrumente und ihrer Auswertung. Berlin: Springer Verlag.

LILJEQUIST, G. H. (1956). Energy exchange of an Antarctic snow-field. Norwegian-British-Swedish Antarctic Expedition, 1949-52, Scientific Results. Vol. II (1) A: short-wave radiation; B: long-wave radiation and radiation balance.

(*Ed*: BAUR, F.) (1953). Linke's Meteorologisches Taschenbuch. II Band: Leipzig.

LÖNNQUIST, O. (1954). Synthetic formulae for estimating effective radiation to a cloudless sky and their usefulness in comparing various estimation procedures. *Arkiv für Geofysik* **2** (12).

LOEWE, F. (1956). Contribution to the glaciology of the Antarctic. *Journal of Glaciology* **2**: 657.

LOEWE, F. (1961). Betrachtungen zur Mehrfachreflektion der Sonnenstrahlung. *Gerlands Beiträge zur Geophysik* **70** (5).

LOEWE, F. (1963). On the radiation economy, particularly in ice- and snow-covered regions. *Gerlands Beiträge zur Geophysik* **72** (6).

MELLOR, M. (1959). A study of factors governing the mass economy of Antarctica. M.Sc. thesis, Meteorology Department, University of Melbourne.

MÖLLER, F. (1944). Das Strahlungsdiagramm. *RfW Berlin 1943 und Meteorologische Zeitschrift* **61**: 37.

MÖLLER, F. (1957). Strahlung in der unteren Atmosphäre. Handbuch der Physik. Geophysik II, Band 48: 155. Springer-Verlag.

NAUTICAL ALMANAC (1961). London.

NICOLET, M. (1948). La mésure du rayonnement solaire. Institut Royale de Météorologie Belgique. Misc. fasc. 21.

NORRIS, D. J., *and* FUNK, J. P. (1961). Radiation observations at Mawson, Antarctica. *Australian Journal of Applied Science* **12**: 148.

RUSIN, N. P. (1958). The radiation balance of the snow cover in the Antarctic. Information Bulletin of the Soviet Antarctic Expedition. No. 2. (Transl. by RADOK, U).

RUSIN, N. P. (1961). Meteorologicheskii i radiatsionyi Rekhim Antarktidy. Gydrometeorolocheskoye Izdatelstvo: Leningrad.

SCHÜEPP, W. (1949). Die Bestimmung der Komponenten der atmosphärischen Trübung aus Aktinometermessungen. *Archiv für Meteorologie Geophysik und Bioklimatologie* B. **1**: 257-346.

SCHULTHESS, E. (1960). Antarctica Artemis Verlags—AG: Zürich.

SCHWERDTFEGER, P. (1964). Effect of polarization of the albedo. *Nature* **202**: 894.

SCHWERDTFEGER, P., *and* WELLER, G. (1967). The measurement of radiative and conductive heat transfer in ice and snow. *Archiv für Meteorologie Geophysik und Bioklimatologie.* Band 15: Heft 1-2, 24.

SHLIAHOV, V. I. (1957). Results of Soviet radiation researches in Antarctica in 1957. Symposium on Antarctic Research: Wellington, N.Z.

STRETEN, N. A. (1963). Some observations of Antarctic katabatic winds. Australian Meteorological Magazine (42).

SWINBANK, W. C. (1963). Long-wave radiation from clear skies. *Quarterly Journal of the Royal Meteorological Society* **89**: 339.

THOMPSON, D. C., *and* MACDONALD, W. J. P. (1962). Radiation measurements at Scott Base. *New Zealand Journal of Geology and Geophysics* **5**: (5).

VOLZ, F. (1956). Optik des Dunstes. Handbuch der Geophysik **8**: 822-897. Verlag Borntraeger: Berlin.

WALKO, P. (1960). The actinometric determination of turbidity parameters and of precipitable water at various altitudes. UGGI Monographic Nr. 4. Symposium on Radiation: Oxford.

WELLER, G. (1967). The effect of absorbed solar radiation on the thermal diffusion in Antarctic freshwater ice and sea ice. *Journal of Glaciology* (No. 48—in press).

WELLER, G., *and* SCHWERDTFEGER, P. (1967). Radiation penetration in Antarctic plateau and sea ice. WMO Technical Note Series. Proceedings of Symposium on Polar Meteorology, Geneva, 1966 (in press).

WEXLER, H. (1941). Observations of nocturnal radiation at Fairbanks, Alaska and Fargo, N. Dak. *Monthly Weather Review*. Suppl. 46: Washington.

WORLD METEOROLOGICAL ORGANIZATION (1953). Commission for instruments and methods of observation. Abridged Final Report of the First Session, Geneva. W.M.O. No. 19, R.P. 9.